JOURNAL OF TELECOMMUNICATIONS AND INFORMATION TECHNOLOGY

4/2001

Special issue edited by Józef Modelski

Part 1

Editorial Board

Editorial Advisory Board

ISSN 1509-4553

JOURNAL OF TELECOMMUNICATIONS AND INFORMATION TECHNOLOGY

Preface

In this special issue, consisting of two parts, the Reader will find papers, selected from over 180 ones, presented during the *13th International Conference on Microwaves, Radar and Wireless Communications* MIKON-2000, which was held at the Wroclaw Technical University, Wroclaw, Poland on 22–24 May 2000.

The MIKON conference has over 30 years history, however only for the fourth time it was being organised as an biannual international event. The first nine conferences were held under the auspices of Polish Academy of Sciences (PAN) on the national scale, with only a limited number of foreign invited speakers. Initially known as microwave solid state technology conference MECS, in 1983 it was trasformed into MIKON. Those nine national conferences created a solid basis for the transforming MIKON into an international conference in 1994. Now it takes place regulary every two years in May in various Polish cities – the biggest research and cultural centres. The MIKON conference has become known as a regional conference in Central and Eastern Europe. The increasing participation of foreign attendees and their papers has resulted in the situation that last year, for the first time, they outnumbered the Polish contributions.

MIKON has been continuously modified and extended, to cover new areas of microwave research and engineering. Due to the fact that telecommunications and radar technology are the principal driving forces behind microwave research, recently MIKON has been transformed into the conference on microwaves, radar, and wireless communications. The MIKON-2000 Technical Program Committee has accepted 168 contributions in all, from 25 countries, mostly from the region of Eastern and Central Europe. We have also heard 20 invited speakers, the world leading experts. Many of the 27 topical sessions were focus on field traditionally addressed at MIKON, such as passive and active components, measurement techniques, CAD and antennas. However, in MIKON-2000 a greater proportion of papers was devoted to radar technology and polarimetry, as well as to microwave and optical communication systems. The strenght of the MIKON-2000 was enhanced by covering almost full range of microwave activities from components, devices, systems, and networks up to applications.

The first part of this special issue comprises 14 papers from the areas of radar technology, radar polarimetry and sensors, antennas and some aspects of communications systems. I hope this volume will find the Reader's interest and will prove to be for practical usage.

Józef Modelski
Guest Editor

Paper

Doppler polarimetric ground clutter identification and suppression for atmospheric radars based on co-polar correlation

Dmitri Moisseev, Christine Unal, Herman Russchenberg, and Leo P. Ligthart

Abstract — A new clutter suppression technique that uses both Doppler and polarimetric information is presented. Polarimetric properties of the target and clutter are calculated per Doppler frequency cell and based on this information clutter suppression is performed. This new clutter suppression technique is demonstrated with radar measurements of precipitation made by the Delft atmospheric research radar (DARR).

Keywords — radar polarimetry, ground clutter suppression, Doppler radar, atmospheric radar remote sensing.

1. Introduction

The performance of a ground-based atmospheric radar is highly influenced by ground clutter. In order to remove this influence, clutter suppression techniques are used. The most common ground clutter suppression technique uses Doppler information, such as the mean Doppler velocity and spectrum width. Ground clutter has a zero mean Doppler velocity and narrow Doppler spectrum. Based on this, reflections that have velocities close to zero are suppressed. The problem of ground clutter suppression becomes more difficult to solve when atmospheric targets with low radial velocities are studied. Such targets as clouds have Doppler velocities close to zero and have narrow Doppler spectra. Therefore to preserve reflections from this kind of targets accurate knowledge of the ground clutter spectrum is required.

There are several methods of ground clutter identification by polarimetric radars reported in the literature. In 1997 by Hagen [1] the use of *Ldr*, which is the ratio of cross-polar reflection to the co-polar one expressed in the linear $v-h$ polarization basis, is discussed for ground clutter detection. It was noticed that *Ldr* for ground clutter is larger than for most of the meteorological targets. However, for the melting layer of precipitation *Ldr* can be rather high and comparable with the one of ground clutter. Another approach described by Ryzhkov [3] uses a cross-correlation coefficient $\rho_{hv}(0)$ between horizontal and vertical co-polar returns. It was reported that for weather echoes, values of the modulus of the cross-correlation coefficient are usually larger than 0.7 and are lower for areas contaminated with ground clutter. Note that even for the melting layer reflections $\rho_{hv}(0)$ is larger than 0.9 as it was presented by Bringi [3]. Therefore the cross-correlation coefficient gives a high contrast between ground and weather echoes and is well suited for ground clutter identification. However, the main disadvantage of this technique is that it rejects all range bins which are affected by the ground clutter and thus gives substantial loss of data.

In order to overcome drawbacks of the Doppler and polarimetric ground clutter suppression techniques it is useful to combine both of them. The use of polarimetry added to Doppler information will give an accurate classification of range-Doppler bins affected by clutter and will lead to the suppression of only a few Doppler cells instead of a complete range bin. In part 2 of this article the formulation of Doppler polarimetry is given. Based on this formulation the co-polar correlation coefficient in the spectral domain, the magnitude of which is the co-polar coherency spectrum, is introduced. The problem of spectral estimates based on actual radar data is also discussed in this part. In part 3 the co-polar coherency spectrum is used for the ground clutter suppression. This ground clutter suppression method is illustrated on precipitation measurements performed by DARR. Part 4 gives conclusions and recommendations for further studies.

2. Radar Doppler polarimetry: definition of the co-polar coherency spectrum

2.1. Theoretical formulation

To describe the time behavior of stationary (in statistical sense) radar targets the covariance matrix $\mathbf{C}(\tau)$ is used. We shall define it similarly to the wave coherency matrix given by Perina [4]. The covariance matrix expressed in an arbitrary polarization basis (x,y) is

$$\mathbf{C}(\tau) = \left\langle \vec{k}(t) \cdot \vec{k}(t+\tau) \right\rangle , \qquad (1)$$

where $\vec{k}(t) = \begin{pmatrix} S_{xx}(t) & \sqrt{2}S_{xy}(t) & S_{yy}(t) \end{pmatrix}^T$ is the target vector obtained from the elements of the scattering matrix and $\langle\rangle$ denotes ensemble average. It should be noted that by radar target covariance matrix is commonly implied the matrix $\mathbf{C}(0)$, see for example [5]. Further, the spectral

covariance matrix $\mathbf{F}(\omega)$ can be introduced. Its elements of which are related to the elements of the covariance matrix as follows:

$$F_{ij}(\omega) = 2\int_{-\infty}^{+\infty} C_{ij}(\tau)\exp(-i\omega\tau)d\tau$$

$$C_{ij}(\tau) = \frac{1}{4\pi}\int_{-\infty}^{\infty} F_{ij}(\omega)\exp(i\omega\tau)d\omega\,, \qquad (2)$$

where $i, j = 1, 2, 3$.

Equation (2) represents the well known Wiener-Khinchin theorem, see for example Davenport and Root [6], which relates correlation functions to power (cross-) spectra.

Based on Eq. (2) the cross-correlation coefficient between horizontal and vertical co-polar returns can be related to power and cross spectra:

$$\rho_{hv}(0) = \frac{C_{13}(0)}{\sqrt{C_{11}(0)C_{33}(0)}} = \frac{\int_{-\infty}^{+\infty} F_{13}(\omega)d\omega}{\sqrt{\int_{-\infty}^{+\infty} F_{11}(\omega)d\omega \cdot \int_{-\infty}^{+\infty} F_{33}(\omega)d\omega}}. \qquad (3)$$

Similar to the definition of the co-polar cross-correlation coefficient, which is given in Eq. (3), we can define a cross-correlation coefficient for every frequency ω. Remembering that $F_{ij}(\omega)d\omega$ gives the variance if $j = i$ and covariance if $j \neq i$ of the signal with the frequency ω, we can introduce the spectral co-polar correlation coefficient $w_{hv}(\omega)$

$$w_{hv}(\omega) = \frac{F_{13}(\omega)}{\sqrt{F_{11}(\omega)\cdot F_{33}(\omega)}}. \qquad (4)$$

The graph of the modules of the co-polar correlation coefficient $w_{hv}(\omega)$ as a function of frequency is called co-polar coherency spectrum after Priestley [8]. The co-polar coherency spectrum $|w_{hv}(\omega)|$ shows the extent to which *hh* and *vv* elements of the scattering matrix are linearly related. The use of this spectrum for ground clutter suppression is further discussed in this article.

2.2. Estimation of co-polar coherency spectrum

The analysis and formulations which were introduced above were done based on infinitely long and continuous measurements. In the case of real radar measurements we deal with the estimation of spectral characteristics from finite measurement samples. In this case estimated Doppler spectrum $I_{ij}^N(\omega)$ is connected to the actual spectrum $F_{ij}(\omega)$ as follows [7, 8]:

$$I_{ij}^N(\omega) = \int_{-\frac{\pi}{T_s}}^{\frac{\pi}{T_s}} W_N(\theta-\omega)F_{ij}(\theta)d\theta\,, \qquad (5)$$

where T_s is the sampling interval ($\frac{\pi}{T_s}$ is the maximum unambiguous Doppler frequency), $W_N(\omega)$ is the spectrum of the covariance lag window and N is the number of samples. If $N \to \infty$, $W_N(\omega)$ will behave like a δ-function and this will lead to

$$\lim_{N\to\infty} I_{ij}^N(\omega) = \int_{-\frac{\pi}{T_s}}^{\frac{\pi}{T_s}} \lim_{N\to\infty} W_N(\theta-\omega)F_{ij}(\theta)d\theta = F_{ij}(\omega)\,. \qquad (6)$$

If N is so small that the spectral width of $W_N(\omega)$ is much larger than the one of $F_{ij}(\omega)$ then

$$I_{ij}^N(\omega) = W_N(0)\int_{-\sigma_w}^{\sigma_w} F_{ij}(\theta)d\theta = W_N(0)\cdot C_{ij}(0)\,. \qquad (7)$$

Based on Eqs. (6) and (7) it can be concluded that if the number of samples is large enough that the spectrum width of the lag window will be much smaller than the width of $F_{ij}(\omega)$, then the estimated Doppler spectrum $I_{ij}^N(\omega)$ will coincide with the actual spectrum $F_{ij}(\omega)$. Moreover, if N is so small that the spectrum width of $W_N(\omega)$ is much larger than the width of $F_{ij}(\omega)$ then the estimated $I_{ij}^N(\omega)$ spectrum will be proportional to $C_{ij}(0)$ and the estimated co-polar coherency spectrum will coincide with the modulus of the correlation coefficient $|\rho_{hv}(0)|$.

3. Ground clutter identification and suppression

In most cases of atmospheric remote sensing the ground clutter has narrow Doppler spectrum and according to Eq. (7) $|w_{hv}(\omega)|$ is roughly equal to $\rho_{hv}(0)$. Since the almost isotropic nature of weather objects their coherency spectrum will be close to unity and not depended on spectrum resolution. Thus, the co-polar coherency spectrum can be used to identify areas of the Doppler spectrum, which are affected by clutter.

To test this new clutter suppression technique, slant profile measurements of precipitation were performed. The elevation angle of the radar was 20 degrees; thus all the clutter reflections are measured by the side lobes of the antennas. Since it is very difficult to predict the polarization state of the side lobes and it is not the topic of this article we will perform all calculations as if the polarization of the side lobes coincide with the polarization of the main lobe.

Measurements of the scattering matrix are performed with three consecutive sweeps of alternating linear polarizations on the receiving and transmitting channels. This cycle takes 3.75 ms. For this particular example about one minute

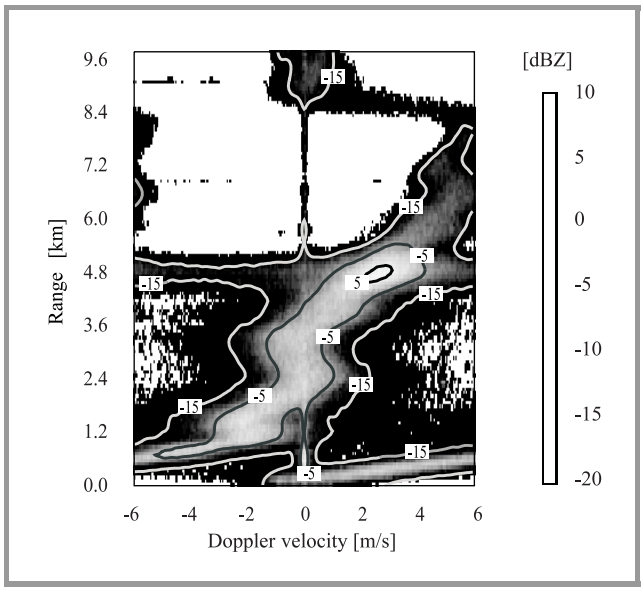

Fig. 1. Doppler spectrum of the precipitation event (HH-polarization). High reflectivity at 4.8 km corresponds to the melting layer. Reflections below the melting layer come from rain. Ice crystals falling out of the cloud cause reflections above the melting layer.

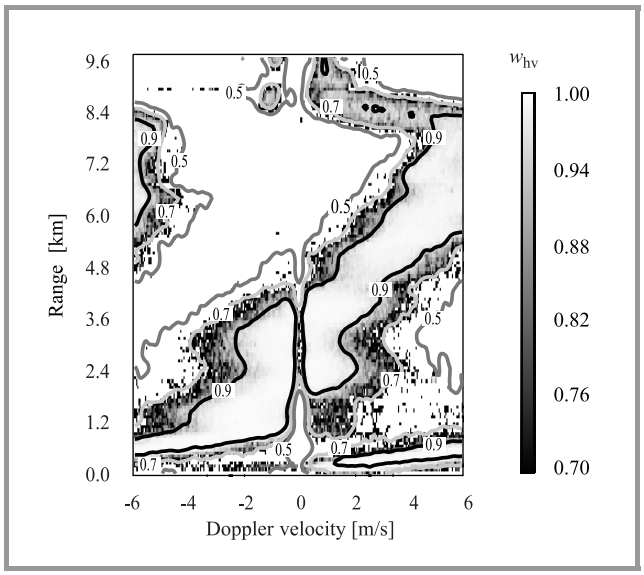

Fig. 2. Co-polar coherency spectrum $|w_{hv}(\omega)|$. The contours represent $|w_{hv}(\omega)|$ values between 0.5 and 1. The gray scaling shows values of between 0.7 and 1. As expected the values of $|w_{hv}(\omega)|$ for weather echoes are larger than 0.7 and for areas affected by ground clutter they are less than 0.7.

of data is collected. Prior to the Doppler processing averaged values of the scattering matrix elements are subtracted from the corresponding time series of scattering matrix elements. This average is performed on the complete data set. This subtraction is identical to suppression of the stable ground clutter.

To obtain Doppler spectra 256 sweeps are used. More details about the Doppler processing are discussed by

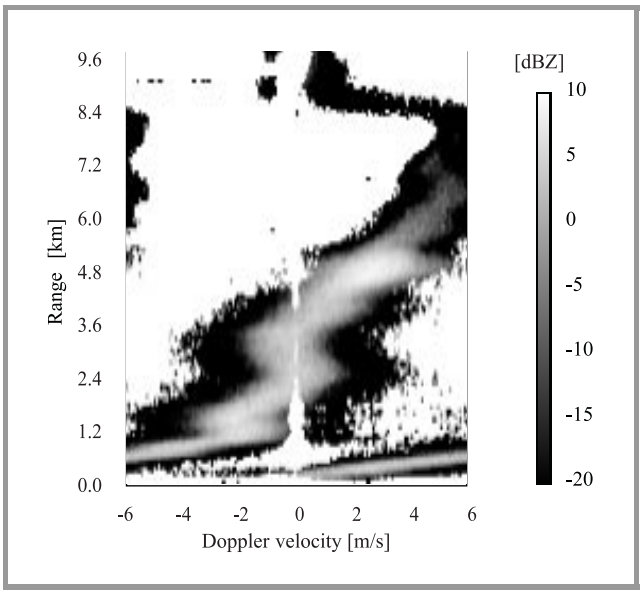

Fig. 3. Doppler spectrum of the precipitation event after clutter suppression. The reflections that have $|w_{hv}(\omega)|$ values below 0.7 are clipped away. This new clutter suppression method shows good performance. It is interesting to note that this suppression has also removed spectral leakage.

Unal [9]. A total of 40 spectra are obtained for each element of the scattering matrix. Based on these spectra the spectral covariance matrix $\mathbf{F}(\omega)$ is obtained and the co-polar coherency spectrum is estimated. In Fig. 1 the Doppler power spectrum for HH-polarization (element of the spectral covariance matrix) is shown. Figure 2 presents the modulus of the co-polar coherency spectrum $w_{hv}(\omega)$. A clear contrast can be seen between ground clutter and atmospheric targets. Therefore in order to suppress ground clutter, areas that have a cross-correlation coefficient below 0.7 are suppressed. The result is shown in Fig. 3.

4. Conclusions

It was shown that Doppler and polarimetric radar signal information can be effectively combined to improve ground clutter suppression. Based on this combination a new ground clutter suppression technique is introduced. This clutter suppression shows high performance especially in the case when ground clutter and target are occupying the same Doppler spectrum area. Moreover, the formulation of Doppler polarimetry is introduced. It is also expected that the further use of Doppler polarimetry will be an important tool for radar targets description.

References

[1] M. Hagen, "Identification of ground clutter by polarimetric radar", in *Proc. 28th Int. Conf. Radar Meteor.*, Austin, Texas, 1997, pp. 67–68.

[2] A. V. Ryzhkov and D. S. Zrnic, "Polarimetric rainfall estimation in the presence of anomalous propagation", *J. Atmosph. Ocean. Technol.*, vol. 15, no. 6, pp. 1320–1330, 1998.

[3] V. Bringi, V. Chandrasekar, P. Meischner, J. Hubbert, and Y. Golenstani, "Polarimetric radar signatures of precipitation at S- and C-bands", *IEE Proc. F*, vol. 138, no. 2, pp. 109–119, 1991.

[4] J. Perina, *Coherence of Light*. London: Van Nostrand Reinhold Company Ltd., 1972.

[5] E. Luneburg, V. Ziegler, A. Schroth, and K. Tragl, "Polarimetric covariance matrix analysis of random radar targets", in *Proc. Targ. Clutt. Scatt. Their Effects Milit. Radar Perform.*, AGARD-CP-501, Ottawa, Canada, 1991, pp. 27-1–27-12.

[6] W. B. Davenport and W. L. Root, *An Introduction to the Theory of Random Signals and Noise*. New York: McGraw-Hill Book Company Inc., 1958.

[7] R. J. Doviak and D. S. Zrnic, *Doppler Radar and Weather Observations*. London: Academic Press, 1992.

[8] M. B. Priestley, *Spectral Analysis and Time Series*. London: Academic Press, 1981.

[9] C. M. H. Unal, D. N. Moisseev, and L. P. Ligthart, "Doppler-polarimetric measurements of precipitation", in *Proc. JIPR'98/PIERS'98*, Nantes, France, 1998.

Dmitri Moisseev
e-mail: D.Moisseev@its.tudelft.nl
IRCTR
Delft University of Technology
Mekelweg 4
2628 CD Delft, The Netherlands

Christine Unal
e-mail: C.Unal@irctr.tudelft.nl
IRCTR
Delft University of Technology
Mekelweg 4
2628 CD Delft, The Netherlands

Herman Russchenberg
e-mail: H.W.J.Russchenberg@irctr.tudelft.nl
IRCTR
Delft University of Technology
Mekelweg 4
2628 CD Delft, The Netherlands

Leo P. Ligthart was born in Rotterdam, the Netherlands, on September 15, 1946. He received an Engineer's degree (*cum laude*) and a Doctor of Technology degree from Delft University of Technology in 1969 and 1985, respectively. He received Doctorates (*honoris causa*) at Moscow State Technical University of Civil Aviation in 1999 and Tomsk State University of Control Systems and Radioelectronics in 2001. Since 1992, he has held the chair of Microwave Transmission, Radar and Remote Sensing in the Department of Information Technology and Systems, Delft University of Technology. In 1994, he became director of the International Research Center for Telecommunications-transmission and Radar. Prof. Ligthart's principal areas of specialisation include antennas and propagation, radar and remote sensing, but he has also been active in satellite, mobile and radio communications.
e-mail: L.P.Ligthart@irctr.tudelft.nl
IRCTR
Delft University of Technology
Mekelweg 4
2628 CD Delft, The Netherlands

Paper

Constant co-polarized echo curves on the Poincare sphere

Zbigniew H. Czyż

Abstract — A set of useful formulae has been presented allowing for computation of the equipower curves on the Poincare sphere of the co-polarized radar returns for both mono- and bi-static scatterings.

Keywords — radar polarimetry, Poincare sphere module of scattering matrix, Kennaugh matrix, Cassini ovals.

1. Introduction

In the English language literature there is a lack of publications treating that very useful "geometrical" presentation of scattering. Basic concepts can be found in technical reports of Kennaugh [1], in Russian book on "Polarization of Radar Signals" written by D. B. Kanareykin [2], and also in the Polish paper presented by this author [3]. But still attempts can be met of researchers trying to find the most convenient ways to draw on the Poincare sphere the curves of constant co-polarized received power scattered backwards from nondepolarizing targets. It is believed that formulae presented beneath will be of some help also for those intending to solve similar problems, i.e., for cross-polarized returns or bistatic scattering.

The method here applied for solution of the problem is based on studies of equation for co-polarized returned power in a most simple form, that means in the so-called "characteristic coordinate system" (CCS) in which Sinclair and Kennaugh matrices depend on minimum number of parameters: two and three real parameters for Sinclair and Kennaugh matrices, respectively. Such approach does not limit the generality of considerations.

2. The co-polarized radar transmission equation

The Jones unit column matrix of monochromatic plane wave of "polarization and phase" P (indicated by the upper index) may be expressed as a function of three the so-called "analytical" angular parameters: γ, δ, ε:

$$[u]_Y^P = \begin{bmatrix} u_Y \\ u_X \end{bmatrix}^P = \begin{bmatrix} \cos\gamma_Y^P \exp\{-j\delta_Y^P\} \\ \sin\gamma_Y^P \exp\{+j\delta_Y^P\} \end{bmatrix} \exp\{-j\varepsilon_Y^P\}. \quad (1)$$

Elements of the matrix depend on the orthogonal null-phase (ONP) polarization basis denoted here by the subscript Y (the lower index). That basis may correspond to the XYZ Cartesian coordinate system, with the propagation axis "Z", or may denote any other ONP basis obtained by applying to the original one a unitary unimodular transformation. Both P and Y can be treated as three parameter tangential phasors (see [4]) on the Poincare sphere. Kronecker square of the Jones matrices eliminates the "phase" parameter:

$$[u]_Y^P \otimes [u]_Y^{P\,*} = \begin{bmatrix} \cos^2\gamma_Y^P \\ \cos\gamma_Y^P \sin\gamma_Y^P \exp\{-j2\delta_Y^P\} \\ \cos\gamma_Y^P \sin\gamma_Y^P \exp\{+j2\delta_Y^P\} \\ \sin^2\gamma_Y^P \end{bmatrix}. \quad (2)$$

So, the resulting unit Stokes four-vector of the wave:

$$[P]_Y^P = \frac{1}{\sqrt{2}} \begin{bmatrix} 1 & 0 & 0 & 1 \\ 1 & 0 & 0 & -1 \\ 0 & 1 & 1 & 0 \\ 0 & j & -j & 0 \end{bmatrix} \begin{bmatrix} \cos^2\gamma_Y^P \\ \cos\gamma_Y^P \sin\gamma_Y^P \exp\{-j2\delta_Y^P\} \\ \cos\gamma_Y^P \sin\gamma_Y^P \exp\{+j2\delta_Y^P\} \\ \sin^2\gamma_Y^P \end{bmatrix} =$$

$$= \frac{1}{\sqrt{2}} \begin{bmatrix} 1 \\ \cos 2\gamma_Y^P \\ \sin 2\gamma_Y^P \cos 2\delta_Y^P \\ \sin 2\gamma_Y^P \sin 2\delta_Y^P \end{bmatrix} = \frac{1}{\sqrt{2}} \begin{bmatrix} 1 \\ \mathrm{q} \\ \mathrm{u} \\ \mathrm{v} \end{bmatrix}_Y^P \quad (3)$$

depends on two, though doubled, parameters 2δ and 2γ which can be interpreted as angular coordinates of the polarization point P on the Poincare sphere. The q, u, v coordinates are the three "normed" Stokes parameters of the point P on the sphere.

Consider, e.g., a simplified model of a rain-drop of the shape of an oblate spheroid with vertical axis of symmetry. Its Sinclair matrix for backscattering can be presented as follows:

$$[A]_Y = \left\{ \begin{bmatrix} A_2 & 0 \\ 0 & A_1 \end{bmatrix} e^{j\mu} \right\}_Y; \quad A_2 \geq A_1 \quad (4)$$

with real positive A_2, A_1, and μ. Diagonal elements may denote, e.g., horizontal and vertical polarizabilities with space attenuation factor included. Incidentally, the form of the above matrix is exactly like in the characteristic ONP polarization basis, corresponding to the CCS in the Stokes parameters space. Any symmetrical Sinclair matrix can be transformed to that form by proper change of the basis.

Using the Kronecker square of that matrix

$$[A]_Y \otimes [A]_Y{}^* = \begin{bmatrix} A_2^2 & 0 & 0 & 0 \\ 0 & A_2A_1 & 0 & 0 \\ 0 & 0 & A_1A_2 & 0 \\ 0 & 0 & 0 & A_1^2 \end{bmatrix}_Y \quad (5)$$

the corresponding Kennaugh matrix can be found as follows:

$$[K]_Y = \tfrac{1}{2}\begin{bmatrix}1&0&0&1\\1&0&0&-1\\0&1&1&0\\0&-j&j&0\end{bmatrix}\begin{bmatrix}A_2^2&0&0&0\\0&A_2A_1&0&0\\0&0&A_1A_2&0\\0&0&0&A_1^2\end{bmatrix}_Y\begin{bmatrix}1&1&0&0\\0&0&1&-j\\0&0&1&j\\1&-1&0&0\end{bmatrix} = \\ = \begin{bmatrix}a_1&b_1&0&0\\b_1&a_1&0&0\\0&0&a_3&0\\0&0&0&-a_3\end{bmatrix}_Y \tag{6}$$

with

$$a_1 = \frac{A_2^2+A_1^2}{2},\quad b_1 = \frac{A_2^2-A_1^2}{2},\quad a_3 = A_2A_1;\quad a_2^2 - a_3^2 = b_1^2$$

(To simplify formulae, in what follows, indices of matrices will be omitted).

For transmit/receive "effective" Stokes four-vectors of complete polarization, corresponding to the unit total intensity, the co-polarized received power is

$$P_c(\mathrm{P}) = P_c(\mathrm{q},\mathrm{u},\mathrm{v}) = \\ = \tfrac{1}{2}[1\ \mathrm{q}\ \mathrm{u}\ \mathrm{v}]\begin{bmatrix}a_1&b_1&0&0\\b_1&a_1&0&0\\0&0&a_3&0\\0&0&0&-a_3\end{bmatrix}\begin{bmatrix}1\\\mathrm{q}\\\mathrm{u}\\\mathrm{v}\end{bmatrix} = \\ = \tfrac{1}{2}\left\{a_1\left(1+\mathrm{q}^2\right)+2b_1\mathrm{q}+a_3\left(\mathrm{u}^2-\mathrm{v}^2\right)\right\} \tag{7}$$

with

$$\mathrm{q}^2+\mathrm{u}^2+\mathrm{v}^2 = 1\,. \tag{8}$$

The last equation presents the Poincare sphere of unit radius in the q, u, v coordinates. For P_c(P) = const., Eq. (7) determines another surface. Its cross-section with the sphere (8) traces curves of constant P_c powers on that sphere.

3. The Poincare sphere model of the backscattering matrix

The Poincare sphere model of a Sinclair and/or Kennaugh scattering matrix will be constructed with the following parameters:

$$r = \frac{A_2+A_1}{2},\quad e = \frac{A_2-A_1}{2},\quad d = \sqrt{A_2A_1}\,. \tag{9}$$

Here r means the radius of the sphere in coordinates

$$x = r\mathrm{q},\quad y = r\mathrm{u},\quad z = r\mathrm{v} \tag{10}$$

what results in the equation of the sphere model:

$$x^2+y^2+z^2 = r^2\,. \tag{11}$$

The Poincare sphere model can show the mechanism of scattering geometrically as follows. Any point P of incident polarization, after inversion through the point I defined by coordinates: $x=-e$, $y=z=0$, and after rotation about the z axis by 180°, determines the scattered polarization point S. The scattered power is equal to the square of the IP distance. However, to obtain the power received by the same transmit/receive antenna, the scattered power should be multiplied by the square of cosine of one half of an angle between the S and P points:

$$P_c(\mathrm{P}) = (\mathrm{IP})^2\cos^2\left(\angle\frac{\mathrm{SP}}{2}\right). \tag{12}$$

4. Construction of constant received power curves by the use of Cassini ovals

Another useful equality has been first derived by Kennaugh. It allows for expressing the co-polarization received power by a product of squares of two distances between P point and the so-called CO-POL NULL points O_1 and O_2 of coordinates: $x=-e$, $y=0$, $z=\pm d$:

$$P_c(\mathrm{P}) = \frac{(\mathrm{O}_1\mathrm{P})^2\times(\mathrm{O}_2\mathrm{P})^2}{(2r)^2} = \frac{c^4}{(A_2+A_1)^2}\,. \tag{13}$$

with

$$c^2 = (\mathrm{O}_1\mathrm{P})\times(\mathrm{O}_2\mathrm{P}) = (A_2+A_1)\sqrt{P_c(\mathrm{P})}\,. \tag{14}$$

Considering P points not necessarily located on the Poincare sphere surface, we obtain for c^2 = const. a surface of rotational symmetry, with the axial cross-section being a Cassini oval with focuses in points O_1 and O_2. That surface is given by the known equation of the Cassini oval:

$$\left.\begin{aligned}&\left[\rho^2+z^2\right]^2+2d^2\left[\rho^2-z^2\right] = c^4-d^4\\&\rho^2 = (x+e)^2+y^2\end{aligned}\right\} \tag{15}$$

for which the following coordinates of its axis and focuses have been determined:

$$y_{axis} = 0,\quad x_{axis} = -e,\quad z(x_{axis}, y_{axis}|P_c = 0) = \pm d\,. \tag{16}$$

Comparing the last expressions with Eq. (15) we see that for $P_c = 0$, resulting in $c = 0$, the surface reduces to two points only, the focuses of the Cassini oval.

5. Cross-section of the Poincare sphere model with parabolic and hyperbolic cylinders

Simpler presentation of the constant received power curves can be found eliminating one of Stokes parameters, v or u, from Eq. (7). That way projections of the P_c(P) = const. curves from the Poincare sphere of unit radius on to the qu and qv planes can be found.

By substituting $v^2 = 1 - q^2 - u^2$ in Eq. (7) we obtain a set of ellipses:

$$P_c(P) = (e + rq)^2 + d^2u^2 = \frac{c^4}{4r^2} = \text{const.} \qquad (17)$$

or, for the model of the radius r, in the xyz coordinate system:

$$\frac{c^4}{4} = r^2\left((e + rq)^2 + d^2u^2\right) = r^2\left(e + x\right)^2 + d^2y^2. \qquad (18)$$

The semi-axes of the new larger ellipses can be found as follows:

$$\left.\begin{aligned} &\frac{4r^2(e+x)^2}{c^4} + \frac{4d^2y^2}{c^4} = 1 = \frac{(e+x)^2}{b^2} + \frac{y^2}{a^2} \\ &a = \frac{c^2}{2d}, \quad b = \frac{c^2}{2r}; \quad a \geq b. \end{aligned}\right\}. \qquad (19)$$

Similarly, by substituting $u^2 = 1 - q^2 - v^2$ in Eq. (7) we obtain a set of hyperbolae:

$$P_c(P) = (r + eq)^2 - d^2v^2 = \frac{c^4}{4r^2} = \text{const.} \qquad (20)$$

and, for the model of the radius r, in the xyz coordinate system:

$$\frac{c^4}{4} = r^2\left((r + eq)^2 - d^2v^2\right) = \left(ex + r^2\right)^2 - d^2z^2. \qquad (21)$$

Parameters a and b of the new larger hyperbolae can be found also similarly:

$$\left.\begin{aligned} &\frac{4e^2\left(x + \frac{r^2}{e}\right)^2}{c^4} - \frac{4d^2z^2}{c^4} = 1 = \frac{\left(x + \frac{r^2}{e}\right)^2}{a^2} - \frac{z^2}{b^2} \\ &a = \frac{c^2}{2e}, \quad b = \frac{c^2}{2d} \end{aligned}\right\}. \qquad (22)$$

It is worth noting that asymptotes of hyperbolae are tangent to the sphere in O_1 and O_2 points. They are crossing at point I' with coordinate $x = -(r^2/e)$ what means that I and I' points are mutual reflections in the sphere surface.
It can be checked easily (by substituting Eqs. (21) or (18) to (15) and eliminating in Eq. (15) y or z, respectively) that projections of constant received power curves obtained by the two methods agree precisely.

6. Other useful formulae

The parameter of constant level of the received signal versus $(P_c)_{\max} = A_2^2$ can be computed from the formulae

$$L = P_c\ [\text{dB}] = 10\log\frac{(P_c)_{\max}}{P_c} = 20\log\frac{c^2_{\max}}{c^2} > 0, \qquad (23)$$

where

$$c^2 = (A_2 + A_1)\sqrt{P_c}, \quad c^2_{\max} = 2r(r+e) = (A_2 + A_1)A_2. \qquad (24)$$

Hyperbolae and ellipses for given L are the following functions of x:

$$z(L,x) = \pm\frac{\sqrt{(ex + r^2)^2 - \frac{c^4}{4}}}{d}, \quad y(L,x) = \pm\frac{\sqrt{\frac{c^4}{4} - r^2\,(e+x)^2}}{d}, \qquad (25)$$

with

$$\frac{c^4}{4} = \left(\frac{r(r+e)}{\log^{-1}(L/20)}\right)^2. \qquad (26)$$

Ellipses can be also presented in cylindrical coordinates by a formula

$$\rho = \frac{c^2}{2\sqrt{r^2 - e^2\sin^2\varphi}}, \qquad (27)$$

where the φ angle is being taken from the xz plane.

7. Conclusions

The problem has been solved for symmetrical Sinclair and Kennaugh matrices. In cases of the bistatic scattering, or matrices corresponding to cross-polarized received powers, we deal with nonsymmetrical matrices. The form of Sinclair matrices in their characteristic ONP polarization bases is antisymmetrical. However, when using the same transmit/receive polarization vectors, the problem remains exactly the same like for the symmetrical matrices. What should be done is to take as the Sinclair scattering matrix its symmetrical part only because the antisymmetrical elements are being eliminated in the transmission equation.

References

[1] E. M. Kennaugh, "Polarization properties of radar reflections". Contract AF 28 (099)-90, Rome Air Development Center, Project Report 389-12 of the Antenna Laboratory, Department of Electrical Engineering, the Ohio State University Research Foundation, Ohio, 1 March 1952.

[2] D. B. Kanareykin, "Experimental determination of polarization invariance for stable targets", in *Polarization of Radar Signals*, D. B. Kanareykin, N. F. Pavlov, and W. A. Potekhin. Moscow: Sov. Radio, 1966 (in Russian).

[3] Z. H. Czyż, "Polarimetric properties of nondepolarizing targets", *Prace PIT*, no. 65, pp. 23–36, 1970 (in Polish).

[4] Z. H. Czyż, "The polarization and phase sphere of tangential phasors and its applications", *Proc. SPIE*, vol. 3120, pp. 268–294, 1997.

Zbigniew H. Czyż was born in Wilno, Poland on Jan. 19, 1930. He received the B.Sc., M.Sc., and Ph.D. degrees from Warsaw University of Technology, Warsaw, Poland, in 1953, 1959, and 1968, respectively. One year of his doctoral studies he spent at the Brooklyn Polytechnic Institute,

Electrophysics Department, Farmingdale, NY. In 1988, he received his habilitation degree (D.Sc.) from Wroclaw University of Technology, Wroclaw, Poland. Since 1952, he has been employed by the Telecommunications Research Institute (Przemysłowy Instytut Telekomunikacji – PIT), Warsaw, Poland, holding position of head of the Microwave Antenna Laboratory (1952–1959), "Independent Scientific Worker" and Docent (1964–1992), and Professor (since 1992). His interests are mainly in the field of microwave reflector antenna design and measurements, and in radar polarimetry. Dr. Czyż was the recipient of Polish Academy of Science, Technical Sciences Division Award (1988): for achievements in the theory of electromagnetic waves – polarization of radar scatterings. He is an author of over 50 papers on radar polarimetry, most of them presented at international conferences, and some prepared in cooperation with the Office of Naval Research in the USA. He is Senior Member of IEEE, member of its Societies: AP, AES, MTT, and GRS. Since 1972 he has served as Secretary of the IEEE Poland Section.

e-mail: godlewska@pit.edu.pl
Telecommunications Research Institute
Poligonowa st 30
04-051 Warsaw, Poland

Paper

24 GHz radar sensors for automotive applications

Michael Klotz and Hermann Rohling

Abstract — Automotive radar systems using integrated 24 GHz radar sensor techniques are currently under development [1]. This paper describes a radar network consisting of four sensors distributed behind the front bumper of an experimental car. Each single sensor measures the target range with high accuracy. A multilateration technique is used in the radar network for precise azimuth angle estimation even in multiple-target situations. The system performance is shown in real traffic situations for parking aid, stop & go and blind spot applications.

Keywords — automotive radar, radar network, radar sensors.

1. Introduction

Automotive radar systems in the 77 GHz domain were recently introduced into the passenger car market as a security and comfort system for the driver. These adaptive cruise control systems (ACC) have a maximum range of 150 m and measure the target range, Doppler frequency and angle using three adjacent and overlapping antenna beams with high resolution and accuracy [2].
For parking aid applications additional ultrasonic sensors with a maximum range of 2 m are used, having limited potential to extend the functionality to other applications like stop & go support of a narrow beam long range radar. For this reason radar systems in the 24 GHz domain which have good performance in range and azimuth angle measurement are of interest and can therefore be applied in different automotive applications like:

- **parking aid** with higher precision, longer range and higher update rates than conventional ultrasonic systems;
- **blind spot detection** with a very cheap sensor technology;
- support of adaptive cruise control systems in **cut-in-and stop & go-situations** due to the fact that the short range sensors can have a higher beam-width than the forward-looking long range sensor;
- **pre-crash detection** with very high detection update rates.

The system described in the following chapters was mainly tested in parking aid and stop & go scenarios with good results and still remaining potential for additional applications.

2. Radar sensor for the frequency 24 GHz

A detailed technical description of the used 24 GHz radar sensors is shown in [3]. The measurement technique is based on a pulse radar principle with very short pulse length of 350 ps and a pulse repetition frequency of 4 MHz. Table 1 shows the main features of the high resolution radar sensors. The sensor measures the target range only, but with high resolution and accuracy. The maximum range is 20 m, the range accuracy is ±3 cm and the achieved range resolution is approximately 6 cm due to the very short transmit pulses.

Table 1
High resolution radar features

Parameter	Min.	Typ.	Max.	Unit
Range	0.15		20	m
Pulse width	300	350	400	ps
Duty cycle		0.175		%
Avg. power	−22	−20	−19	dBm
Peak power	4	5	6	dBm
Power EIRP			20	dBm
S/N	30	32	34	dB

A block diagram of a sensor is shown in Fig. 1. The complete range up to 20 m can be scanned by setting the adjustable delay for the transmit pulses used for the mixer. The reflected and received pulses are mixed down with the

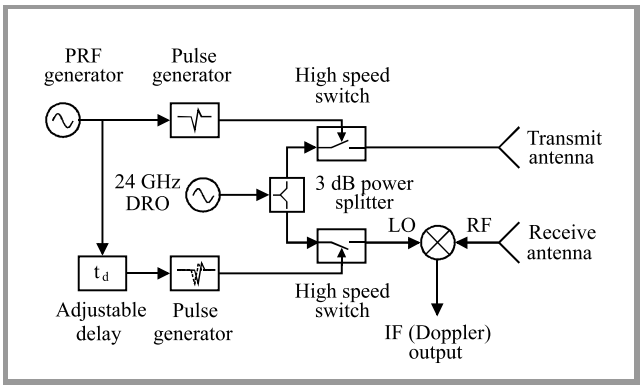

Fig. 1. Sensor block diagram. Explanations: IF – intermediate frequency, LO – local oscillator, PRF – pulse repetition frequency (in this case 4 MHz), RF – radio frequency, t_d – delay time, DRO – dielectric resonator oscillator.

delayed transmit pulses. The sensor output is an analog IF-output signal.
Reflecting targets in the sensor's field of view result in amplitude peaks of integrated pulses energy in the sensor IF-output signal. The corresponding amplitude depends on the target's radar cross-section and on the signal phase. The sensor IF-output signal is processed using conventional envelope detection methods. For signal baseline adaptation a special filtering is used. The signal difference between IF-output and estimated baseline is then applied to a CFAR threshold calculation algorithm taking the signal noise into consideration. The noise-adaptive threshold is used for the envelope detection. Range information of all detected targets is then sent to the radar decision unit for the following data fusion and azimuth angle estimation.

3. Radar network architecture

An experimental car fully equipped for adaptive cruise control usage [2] has been used for tests and to obtain realistic data. The front bumper of the vehicle is equipped with a short range radar sensor network consisting of four sensors with separate control units and a central processor for the data fusion as shown in Fig. 2.

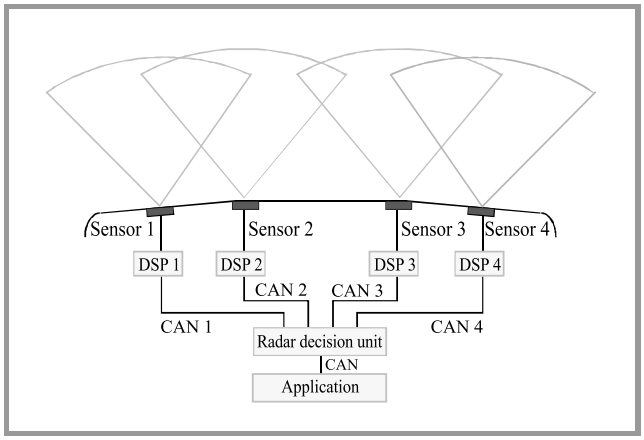

Fig. 2. System architecture overview. Explanations: CAN – controller area network (a serial automotive bus), DSP – digital signal processor.

The sensor IF-output signals are processed separately in the DSP control units and four target lists are sent to the central processor (radar decision unit) via CAN bus. Each single sensor measures the target range only. The data fusion is performed in the radar decision unit. Output of this central processor is an object map including distance information for all detected objects as well as an estimated relative velocity and the angular positions of the objects in azimuth.
For the object map update rates of 20 ms are achieved so far which is planned to be reduced in future. The object maps are finally used by further vehicle applications e.g. for activating the vehicle brakes.

4. Data fusion overview

The radar decision unit uses single sensor range information for angle estimation of the detected objects and for estimation of relative velocities of all detected objects in the sensor's field of view. The processing steps performed in the radar decision unit are shown in Fig. 3.

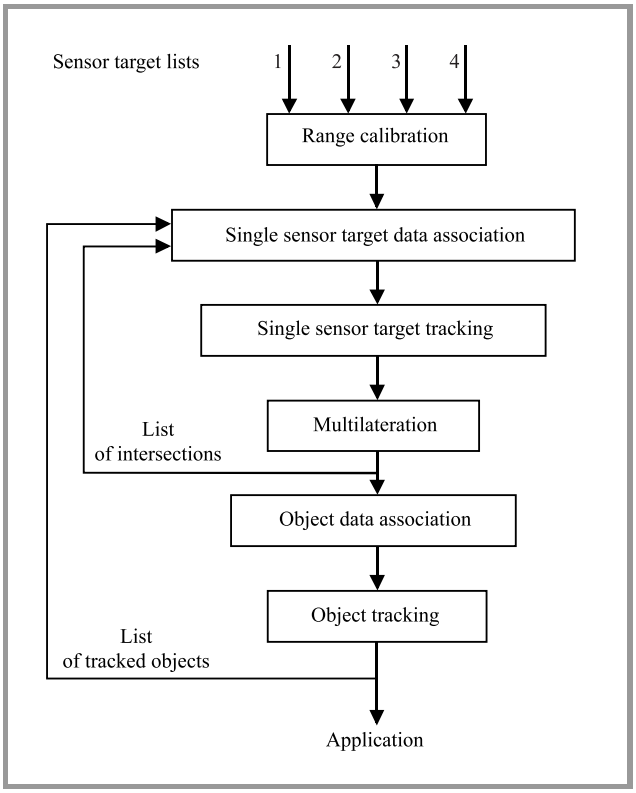

Fig. 3. Data fusion overview.

The transmitted sensor target lists are first corrected concerning their range information. Due to the fact that the distances between the sensors within a vehicle bumper are very small, a very precise range measurement is of great importance for very accurate angle estimation. A measured distance precision of approximately ± 3 cm in a complete measurement range of up to 20 m is necessary to achieve precise angle estimation results.
The data fusion is separated into more than one tracking step. First a single sensor target data association finds the correct sensor target tracks for the targets detected in the last cycle for each sensor separately. The single sensor target tracker tracks the targets in order to close detection gaps caused by limited probability of detection. A radial velocity for each tracked single sensor target can be estimated with very high precision because of the sensor's very precise distance measurements. This is done by conventional α-β-tracking filter techniques.
Due to the fact that the sensor shown in Fig. 1 has only a single channel IF-output, the signal amplitude even of reflectors with high radar cross-sections can be very tiny depending on the signal phase and in some cycles the target might not be detected. That explains the importance of the single sensor tracker.

The sensor tracks are applied to least-squares estimation techniques to really make usage of the redundancy in the system to minimise the errors of estimated range and angle information in the multilateration step. The resulting distance error for the detected and measured object is less than the error of a single sensor distance measurement due to the least-squares estimation. The output information of the multilateration step is a list of intersections for all detected objects. This is an update of the position information for all objects including distance and angle. These intersections are associated to object tracks in the next step and then tracked by the object tracker.

The resulting output of the complete data fusion is a list of tracked objects. For all objects distance, angle and estimated velocity are calculated and delivered to the specific application like the ACC distance control algorithms.

The feedback of all obtained information within the data fusion process showed to be very important for all data association steps. The list of intersections and the list of the resulting tracked objects are used for data association in the single sensor tracker as shown in Fig. 3.

In parallel to the described processing using least-squares methods for position calculation, Kalman-tracking filters were implemented and first simulated. Similar results can be achieved with Kalman-filters with the difference that the Kalman-filter comprises the steps of multilateration and object tracking in Fig. 3 within a single optimal filter algorithm. This makes the Kalman-filter the more elegant way of filtering with finding a precise position solution for the detected objects in parallel. The Kalman-filter was processed in a serial structure in this case. For the current system the least-squares method was preferred, but further optimisations will surely include a Kalman-filter.

5. Experimental results

The experimental system integrated in an experimental car is shown in Fig. 4. The sensors can be covered by an additional radome in the shown bumper or mounted directly behind a normal vehicle bumper. This makes the complete radar system invisible compared with an ultrasonic system, an interesting feature for design aspects. Different traffic situations were tested with this system.

Fig. 4. Experimental vehicle equipped with a short range radar sensor network.

Until now the considered traffic scenarios included many parking aid situations to achieve good performance in a less critical application. But also stop & go tests e.g. the passing of parked cars or the following of other cars were performed successfully. The system shows good performance to support a long range radar in stop & go and cut-in situations. Blind spot surveillance only needs presence detection with precise distance measurement which can be done very well with a single sensor.

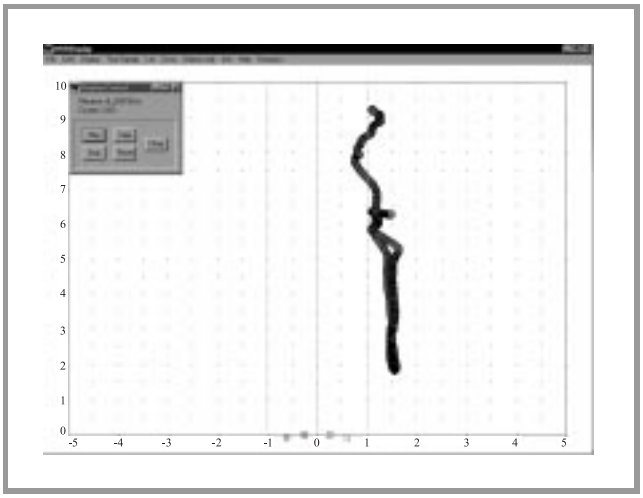

Fig. 5. Object trajectory when approaching and receding a street lamp post.

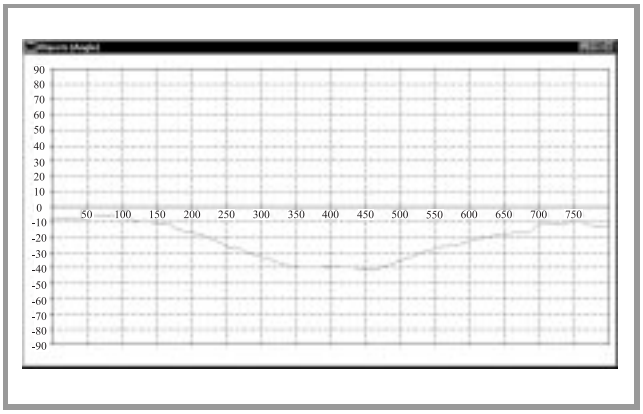

Fig. 6. Estimated angle for the last 800 cycles (16 s).

Figure 5 shows a recorded situation in an *x*-*y*-plot where the experimental car approached and receded a lamp post (10 cm diameter) on the right side of the road. The driving lane is indicated with two straight lines at ± 1 m from the vehicle center line. The maximum distance shown is 10 m. The calculated trajectory of the object during the complete

measurement is shown. An estimated angle of the object in this situation can be seen in Fig. 6. The angular range in this measurement is between approximately 5° up to 40°. Precision of the estimated angle is high in short distances where all sensors detect the object and redundancy maximises the accuracy. Additionally no false alarms can be observed in the data fusion output during the whole measurement (Figs. 5 and 6).

6. Conclusion

It was shown that new radar technology in conjunction with modern digital hardware are well suited for interesting automotive applications meeting the key product parameters like performance, size, price and high update rates. Beyond already introduced ACC radar systems, additional applications can be covered with a multifunctional short range radar network in vehicles. This article shows an interesting sensor concept which can be used for such a system. An experimental vehicle is equipped with such a sensor network to get experiences with measurements in realistic street situations. The system architecture was described and an overview of the signal processing steps was presented. Especially the data fusion part comprises very important parts of the complete processing to achieve high accuracy with this system. Convincing results from realistic street traffic situations confirm the feasibility of the complete system and are encouraging for further research activities.

References

[1] M. Klotz and H. Rohling, "A high range resolution radar system network for parking aid applications", in *5th Int. Conf. Radar Syst.*, Brest, France, May 1999.

[2] H. Rohling, M.-M. Meinecke, M. Klotz, and R. Mende, "Experiences with an experimental car controlled by a 77 GHz radar sensor", in *Int. Radar Symp.*, Munich, Germany, Sept. 1998, vol. 1, pp. 345–354.

[3] W. Weidmann and D. Steinbuch, "A high resolution radar for short range automotive applications", in *28th Eur. Microw. Conf.*, Amsterdam, Netherlands, 1998, pp. 590–594.

Michael Klotz received the Diplom-Ingenieur degree in electrical engineering in 1996 from the Technical University of Braunschweig, Germany. Since 1997 he is working on sensor fusion, radar signal processing, automotive radar system development, radar tracking algorithms for different automotive applications. The work includes theoretical analysis and also direct practical implementation. After two years at the Technical University of Braunschweig he continues his research since 1999 at the Technical University of Hamburg-Harburg working on a Ph.D. thesis.
e-mail: klotz@tu-harburg.de
Department of Telecommunications
Technical University of Hamburg-Harburg
Eißendorfer Straße 40
D-21073 Hamburg, Germany

Hermann Rohling received the Diplom-Mathematiker degree from the Technical University of Stuttgart in 1977 and the Ph.D. degree from the TU Aachen, Faculty of Electrical Engineering in 1984. Prof. Rohling is currently with the Department of Telecommunications, TU Hamburg- Harburg. His research interests are in radar, mobile communications, wireless local loops, multicarrier digital transmission techniques, multiple access techniques, detection, estimation, signal theory and DGPS for high precision navigation. He is a member of the german societies ITG and DGON.
e-mail: rohling@tu-harburg.de
Department of Telecommunications
Technical University of Hamburg-Harburg
Eißendorfer Straße 40
D-21073 Hamburg, Germany

Paper

Generalized radar/radiometry imaging problems

Ivan Prudyus, Sviatoslav Voloshynovskiy, Andriy Synyavskyy,
Taras Holotyak, and Leonid Lazko

Abstract — In the paper the results of spatio-temporal imaging simulation based on radar, synthetic aperture radar (SAR) and radiometry systems are presented. The analytical relationship between object scattering/emitting and the formed image is given and the general approach for the description of imaging system by means of Frendholm equation solution is developed. The potential limit of image resolution based on Rao-Cramer inequality is estimated.

Keywords — radiometry systems, synthetic aperture radar, spatio-temporal imaging.

1. Introduction

Resolution of radar and radiometry imaging systems is always constrained because of their finite spatio-temporal bandwidth that is determined by the constructive and technological particularities. That causes the decrease of received image quality. Advances in modern image and signal processing techniques open the new possibilities of real time image processing. Thus, the problem of adequate simulation of image formation for the development of optimal algorithms of resolution increasing and obtained image quality improving is very actual.

In this paper three main classes of imaging systems (monostatic radar, SAR and radiometer) are considered [1]. The distortions caused by imaging systems are determined as the analytical relation between scattering/emitting object's ability and the obtained image. Scattering $Q(x, y)$ is a local object characteristic that is described by relation between incident and reflected waves. Emitting $Q_p(x, y)$ property is defined by radiating particularities of investigated object.

2. Radar image formation

In radar imaging systems the range portrait is formed based on the delayed scattered signal from the different object's parts [2, 3]. This enable to obtain one-dimensional object presentation during one radiation period. In this case, the delay determinates coordinates of scattering area, signal magnitude permits to estimate scattering coefficient and antenna directional pattern has to satisfy the condition of uniform object radiation and reflected-signal receiving (Fig. 1). This principle is widely used for two-dimensional radar imaging [2 – 6], where resolution in second coordinate is satisfied by scanning with narrow antenna directional pattern.

Developed model of radar imaging system was created under assumption about flat surface of investigated objects, isotropic scattering property of the object's elements, and absence of secondary reflection:

$$s_{echo}(t) = \int_0^{T_{rad}} Q\left[\sqrt{c^2(t-\tau)^2 - H^2}\right] s_{rad}(\tau) \cdot \frac{c^2(t-\tau)\,d\tau}{\sqrt{c^2(t-\tau)^2 - H^2}}, \tag{1}$$

where $s_{rad}(t)$ is the radiated signal; T_{rad} denotes the radiated signal duration; c is the wave propagation velocity; H is the altitude of radar position.

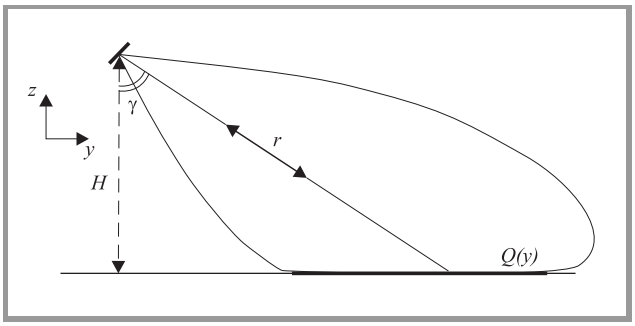

Fig. 1. The geometry of radiation at the range portrait formation by radar system.

Temporal function of received signal $s_{echo}(t)$ transformed into corresponding spatial coordinate system is a range portrait $I(Y)$ and Eq. (1) can be rewritten as:

$$I(Y) = \int_{y_{\min}}^{y_{\max}} Q(y)\, G_d[y, Y]\, dy, \tag{2}$$

where $G_d[y, Y]$ denotes the transform kernel Eq. (2) or system function determined by radiated signal; $(y_{\max}, y_{\min})$ is interval of scattering property investigating $Q(y)\, G_d[y, Y]$ describes the temporal distortion features. In the case of $G_d(t, \tau) = s_{rad}(t - \tau)$, Eq. (2) will be presented by a convolution, and distortion will be invariant in respect to the range coordinate.

3. Radar imaging system with synthetic aperture

To satisfy high quality of remote sensing, multiposition radar systems with coherent processing, i.e. SAR are widely

used, that permits to significantly improve cross-range resolution [4, 5]. Oppositely to ordinary radar, the formation of synthesized directional pattern is performed by corresponding spatio-temporal processing (Fig. 2). In each discrete position with step Δx the signal $s_{rad}(t)$ is radiated and echo-signal is received. Taking into account spatial filtering properties of the transmitting and receiving antennas, echo-signal $s_{rec}(t)$ can be presented according to Eq. (1). One of the particularities of these systems is Doppler frequency shift effect that depends on the wave propagation direction.

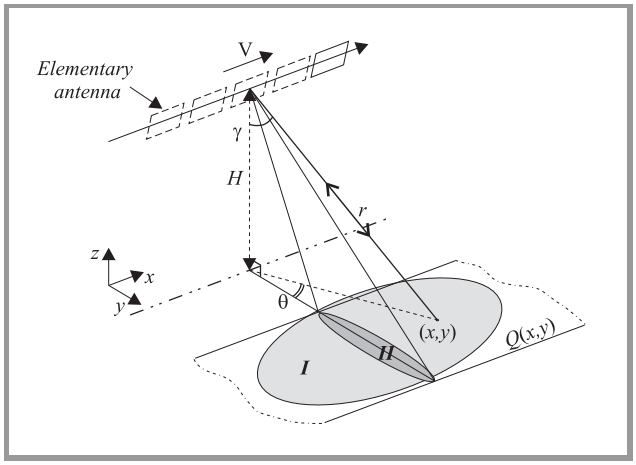

Fig. 2. Aperture synthesizing in radar imaging systems. Explanations: *I* – elementary antenna pattern, *II* – synthetic aperture pattern.

Synthesis process consists in the coherent summing of the received signals

$$U^i(y) = \sum_{k=-L}^{L} C_k s_{rec}^{i+k}\left(\frac{2\sqrt{y^2+H^2}}{c}\right), \qquad (3)$$

where $U^i(y)$ is the complex discrete-continuous SAR image. Complex coefficients C_j are equivalent to the current distributions in the synthetic aperture. Depending on the choice of C_j Eq. (3) gives a possibility to obtain different synthetic aperture directional patterns, to select the orientation direction of directional antenna pattern main lobe, to focus the synthetic aperture on the certain range. Model (3) does not permit to obtain the necessary resolution in the range coordinate and compensate the Doppler frequency shift that causes resolution decreasing.

The developed model was created under assumption of discrete system carrier moving with synthesizing step Δd. Taking into account Eqs. (1), (2) and (3) SAR model can be expressed as:

$$I(X,Y) = \int_{v_{\min}}^{v_{\max}} \int_{y_{\min}}^{y_{\max}} Q\Big((v-X),y\Big)\, G_{sar}[v,y,Y]\, dydv, \qquad (4)$$

where transformation kernel $G_{sar}[v,y,Y]$ is being defined SAR carrier altitude H, its velocity V, synthesizing step Δd, as well as radar parameters: waveform of radiated signals $s_{rad}(t)$, its carrier frequency ω_0, complex coefficients of coherent processing C_k, directional properties of transmitting $F_{tran}(\gamma,\theta)$ and receiving $F_{rec}(\gamma,\theta)$ antenna directional patterns, and described by the following equation:

$$G_{sar}[v,y,Y] = c^2 \cdot \sum_{k=-M}^{M} C_k F_{tran}[\gamma,\theta]\cdot F_{rec}[\gamma,\theta] \times$$
$$\times \frac{D^2+H^2}{T}\cdot s_{rad}\left(\frac{2Y}{c}-\frac{\sqrt{D^2+H^2}}{c}\right)\exp\left\{\frac{-j2\omega_0\sqrt{D^2-y^2}\,V}{c^2\sqrt{D^2+H^2}}\times\right.$$
$$\left.\times\left(2Y-\sqrt{D^2+H^2}\right)\right\}, \qquad (5)$$

where $\theta = \left(\operatorname{arctg}\left(\frac{\sqrt{D^2-y^2}}{y}\right)\right)$, $\gamma = \left(\arccos\left(\frac{H}{\sqrt{D^2+H^2}}\right)\right)$ and $D = \sqrt{(v+k\Delta d)^2+y^2}$.

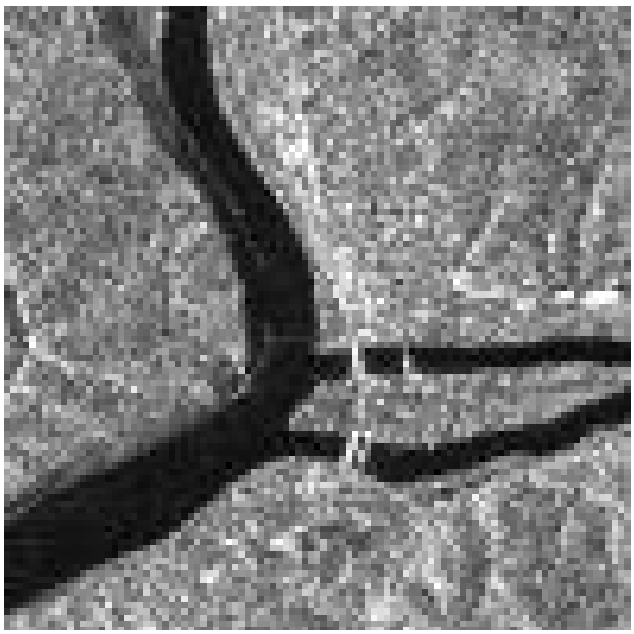

Fig. 3. Tested scattering ability $Q(x,y)$.

In alternative to SAR models based on Radom transform [6] model (4) does not need the coordinate transformation, that permits to simplify the processing algorithms. To show the particularities of the above mentioned model the test image presented in Fig. 3 was chosen. The simulation was performed for Gaussian radiated signal and uniform field distribution in the elementary transmitting and receiving antennas and different kinds of coherent signal processing methods (Fig. 4). Obtained results confirm possibility to form the narrow directional pattern of synthesized aperture by means of coherent summation with quadratic phase and time delay compensation. Kernel (5) shows that SAR distorting impact is invariant to x, and non-invariant to y that is explained by different nature of image formation in these coordinates.

a)

b)

c)

Fig. 4. Obtained SAR image $I(X,Y)$ with 5 elements (a), with 100 elements and without quadratic phase delay compensation (b), with 100 elements and corresponding quadratic phase delay compensation (c).

4. Radiometry imaging systems

In radiometry systems image formation process is being performed by two-dimensional scanning [7, 8]. Radiometry receiver is energy device, thus, the received image characterizes energetic properties of the studied object emission. This class of systems can be described by following model:

$$I(X,Y)=\int_{\vartheta_{\min}}^{\vartheta_{\max}}\int_{\eta_{\min}}^{\eta_{\max}} Q_p(\eta,\vartheta)\cdot G_{pasiv}[X-\eta,Y-\vartheta]\,d\eta\,d\vartheta\,, \tag{6}$$

where $(\eta_{\max},\eta_{\min},\vartheta_{\max},\vartheta_{\min})$ denotes the scanning region; $G_{pasiv}[X-\eta,Y-\vartheta]$ is transformation kernel and depends on field distribution in aperture $e(x,y)$:

$$G_{pasiv}[\eta,\vartheta]=\left|\Im\{e(x,y)\}\right|^2, \tag{7}$$

where $\Im\{e(x,y)\}$ denotes two-dimensional Fourier transform.

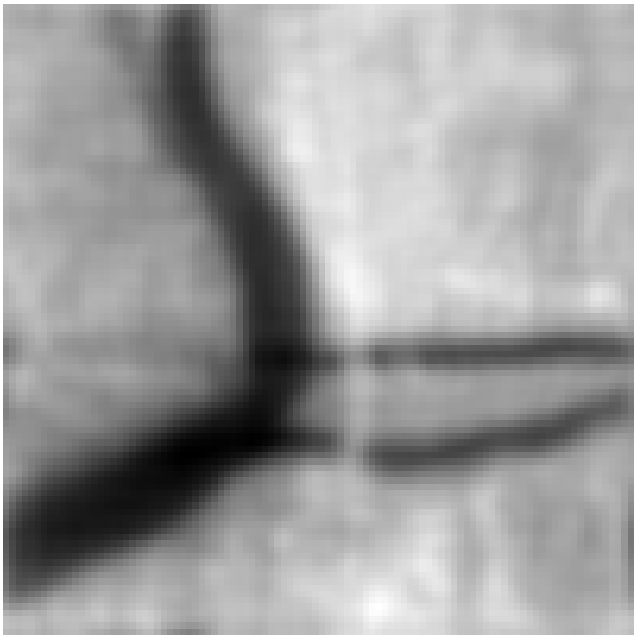

Fig. 5. Radiometry image $I(X,Y)$ obtained on the base of the model (7).

Image formed by radiometry systems according to Eq. (6) is presented in Fig. 5. The distortions caused by radiometry imaging systems have spatially invariant character and are determined by the form of a system function. The significant losses in high spatial frequency band cause typical blurring of the obtained image.

5. Generalized linear imaging model

The presented above models of the image formation systems Eqs. (2), (4) and (6) are deterministic ones. However, the

real systems usually are under impact of many stochastic factors, such as received noise, error of imaging system geometrical parameters estimation, system parameters errors (radiated signal and direction pattern forms). The complicated stochastic nature of these parameters do not allow to obtain precise statistic model of radar/radiometry imaging systems. Taking into account large number of stochastic parameters and the linearity of image formation models the additive Gaussian component can be assumed due to central limit theorem assumption. In this case the generalized model of radar/radiometry imaging systems is described by the following expression:

$$I(X,Y) = \int_{x_{\min}}^{x_{\max}} \int_{y_{\min}}^{y_{\max}} Q(x,y) \cdot G[x,X,y,Y]\, dydx + n(X,Y), \tag{8}$$

where $G[x,X,y,Y]$ is the point spread function, and n is the additive Gaussian component.

Based on the presented models, the synthesis of image processing algorithms is possible and quality improving can be formulated based on the inverse solution of first kind Frendholm equation. Correctness and robustness issues of this problem solution will be determined by kernel form [9], type of systems and their parameters that have also impact on the noise statistics.

This approach gives possibility to reduce blurring impact of point spread function and remove the noise component. The synthesized based on this approach SAR image processing algorithms permit automatically to compensate the quadratic phase distortions and moving of SAR carrier.

6. Potential limit of restoration accuracy. Restoration methods

A lot of methods of Frendholm integral equation solution are known [9 – 14]. Deterministic methods based on prior information are given in [3]. Selection of solution methods is being performed according to the type of integral equation kernel or structure and size of equation system matrix. Singular operators are characterized by nonstability of solution to calculation errors, imprecission of initial data or stochastic component existing in right part of equation.

Radar and radiometry image restoration (8) are often performed under significant noise impact. Stochastic character of the radar image formation shows necessity to use stochastic methods of problem (8) solution. These methods give possibility not only to find stochastically correct solution, but also to estimate potential solution limit.

Problem (8) can be presented by system of linear equations:

$$X = GA + n, \tag{9}$$

where G is $M \times M$ matrix with $g_{i,j}$ elements; X and A are obtained and original image respectively; n is random vector with Gaussian distribution $N(0, \sigma_n^2)$. Each element x_i of vector X can be presented by linear combination of unknown parameters a_j. In the case of prior information about distribution law of a_j absence, Eq. (9) can be solved by maximum likelihood (ML) principle [15]. Element x_i has the Gaussian distribution with mean $\sum_{j=1}^{M} g_{i,j} \cdot a_j$ and variance σ_n^2. Then taking into account statistical independence of x_i, likelihood function can be written as:

$$p(X|A) = \prod_{i=1}^{M} p(x_i \mid A) =$$
$$= \frac{1}{\left(\sqrt{2\pi\sigma_n^2}\right)^M} \exp\left\{ -\sum_{i=1}^{M} \left[\left(x_i - \sum_{j=1}^{M} g_{i,j} a_j \right)^* \times \right.\right.$$
$$\left.\left. \times \left(2\sigma_n^2\right)^{-1} \left(x_i - \sum_{j=1}^{M} g_{i,j} a_j \right) \right] \right\}. \tag{10}$$

Solving Eq. (9) by means of ML function corresponds to solving of equations' system $G^T X = G^T G A$ that coincides with the least squares approach [9]. Potential accuracy of Eq. (9) solution can be found from Rao-Cramer inequality [15]. From Eqs. (10) and (11) the accuracy of unknown parameter a_j based on ML principle is calculated as its estimation variance:

$$E\left[\hat{a}_{i_{ml}} - a_i\right]^2 \geq \left(-E\left[\frac{\partial^2 \ln\left(p(X \mid A)\right)}{\partial a_i \partial a_i} \right] \right)^{-1} =$$
$$= \sigma_n^2 \left(\sum_{l=1}^{M} |g_{l,i}|^2 \right)^{-1}, \qquad i = \overline{1, M}. \tag{11}$$

The found accuracy is the same for all unknown parameters and defined by the relation between random component variance and sum of squared column's elements of matrix G. Inequality (11) gives possibility to estimate potential accuracy of the radar/radiometry image restoration. Precision of the restoration without prior information is equal to the relation of noise variance to the squared norm of point spread function. In the case of spatially variant linear operators, e.g. Eqs. (2) or (4), point spread function changes its form in dependence on the image coordinates, therefore, accuracy will be defined by different relationship.

7. Conclusions

The results of radar and radiometry imaging systems analysis show possibility to describe these system by the linear model. The analytical form of operator transforms for efficient image formation simulation is determined for the classical types of these systems. Blurring of radar and radiometry images is caused by the finite spatio-temporal bandwidth. Nonoptimality of the coherent processing in SAR also decreases image quality. Based on the developed models the approach to radar and radiometry image quality improving that consists in the image processing by means of restoration methods synthesized by the mentioned models is generalized. The potential limit of image restoration accuracy under Gaussian noise impact is determined.

Variance of image estimation is proportional to the noise energy and inversely proportional to the squared norm of point spread function, that permits to make some recommendations about wave form type and antenna parameters. According to the developed model of radar range portrait formation the point spread function corresponds to radiated signal form that points out on the possibility of signal with large base usage [16]. This kind of signals has high energy because of large duration and wide band because of the complicated modulation. Spatial properties of the imaging systems are defined by antenna parameters and directly depended on the aperture magnitude-phase distribution. Thus, usage of complicated distributions permits to satisfy the robustness of image restoration algorithms to noise level and to obtain high accuracy.

References

[1] M. I. Skolnik, *Spravočnik po Radiolokacii*. Vol. 4. Sov. Radio, 1978 (transl. Engl).

[2] V. Guglielmi, F. Castanie, and P. Piau, "Application de methodes super-resolvantes au traitement des donnees d'un radar a synthese d'ouverture", in *Proc. 5 Int. Conf. GRETSI'95*, Juan-Les-Pins, France, 1995, pp. 1097–1100.

[3] Je. I. Klepfer, I. N. Prudyus, A. T. Synyavskyy, and L. V. Lazko, "Vikoristannja nelinijnich obmežen' v iteracijnich metodach vidnovlennja radiolokacijnich signaliv", *Radiotechnika ta Telekomunikacii: Visnik DU "LP"*, no. 387, pp. 36–45, 2000.

[4] I. N. Prudyus, A. T. Synyavskyy, and V. P. Ostap, "Simulation of spatial-temporal signal processing in imaging systems with synthetic aperture", in *Proc. 3rd Int. Conf. Anten. Theory Techn. (MKTTA'99)*, Sevastopol, Ukraine, 1999, pp. 233–236.

[5] I. N. Prudyus, A. T. Synyavskyy, and V. P. Ostap, "Modeljuvannja procesu formuvannja radiolokacijnich zobražen' v sistemach z sintezovanoju aperturoju", in *Proc. Int. Conf. MME'99*, Lvov, Ukraine, 1999, pp. 221–222.

[6] M. Lindberg, "Radar image processing with the radon transform". Technical reports. European Consortium for Mathematics in Industry. Programme in applied mathematics, no. 5, 1997.

[7] I. N. Prudyus, Z. D. Grytskiv, and S. V. Voloshynovskiy, "Radiometry image processing based on nonlinear iterative methods", in *Proc. Workshop Des. Methodol. Signal Proc.*, Zakopane, Poland, Aug. 1996, pp. 21–27.

[8] I. N. Prudyus, S. V. Voloshynovskiy, and T. S. Holotyak, "Investigation of spatial antenna system characteristics in active and passive imaging systems", in *Proc. Int. Conf. (TCSET'2000)*, Lvov-Slavsko, Ukraine, 2000, pp. 124–125.

[9] A. N. Tichonov and V. Ja. Arsenin, *Metody Rešenija Nekorrektnych Zadač*. Nauka, 1979.

[10] G. I. Vasilenko and A. M. Tatarinov, *Vosstanovlenie Izobraženij*. Radio i Swjaz', 1986.

[11] M. Kilmer and D. P. O'Leary, "Choosing regularization parameters in iterative methods for ill-posed problems". Technical reports CCR 95-03126, CCR 97-32022, University of Maryland, Dept. of Computer Science, College Park, MA, 1997.

[12] J.-L. Starck, F. Murtagh, and A. Bijaoui, "Multiresolution support applied to image filtering and restoration", *Comp. Vis., Graph. Image Proc.*, no. 34, pp. 234–250, 1996.

[13] M. Nielsen, L. Florack, and R. Deriche, "Regularization and scale space". Rapport de recherche, Institut national de recherche en informatique et en automatique; no. 2352, programe 4 (Robotique, image et vision), Sophia-Antipolis, France, 1994.

[14] J. G. Nagy and D. P. O'Leary, "Fast iterative image restoration with a spatially-varying PSF", *SIAM J. Sci. Comput.*, no. 2, pp. 474–489, 1997.

[15] G. Van Tris, *Teorija Obnaruženija, Ocenok i Modulacii*. Sov. Radio, 1972.

[16] I. N. Prudyus, M. M. Sumyk, and A. T. Synyavskyy, "Stability of matched filtering of polyphase signals to Doppler shift", in *Proc. Reg. Conf. Milit. Commun. Inforam. Syst. (RCMCIS'99)*, Zegrze, Poland, Oct. 1999, pp. 104–109.

Ivan Prudyus received the Ph.D. degree in radio engineering from Kaunass Polytechnic Institute in 1980. From 1981 he has worked as Associate Professor at Radio Devices Department of Radio Engineering Faculty, Lvov Polytechnic Institute, and from 1991 he is a Dean of Radio Engineering Faculty, Lvov Polytechnic National University, Lvov, Ukraine. His research interests include antenna and VHF technique, signal processing, systems of recognition and control, receive information systems. He is Lecturer of theory of antennas and VHF devices, telecommunication devices, electromagnetic compatibility.
iprudyus@polynet.lviv.ua
Radio Engineering Faculty
Lvov Polytechnic National University
S. Bandery st 12
Lvov, 79013, Ukraine

Sviatoslav Voloshynovskiy received the Ph.D. degree in radio engineering from Lvov Polytechnical National University in 1996. From 2000 he is an Associated Professor of Department of Radio Electronic Devices and Systems at Lvov Polytechnic National University, Lvov. Also, he is an Assistant Professor of Computer Science Department, University of Geneva, Switzerland. His research interests include radar and radiometry imaging system, antenna design, adaptive image restoration, image enhancement, image compression, and inverse problems.
svolos@cui.unige.ch
CUI, University of Geneva
24 Genral Dufour
4 Geneva 1211, Switzerland

Andriy Synyavskyy was born in Lvov, Ukraine in 1974. He received the radio-engineering diploma and M.Sc. degree from Lvov Polytechnic National University in 1996 and 1997, respectively. After postgraduate courses he joined the Lvov Polytechnic National University on Radio Engineering Faculty in 2000, where is currently working as Junior Scientist above the research projects in the areas of signal/image processing and toward the Ph.D. degree in television- and radio-engineering. His research interests include the description, modeling and characterization of high-resolution radar imaging processes, deterministic and stochastic investigation of microwave scattering as well as creation of radar signals processing methods.
sinat@polynet.lviv.ua
Lvov Polytechnic National University
S. Bandery st 12
Lvov, 79013, Ukraine

Taras Holotyak received the M.Sc. and Ph.D. degrees from Lvov Polytechnic National University in 1997 and 2001, respectively, all in radio engineering. In 2001 he joined the Department of Radio Electronic Devices and Systems at Lvov Polytechnic National University, Lvov, Ukraine, where he is now an Assistant Professor. His research interests are in remote sensing, digital image processing, and computer vision, focusing on radiometry image formation, nonlinear adaptive image restoration, and human visual systems models.
taras@polynet.lviv.ua
Lvov Polytechnic National University
S. Bandery st 12
Lvov, 79013, Ukraine

Leonid Lazko was born in 1975 in Kremenets. From 1992 till 1997 he studied in Lvov Politechnic National University. He received the eng. degree in radio engineering from Lvov Polytechnic National University, Ukraine, in 1997. Currently he is on postdoctoral studying and works toward the Ph.D. degree. His research interests include digital image processing, radar imaging, antenna array, regularization of ill-posed problems, spectrum exstrapolation technique.
Lvov Polytechnic National University
S. Bandery st 12
Lvov, 79013, Ukraine

Paper

A dedicated computer system for FM-CW radar applications

Silvester H. Heijnen, Jaques S. van Sinttruijen, Fred W. van der Zwan, and Leo P. Ligthart

Abstract — In this paper, a DSP based computer system for FM-CW radar applications is described. Besides data acquisition and storage, the computer system will also be used for front-end data processing and system control. Processing includes filtering and clutter suppression. The radar for which the computer is designed is a multi parameter atmospheric profiler capable of doing Doppler and polarimetric measurements. The computer system will allow for a measurement of the full polarimetric scattering matrix over 512 range cells and 512 Doppler cells in 2 s. Radar system control includes the timing and the settings of the radar system together with linearity correction of the sweep oscillator.

Keywords — radar, data processing, system control, filtering and clutter suppression.

1. Introduction

At the International Research Centre for Telecommunications-transmission and Radar (IRCTR, a department of the Delft University of Technology in the Netherlands) a new transportable atmospheric radar system (TARA) [1], is under construction. The main area of application of the system will be in the field of atmospheric remote sensing. Transportability will allow for studies of the atmosphere at different geographical location, but imposes severe constrains on the construction of the system. Being a research tool, the system has to be as flexible as possible to adapt the system to the measurement conditions. Therefore, the FM-CW principle is used allowing for easy changes in system settings. FM-CW also has the advantage of low peak power allowing for an all solid-state design. A consequence is the need for two antennas to isolate the transmitter from the receiver. In atmospheric remote sensing the targets usually have a low radar cross-section. On the other hand obstacles like trees and buildings have a high radar cross-section giving rise to large clutter contributions. One way to reduce clutter contributions is to reduce the antenna sidelobes in the direction of the obstacles. Clutter can also be removed in the Doppler domain as it has a low to zero Doppler velocity. The transmit frequency is chosen to be 3.3 GHz allowing for studies of clear-air turbulence as well as studies of clouds and rain. The bandwidth of the system can be changed between 2 and 50 MHz. The TARA system has Doppler and polarisation capability. For 3D wind field measurements, off-axis beams are available in two orthogonal directions. In Table 1 a summary of the system specifications is given. A technical drawing can be found in Fig. 1. Clearly visible is the dual antenna system with large shields. The shields will reduce the far sidelobes of the antennas. TARA is constructed in a twelve-meter long standard container. The front part of the container is used as measurement chamber. During the construction phase, new developments were found in the field of antenna research and real-time data processing.

In a FM-CW system, range dependent reflectivity information is contained in the frequency spectrum of the beat signal, which is generated by comparing the received signal with the transmitted signal using a mixer. Doppler information is contained in the reflective phase differences between successive measurements of the same target. Multiple Fourier transforms are used to retrieve information from the raw data. The computer system described in this paper is capable of doing these multiple Fourier transforms in real-time. The other functionality of the computer system is radar-system control. This includes beam switching and polarisation switching but also linearisation of the frequency sweep. It will be shown that in a FM-CW system, nonlinearities of the frequency sweep will limit the achievable resolution. The linearisation scheme used in the TARA system is discussed as well as the realised linearity.

2. Computer architecture

The primary function of the computer is the front-end data processing. As was explained before, processing involves multiple FFT's. They are implemented in hardware using the PDSP16510 from Plessey. This chip is capable of doing a 1024-point 16-bits complex FFT in 96 μs. DATA is digitised with a 16-bit 2-MHz ADC and stored into a local memory before down loading into the first FFT chip. The output of the FFT chip is loaded into the memory of a DSP that is used for correction of shifts occurring in the FFT process for each individual sweep. The information in the output data of the first FFT contains the reflectivity per range resolution cell. A total of 512 sweeps is stored and, subsequently, a second FFT is calculated now per range resolution cell. The output data of this second FFT contains the Doppler spectrum. Each Doppler spectrum is filtered and the clutter is suppressed. This is done in the Doppler domain by omitting the zero velocity Doppler resolution cell. After clutter suppression, the first three moments of the Doppler spectra, being the reflectivity, the averaged Doppler speed and the Doppler spectral width, are

Table 1
Specifications of the TARA system

Parameter	Value	Additional remarks
Type	FM-CW	
Central frequency	3.3 GHz	
Transmitted power	100 W	can be attenuated in 10 dB steps
Dynamic range	80 – 90 dB	
Noise figure	∼1 dB	
Sweep bandwidth	2 – 50 MHz	computer controlled
Sweep shape	triangular, saw tooth	can be arbitrarily
Sweep time	> 1 ms	can be staggered
Sampling	< 2 MHz	16-bits ADC
Samples per sweep*)	1024	
Sweeps per Doppler spectrum*)	512	
Polarisation (linear)	HH, HV, VH, VV	antennas controlled independently; central beam only; offset beams are single linearly polarised
Resolution aspects		
Max. range	38 km	@ 2 MHz bandwidth
Min. range resolution	3 m	@ 50 MHz bandwidth
Unambiguous Doppler speed	∼22.7 m/s	max. @ 1 ms sweep time
Doppler resolution	∼8.9 cm/s	@ 1 ms sweep time
Sensitivity*)	@ 5 km	@ 1 km
Reflectivity	$\leq 2.3 \cdot 10^{-14}$ m^{-1}	$\leq 0.9 \cdot 10^{-15}$ m^{-1}
Radar cross-section	$\leq 1.8 \cdot 10^{-8}$ m^2	$\leq 2.8 \cdot 10^{-11}$ m^2

*) SNR = 0 dB, resolution = 40 m

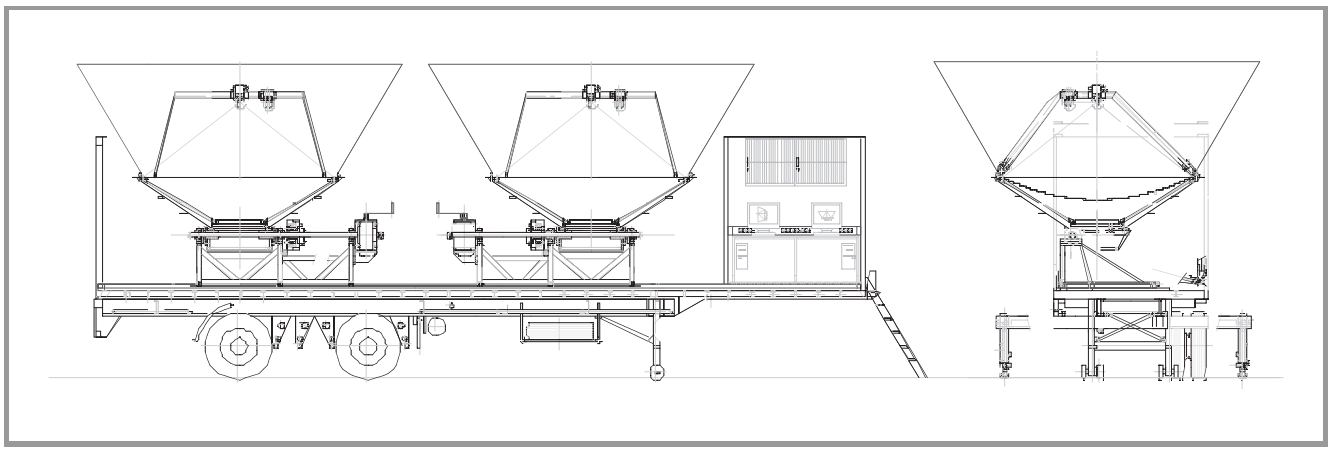

Fig. 1. Technical drawings of the TARA radar system. Clearly visible is the dual antenna system with large shields.

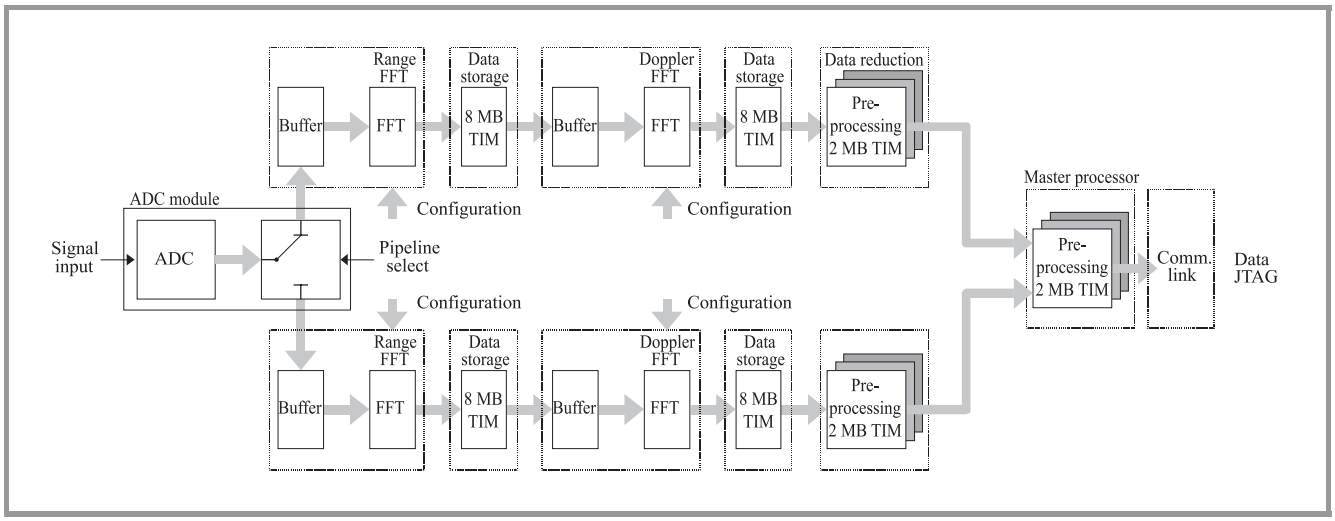

Fig. 2. Block diagram of the spectrum processor for the TARA system.

calculated. To remove noise contributions in the reflectivity, the Doppler spectra are clipped before the calculation of the moments is executed. All these calculations are done in a single DSP. After processing, data is transferred into a last DSP were data displaying and archiving is handled. The minimum sweep time in the system is 1 ms. To guarantee continuous data throughput, a dual pipeline architecture is used, see Fig. 2. A photograph of the system is shown in Fig. 3.

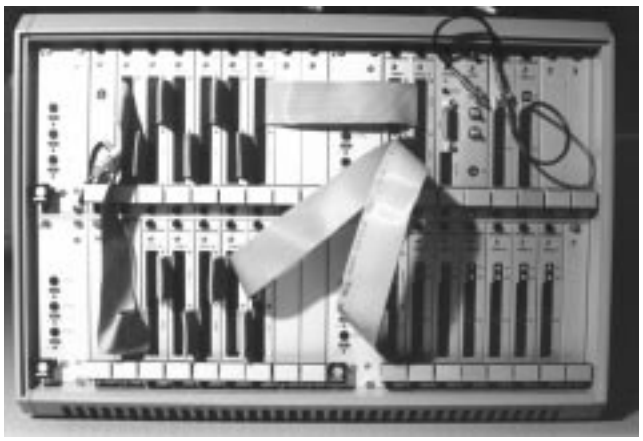

Fig. 3. Photograph of the computer system. The left upper quadrant contains the ADC and one pipeline of the spectrum processor. The second pipeline is placed in the left lower quadrant. The right upper quadrant contains the master processor and the linearisation module. The right lower quadrant contains the I/O modules for system control.

The second function of the computer system is control of the radar hardware. This includes, but is not limited to, polarisation and beam switching, bandwidth and frequency agility. All settings can be changed on a sweep to sweep base. Delayed sampling is used to allow the system to relax after switching such that stability during the measurements is guaranteed. This means that of a sweep of 1 ms only 875 μs are used for sampling.

System control also includes linearisation of the frequency sweep. In FM-CW systems, range resolution is on the one hand determined by the bandwidth of the system and on the other hand by frequency-sweep linearity. Nonlinearities will lead to spectral leakage and thus deteriorate the resolution. It can be shown that the nonlinearities should be limited to less than 0.05% of the bandwidth for the spectral leakage to remain within acceptable limits. In general, a VCO does not comply with this specification and the frequency curve has to be linearised.

Linearisation of the sweep can be done in several ways. In the TARA system it is done in a feed-forward way. This means that off-line the voltage depending frequency in the system is measured. This measurement is done in a sta-

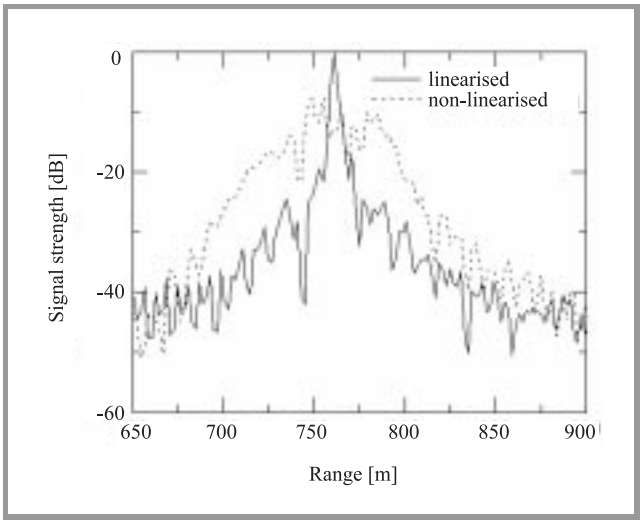

Fig. 4. Resolution of the TARA system with and without linearisation correction. Clearly visible is the dramatic improvement in resolution and the corresponding increase in signal strength.

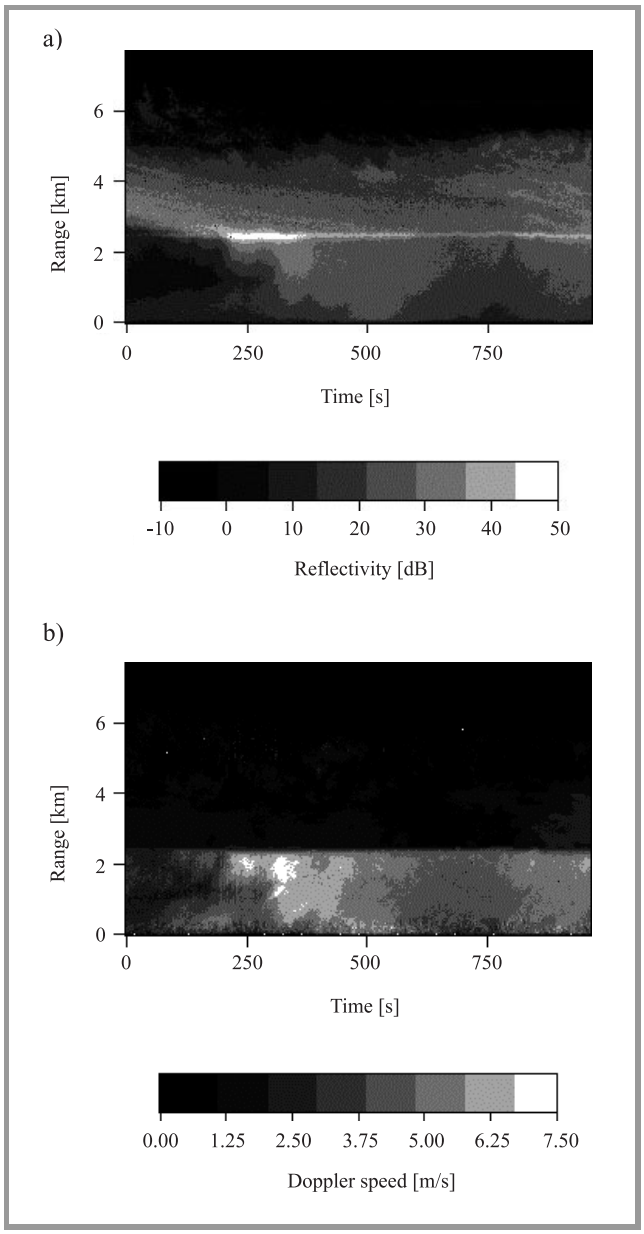

Fig. 5. Measurements with the TARA computer system: (a) the reflectivity and (b) the average Doppler speed. Sweep time: 1 ms, bandwidth: 15 MHz, 512 range cells and 512 Doppler cells. As the system is not calibrated, the reflectivity is given in dB.

tionary state. From the measured frequency characteristic, a correction table is calculated. Before starting measurements, a control signal for the VCO is calculated from the table and this is stored into a RAM-memory. During each sweep this memory is played back generating a linear frequency sweep. This set-up only works if two conditions are fulfilled. First, the VCO must be fast enough such that the sweep can be considered to be a sequence of stationary states. Second, the system must be stable and reproducible during very long times for the correction table to remain valid. To fulfil the first condition, a VCO is taken that can sweep over 200 MHz in less than 100 ns. As the sweep time for the TARA system is in all cases longer than 1 ms, while the bandwidth is less than 50 MHz, the first condition is met. To guarantee system stability, the VCO is temperature stabilised to within 1°C. In Fig. 4, the realised range spectrum is shown. For this measurement an internal delay line of 5 μs is used. The beat signal is Fourier transformed to give the reflected signal as a function of range. In the case of non linearisation correction, the delay line shows as a very broad peak extending over roughly 100 m in range. In the case the sweep is linearised, the delay line shows up as a very narrow peak within one resolution cell. This indicates linearity within the desired limits. As the spectral peak narrows, the signal strength increases. The correction table used for this measurement was more than two months old. New correction tables can easily be calculated every week or even more often making sure that linearity is not a limitation to the resolution.

3. Measurements

Although the TARA system is not yet fully operational, first measurements were done using an antenna set of a different radar system. These measurements were done during a day of light rain using a bandwidth of 15 MHz and a sweep time of 1 ms. The Doppler spectrum was calculated at 512 range cells using 512 sweeps. The first two moments of the spectrum, the reflectivity (un-calibrated) and the average Doppler speed (calibrated), are shown in Fig. 5. This typical example shows a sharp transition, the bright band or melting layer, at 2.5 km where the 0° isotherm is positioned. Above this melting layer the average Doppler speed is very low. Below this layer the velocities increase showing a downward movement towards the radar system. The quality of the measurement shows the real time possibility of the computer system and the validity of the linearisation scheme.

Acknowledgement

The work described in this article was done under financial support of the Dutch Technology Foundation “STW”. The authors wish to thank the people from Prodrive in Eindhoven, The Netherlands, for helping in developing and building the computer system.

References

[1] S. H. Heijnen and L. P. Ligthart, “TARA: development of a new transportable atmospheric radar”, in *5th Int. Conf. Radar Syst.*, Brest, France, May 1999.

Silvester Henri Heijnen was born in Geleen, the Netherlands, on July 15, 1964. He finished the University in 1983 with a degree in physics. His Ph.D. was done at a research institute for thermonuclear plasma physics research in Hol-

land and culminated in a thesis on the application of short-pulsed radar for measuring electron density profiles in thermonuclear plasmas. After this he worked for one year in the Forshungs Anlage in Jülich, Germany. In 1995, he joined the International Reseach Centre for Telecommunications-transmission and Radar, IRCTR, Delft University of Technology, the Netherlands, to work on the realisation of the Transportable Atmospheric Radar, TARA. Currently, he is working in the remote sensing group of IRCTR on the interpretation of TARA data.

S.H.Heijnen@irctr.tudelft.nl
IRCTR
Delft University of Technology
Mekelweg 4
2628 CD Delft, The Netherlands

Jaques S. van Sinttruijen
IRCTR
Delft University of Technology
Mekelweg 4
2628 CD Delft, The Netherlands

Fred W. van der Zwan
F.Zwan@irctr.tudelft.nl
IRCTR
Delft University of Technology
Mekelweg 4
2628 CD Delft, The Netherlands

Leo P. Ligthart – for biography, see this issue, p. 6.

Paper

The simple analysis method of nonlinear frequency distortions in FMCW radar

Krzysztof S. Kulpa, Andrzej Wojtkiewicz, Marek Nałęcz, and Jacek Misiurewicz

Abstract — The paper presents a simple method for estimating nonlinear frequency distortions of linear frequency modulated (LFM) signals used in FMCW radars. This method, derived from the polynomial model of the nonlinear FM signal phase, is based on finding the maximum of two-dimensional chirp-like transform of the IF video signal. The IF signal is obtained by mixing transmitted FM signal with its delayed copy. Using suggested transform we show that the presented method is able to detect and classify signal distortions.

Keywords — radar, nonlinear frequency distortions, linear frequency modulation.

1. Introduction

In many applications such as radars, sonars, biomedical engineering etc. the constant amplitude complex harmonic signals

$$s(t) = S_0 \exp(j\phi_M t) \tag{1}$$

with varying frequency are used. The signal phase $\phi_M(t)$ can be modeled by the M-th order polynomial

$$\phi_M(t) = \sum_{m=0}^{M} a_m t^m \tag{2}$$

with coefficients a_m. For example the chirp signal corresponds to the second order phase polynomial ($M = 2$) and so-called quadratic frequency modulated (FM) signal corresponds to the third order phase polynomial ($M = 3$). To estimate unknown parameters of frequency modulated (FM) signal, well-known time-frequency analysis, both linear (spectrogram, scalogram) and bilinear (such us Wigner-Ville distribution) are commonly used.

These tools are, however, inefficient for nonlinear frequency modulation. The recent works [6 – 8] on generalization of Wigner-Ville distribution are very useful for analyzing the signal (1) for $M > 2$ and for estimating instantaneous signal frequency $f(t) = \frac{1}{2\pi}\frac{d\phi_M(t)}{dt}$.

One of the most important practical problems is to estimate phase coefficients a_M of unknown signal contaminated by white Gaussian noise. Such estimation allows identification and classification of polynomial phase signals [2 – 4]. These methods, however, are not well suited to such problem.

The paper presents a simple method for analyzing nonlinear distortions of LFM signals used in FMCW radars [1]. In theory, the radar transmitter generates continuous wave $s(t)$ with sawtooth frequency modulation ($M = 2$) of period T. The return echo reflected from a stationary target at distance R from the radar can be considered as the delayed and attenuated copy of the transmitted signal with time delay equal to $\tau = 2R/c$, where c is the light velocity. This received signal is mixed with transmitted signal and at the output of a homodyne receiver the pure harmonic video signal is obtained. The video signal frequency f_R is equal to $\alpha\tau$, where $\alpha = \Delta f/T$ is the slope of frequency modulation and Δf is signal frequency deviation. In FMCW radar the unknown frequency f_R is estimated by finding the maximum of signal $y(t) = s(t)s^*(t-\tau)$ spectrum (* denotes complex conjugation). In practice, the transmitted signal $s(t)$ has nonlinear frequency modulation. Its phase can be modeled by the polynomial (2) of higher order ($M > 2$) with non-zero coefficient a_M. In the paper we restrict analysis to the third order ($M = 3$), however our method can be easily extended for higher order ($M > 3$) effects.

2. Statement of the problem

Let us assume that the signal transmitted by the FMCW radar is given by:

$$s(t) = S_0 \exp\left(j\,\phi_3(t)\right), \tag{3}$$

where $\phi_3(t)$ is periodical function with the period T, and for time interval $0 \le t < T$

$$\phi_3(t) = a_0 + a_1 t + a_2 t^2 + a_3\left(t - \frac{T}{2}\right)^3 \tag{4}$$

is the third order polynomial (for convenience, we use slightly different notation than (2)). The instantaneous angular frequency $\omega(t) = d\,\phi_3(t)/dt$ of the signal (3) (for $0 < t < T$) is equal to

$$\omega(t) = a_1 + 2a_2 t + 3a_3\left(t - \frac{T}{2}\right)^2, \tag{5}$$

where $a_1/(2\pi)$ is the carrier frequency f_0, $2a_2/(2\pi)$ is the slope of frequency modulation α, and the third term in Eq. (5) is responsible for quadratic modulation distortion. After mixing the signal $s(t)$ with the return echo $s^*(t-\tau)$ we obtain (for $\tau < t < T$)

$$y(t) = s(t)\,s^*(t-\tau) = Y_0 \exp\left(j\phi(t)\right). \tag{6}$$

The differential phase $\phi(t) = \phi_3(t) - \phi_3(t-\tau)$ is given by:

$$\phi(t) = b_0 + b_1 t + b_2 \left(t - \frac{T}{2}\right)^2, \tag{7}$$

where

$$b_0 = a_1\tau - a_2\tau^2 + a_3\tau^3 + \frac{3}{2}a_3\tau^2 T, \tag{8}$$

$$b_1 = 2a_2\tau - 3a_3\tau^2, \tag{9}$$

$$b_2 = 3a_3\tau. \tag{10}$$

To simplify further considerations we have assumed unit amplitude of the signal ($S_0 = 1$) and we do not take into consideration initial phase b_0. To measure nonlinear effects of modulation, the unknown parameters b_1 and b_2 of the signal

$$x(t) = \exp\left(j\left[b_1 t + b_2\left(t - \frac{T}{2}\right)^2\right]\right) \tag{11}$$

have to be estimated. For small nonlinear distortions the second term in Eq. (9) is negligible and we can assume $b_1 = 2a_2\tau$. The parameter b_1 is the unknown angular frequency of the signal, proportional to time delay τ (range to the target), and $b_2 = 3a_3\tau$ is the unknown quadratic modulation distortion. It must be noted that due to distortions the signal (11) is an LFM signal instead of a pure harmonic signal.

3. Estimation of unknown parameters

In the modern digital FMCW radar receivers the video signal (11) is sampled with sampling period $\Delta T = T/N$, where N is a natural number (typically $N = 1024, 2048, \ldots$). A discrete-time version of Eq. (11) has the form

$$x(n) = \exp\left(j\left[n\theta_R + \gamma\theta_R(n - N/2)^2\right]\right), \tag{12}$$

where $\theta_R = \omega_R\Delta T$ is the unknown range angular frequency normalized with respect to sampling frequency $f_s = \frac{1}{\Delta T}$ and the parameter

$$\gamma = \frac{3a_3 T}{2a_2 N} \tag{13}$$

is an unknown coefficient of nonlinear distortions.

Let us apply the idea of the matched filter to the estimation of unknown parameters θ_R and γ of a deterministic signal (12) contaminated by additive white Gaussian noise. If the impulse response $h(n)$ of the deterministic $N-1$ order FIR filter fulfills the condition

$$h(n) = x^*(N-1-n) \tag{14}$$

then the filter is matched to the signal $x(n)$ and its response

$$z(n) = \sum_{k=0}^{N-1} x(n-k)\,h(k) = \sum_{k=0}^{N-1} x(n-k)\,x^*(N-1-k) \tag{15}$$

for $n = N-1$ is equal to the signal energy E

$$z(N-1) = \sum_{k=0}^{N-1} \left|x(k)\right|^2 = E. \tag{16}$$

The energy E is obtained only when estimated values $\hat{\theta}_R$ and $\hat{\gamma}$ of matched filter impulse response are equal to actual values θ_R and γ of the analyzed signal. In the estimation process it is necessary to search for values $\hat{\theta}_R$ and $\hat{\gamma}$ that maximize (15) for $n = N-1$, or equivalently to maximize absolute value of the two-dimensional transform

$$X(\theta_R, \gamma) = \sum_{k=0}^{N-1} x(N-1-k)\exp\left(-j\left[(N-1-k)\theta_R + \gamma\theta_R\left(\tfrac{N}{2}-1-k\right)^2\right]\right). \tag{17}$$

For $\gamma = 0$ Eq. (17) becomes the classical discrete Fourier transform (DFT) of the signal $x(n)$, often used for estimating range frequency $\hat{\theta}_R$ in FMCW radars with linear frequency modulation. The second order term in Eq. (17) (for $\gamma \neq 0$) can be interpreted as the correction of nonlinear effects. In general, Eq. (17) can be treated as the extended, generalized chirp transform, which allows detection and estimation of modulation distortions. It is worth to notice that transform (17) is a special case of the so-called generalized chirp transform (GCT) and the estimated values $\hat{\theta}_R$ and $\hat{\gamma}$ are the maximum likelihood estimates of θ_R and γ parameters [5].

4. Measurement results and conclusions

To verify the ability of the transform (17) to detect and estimate nonlinear distortions in FMCW radar signal, the recorded and simulated nonlinear modulated FMCW signals were tested. In Fig. 1 the recorded signal transform is presented. It is easy to notice that the transform (17) of recorded signal reaches its maximum for γ approximately equal to -1%.

For comparison purposes in Fig. 2 the transform of simulated signal with -1% third order component is presented. These two figures are very similar, but it can be easily seen that recorded signal transform is less symmetrical than the simulated one. This is due to the presence of higher order nonlinear distortions in the recorded signal. Further investigations show that the fourth order component causes vertical asymmetry, and the fifth order term causes horizontal asymmetry. This example proves that the presented method may be used successfully to estimate third order nonlinear coefficients and to detect higher order effects.

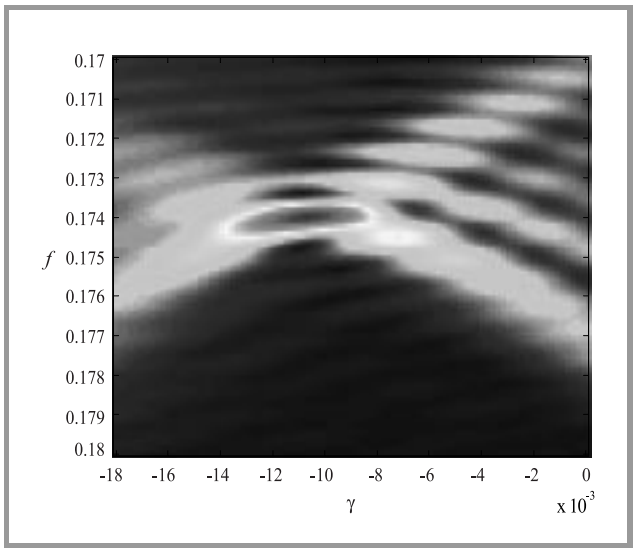

Fig. 1. Recorded signal transform (17) magnitude; $f - \gamma$ plane ($f = \theta_R / 2\pi$).

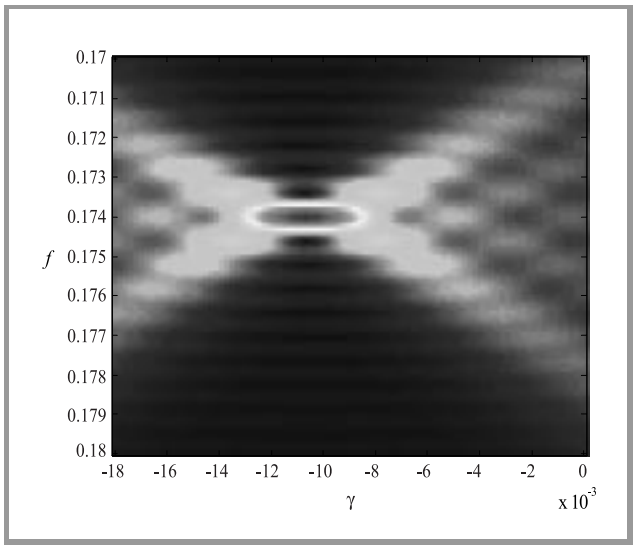

Fig. 2. Simulated signal transform (17) magnitude.

References

[1] A. Wojtkiewicz, J. Misiurewicz, M. Nałęcz, K. Jędrzejewski, and K. Kulpa, "Two-dimensional signal processing in FMCW radars", in *Proc. XX KKTOiUE*, Kołobrzeg, Poland, 1997, pp. 475–480.

[2] S. Peleg and B. Porat, "Estimation and classification of polynomial-phase signals", *IEEE Trans. Inform. Technol.*, vol. 37, no. 2, 1991.

[3] S. Peleg and B. Porat, "The Cramer-Rao lower bond for signals with constant amplitude and polynomial phase", *IEEE Trans. Signal Proc.*, vol. 39, no. 3, pp. 749–752, 1991.

[4] S. Peleg, B. Porat, and B. Friedlander, "The achievable accuracy in estimating the instantaneous phase and frequency of a constant amplitude signals", *IEEE Trans. Signal Proc.*, vol. 41, no. 6, pp. 2216–2224, 1993.

[5] B. Boshash, "Estimating and interpreting the instantaneous frequency of a signal" (Part 2), *Proc. IEEE*, vol. 80, no. 4, pp. 540–568, 1992.

[6] M. Benidir and A. Oudali, "Polynomial phase signal analysis based on the polynomial derivaties decomposition", *IEEE Trans. Signal Proc.*, vol. 49, no. 7, pp. 1954–1965, 1999.

[7] B. Barkat and B. Boashash, "Instantaneous frequency estimation of polynomial FM signals using the peak of PWVD: statistical performance in the presence of additive Gaussian noise", *IEEE Trans. Signal Proc.*, vol. 47, no. 9, pp. 2480–2490, 1999.

[8] B. Barkat and B. Boashash, "Design of higher order polynomial Wigner-Vilde distributions", *IEEE Trans. Signal Proc.*, vol. 47, no. 9, pp. 2608–2611, 1999.

Krzysztof S. Kulpa was born in Warsaw, Poland on April 13, 1958. He received the M.Sc. and Ph.D. degrees in electronic engineering from Warsaw University of Technology in 1982 and 1987, respectively. Since 1982 he has been in the Institute of Electronics Fundamentals at Warsaw University of Technology on the posts of a Teaching Assistant and Assistant Professor. His teaching activities included the areas of measurements and digital signal processing. In the years 1988–1990 he was also at the Technical University of Bialystok, Bialystok, Poland. His professional experience includes training visits in IBM Spain or Elmer-Perkins in England, as well as being a technical consultant in CNPEP RADWAR in Poland. He was involved with several research and development projects, granted from the Polish radar industry, in the area of digital processing of radar signals. His interests include Kalman filtering and object tracking problems, adaptive MTI filtering, and continuous wave radars.
e-mail: k.kulpa@ise.pw.edu.pl
Institute of Electronic Systems
Warsaw University of Technology
Nowowiejska st 15/19
00-665 Warsaw, Poland

Andrzej Wojtkiewicz was born in Nowogrodek (Poland) in 1938. He received the M.Sc. and Ph.D. degrees from the Gdansk University of Technology (Poland) in 1961 and 1971, respectively, both in electronic engineering. Since 1974 he has been with the Warsaw University of Technology, where he currently holds the position of Professor. His fields of interest concentrate on analysis and design of digital filters, adaptive signal processing and parameter estimation, applied primarily in digital processing of radar signals. He has authored and co-authored more than 100 research papers and technical reports in his areas of interest. He is also author of the book, *Introduction do Digital Filter Synthesis* (1984). He has been a member of the IEEE.
e-mail: a.wojtkiewicz@ise.pw.edu.pl
Institute of Electronic Systems
Warsaw University of Technology
Nowowiejska st 15/19
00-665 Warsaw, Poland

Marek Nałęcz was born in Warsaw (Poland) in 1961. He received the M.Sc. degree in 1984 and the Ph.D. degree in 1992 from the Warsaw University of Technology, both in electronic engineering and both conferred with honors. Since 1984 he has been with the Warsaw University of

Technology, where he currently holds the position of Assistant Professor. His early works were devoted to the analysis of switched-capacitor circuits. Now his fields of interest concentrate on digital processing of radar signals, applications of digital signal processors, adaptive filters, modern spectral estimation methods and robust algorithm of system identification. He has authored and co-authored more than 50 research papers, conference papers and technical reports in his areas of interest. He has been a member of the IEEE.

e-mail: m.nalecz@ise.pw.edu.pl
Institute of Electronic Systems
Warsaw University of Technology
Nowowiejska st 15/19
00-665 Warsaw, Poland

Jacek Misiurewicz was born in Warsaw, Poland on March 26, 1965. He received the M.Sc. and Ph.D. degrees in electronic engineering from Warsaw University of Technology in 1988 and 1996, respectively. Since 1988 he has been in the Institute of Electronics Fundamentals at Warsaw University of Technology on the posts of Teaching Assistant and Assistant Professor in the area of digital signal processing. He was involved with several research and development projects, granted from the Polish radar industry, in the area of digital processing of radar signals. His interests include non-uniform sampling problems, MTI filtering and filter design, as well as programmable logic applications and real-time programming. He was a member of an Organizing Committee of National Circuit Theory conferences in 1991 and 1992. He is a member of the IEEE since 1993, and IEEE Poland Section Newsletter Editor since 1998.

e-mail: j.misiurewicz@ise.pw.edu.pl
Institute of Electronic Systems
Warsaw University of Technology
Nowowiejska st 15/19
00-665 Warsaw, Poland

Paper

The priority assignment for detected targets in multifunction radar

Wojciech Komorniczak, Tomasz Kuczerski, and Jerzy F. Pietrasiński

Abstract — In a multifunction radar there is necessity to manage its very limited resources. This management should concern, among others, detected targets importance description. So information of those with lower priority will be refreshed more rarely. Presented paper describes system that assigns ranks for all detected objects in real time and then puts targets in order of priority. The system is based on structure of artificial neuron. Methods of neuron learning are discussed.

Keywords — multifunction radar, target identification, priority assignment, resources management.

1. Introduction

The multifunction radar (MFR) is a device that can detect and then track many targets. Because of limitations concerning available radar resources (in a domain of time and energy) MFR should be equipped with advanced resource management system. With reference to detected objects the task of management system is, among others, to rank targets in order of their increasing priority. The ranking procedure is necessary because in situation when a lot of objects are detected, the MFR resources will be assigned to those with the highest priority. As a result of this attitude the information about targets with lower rank will be refreshed more rarely.

There are no publications related to detected objects priority assignment. Therefore, on the basis of tactics of air forces and from the other hand anti-aircraft defense, following features of objects were recognized as important from the point of view of ranking procedure:

- membership (friend or foe),
- flight direction,
- diagonal range,
- altitude,
- radial velocity,
- azimuth,
- acceleration.

One of the units of the MFR resource management system (Fig. 1) is a priority assignment module.

Generally, the structure mentioned above shows model of a MFR resource management system. The input data source is target generator. The detection and IFF simulation modules approach the model operation to real conditions.

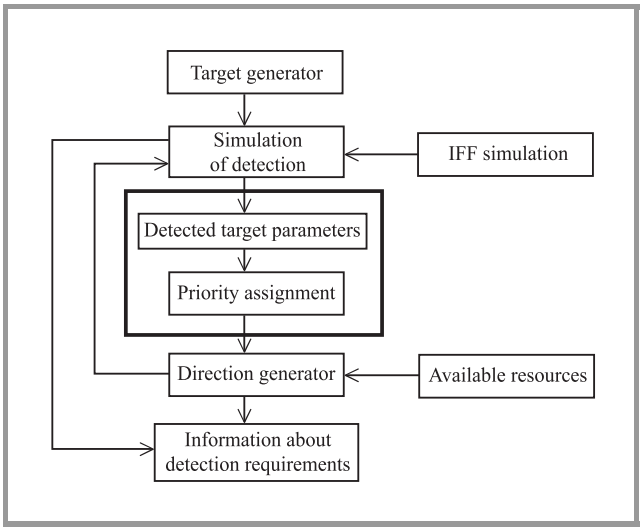

Fig. 1. The MFR resource management system model.

2. The priority assignment module model

Features of detected targets listed above can be transformed to related signals. The signals determine the input vector that is formed in the detected target parameters module. The example vector x_i can be as follows:

x_1 – diagonal range [km],

x_2 – radial velocity of object [m/s],

x_3 – signal: friend ($x_3 = 0$), foe ($x_3 = 1$),

x_4 – acceleration of object [m/s^2],

x_5 – object rank ($x_5 = 0.5$, in case when object is pointed by upper command, can assume value $x_5 > 0.5$ for important one or $x_5 < 0.5$ for not important).

As it is shown in Fig. 2, components of x vector are multiplied by weights w_i in the W-block. Then the input stimulation signal is calculated as a weighted sum of x

$$u = \sum_{i=1}^{5} \boldsymbol{w}_i \boldsymbol{x}_i . \qquad (1)$$

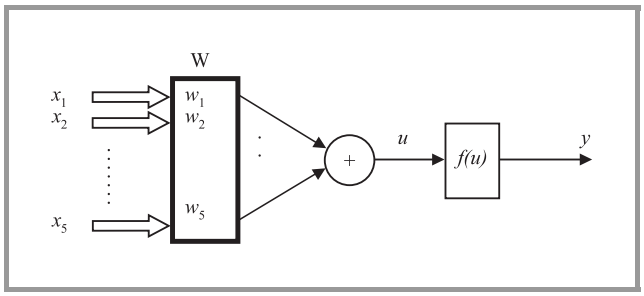

Fig. 2. The priority assignment module.

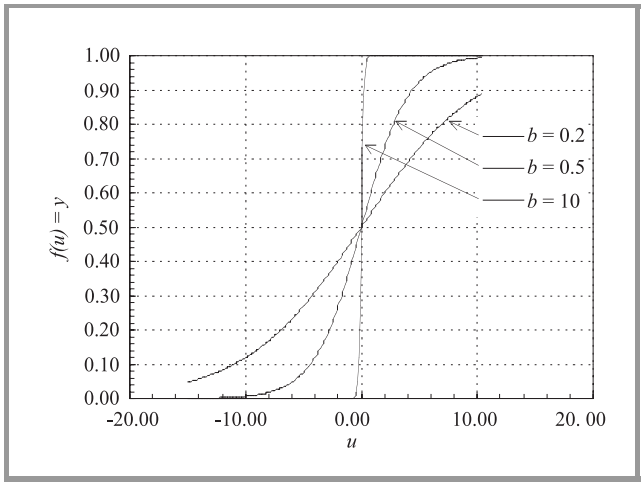

Fig. 3. Activation function of the module.

On the output of module there is a nonlinear operation $f(u)$ according to activation function (2) (Fig. 3):

$$f(u) = \frac{1}{1+\exp(-bu)}\,. \tag{2}$$

The slope of the function depends on the parameter b. The value of b will be fixed on the testing stage. For parameter $b \to \infty$ there is the function in a form as follows:

$$f(u) = \begin{cases} 1, & u > 0 \\ 0.5, & u = 0 \\ 0, & u < 0 \end{cases}\,. \tag{3}$$

3. Weight coefficients calculation method

Due to application of the structure presented in Fig. 2 with nonlinear output element, to calculate values of the weight coefficients it is possible to use learning method with back propagation [2]. This method relies on minimizing of mean square error that arises on output. It can be defined as:

$$q = \frac{1}{2}\sum_{j=1}^{N}(\delta^{(j)})^2\,, \tag{4}$$

where:

$\delta^{(j)} = z^{(j)} - y^{(j)}$,

$z^{(j)}$ – requested value of the target rank in jth step of learning,

$y^{(j)}$ – output value of the target rank calculated in jth step of learning for $w^{(j)}$ weight coefficients:

$$y^{(j)} = f\Big(\sum_{i=1}^{5}(\boldsymbol{w}_i^{(j)} \cdot \boldsymbol{x}_i^{(j)})\Big)\,, \tag{5}$$

N – number of learning pairs: $< x^{(i)}, z^{(i)} >$,

U – learning set,

$$U = \ll \boldsymbol{x}^{(1)}, z^{(1)} >, \ll \boldsymbol{x}^{(2)}, z^{(2)} >, \ldots, \ll \boldsymbol{x}^{(N)}, z^{(N)} \gg\,. \tag{6}$$

According to gradient method of error q minimizing it is possible to apply weight coefficients calculating algorithm on the basis of the learning set as follows:

$$w_i^{(j+1)} - w_i^{(j)} = \Delta w_i^{(j)} = -\eta\,\frac{\delta q^{(j)}}{\delta w_i^{(j)}}\,, \tag{7}$$

where η is the learning coefficient.

Starting values of weight coefficients are fixed randomly. It is possible to set the weights to $w_i = 0.5$. It is important to assure the same conditions for the training results comparing.

The weight coefficients selection algorithm ensures the minimization of the error q for established learning set U. Because of the structure mentioned above and learning methods are compatible with nonlinear neuron model and nonlinear neuron learning algorithm [2], system has ability to generalize the target rank. Thanks to it there is a possibility to assign the priorities for all objects, even those not included in learning process. The next stage consists of verification such a module as a part of MFR resource management system.

It is worth to pay attention that the module has ability to acquire the knowledge during operation with real targets. In the case of wrong defined rank value, the system operator can manually set the requested z value and repeat learning according to algorithms (4) and (7).

4. Learning sets generating methods

Learning set U described by Eq. (6) consists of value pairs that input signal and requested output signal value z. Generation of this can be performed in two ways:

a) simulation method with using target generator (Fig. 1),

b) using registered real signals.

Both methods require operator – expert. He uses its own knowledge and experience, on the basis of information X shown on, for example, radar display and finally can rank the targets according to their importance. Due to established model (Fig. 3) of output signal, the rank of each

target is a number from range (0, 1). A block diagram of learning sets generating method of sets U is presented in Fig. 4.

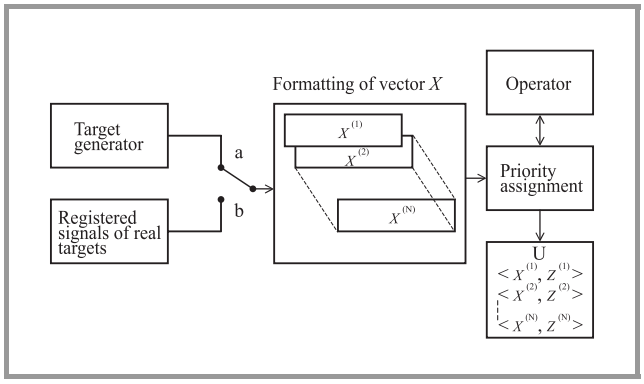

Fig. 4. Learning sets generating model.

In the case of simultaneous occurring of N targets on radar display the operator has to put them in order by assigning to each object the value of the rank z. Estimation of the minimum size of the learning set $N_{\min}$ can be assumed on the basis of the literature [1]. It is equal twice number of all weight coefficients of module. For input signal defined as a vector of 5 elements $N_{\min} = 10$.

5. Conclusions

The proposed structure of the module (Fig. 2) enables correct realization of the priority assignment process. It has ability to learn due to possibility of weight coefficient w_i correction according to learning algorithm (8). For effective program work the learning set must be complete. It must fulfil requirements as follows:

- each input signal class must be presented;
- the learning data must consist of several subgroups relating to specific pattern;
- in each class its statistical changeability must be considered; for example the error of target parameters measure;
- to avoid excessive adaptation, the learning data must be put in random order; the value of N must not excess $N_{\min}$.

The learning process should be realized for many various data sets, but with using the same starting point. After each learning, it is important to save values of weight coefficients for verification using testing set of large number of elements. In the case of not satisfying error q level the module must be rebuild. It can be done for example by using cascade learning algorithm proposed by Fahlman [1].

References

[1] S. Osowski, *Neural Networks*. Warszawa: WNT, 1996 (in Polish).

[2] R. Tadeusiewicz, *Neural Networks*. Warszawa: AOF RM, 1993 (in Polish).

Wojciech Komorniczak received the M.Sc. degree in electronics from Military University of Technology (MUT), Warsaw, Poland in 1997. He is currently the assistant in MUT in the Institute of Radar Technology, Faculty of Electronics. The area of his interests concerns the multifunction radar resources management and the threat assessment problems. From the beginning of 2001 he is a Ph.D. student in École Nationale Supérieure des Télécommunications de Bretagne, Brest, France.
wojciech.komorniczak@enst-bretagne.fr
Faculty of Electronics, Institute of Radar Technology
Military University of Technology
Gen. S. Kaliski st 2
00-908 Warsaw, Poland

Tomasz Kuczerski received the M.Sc. degree in electronics from the Military University of Technology (MUT), Warsaw, Poland, in 1993. He is an assistant in Radar Theory and Techniques Section in the Institute of Radar Technology, MUT. His research interests include radar theory, signal processing and artificial intelligence problems.
tkuczerski@wel.wat.waw.pl
Faculty of Electronics, Institute of Radar Technology
Military University of Technology
Gen. S. Kaliski st 2
00-908 Warsaw, Poland

Jerzy F. Pietrasiński received the M.Sc. degree in electronics from the Military University of Technology (MUT), Warsaw, Poland, in 1973. He received the Ph.D. degree in telecommunications from the MUT in 1979. He is an Assistant Professor, a chief of Radar Theory and Techniques Section in the Institute of Radar Technology, MUT. His research interests include radar theory, signal processing and radar resource management problems. He is a voting member of the Polish team in the Sensors & Electronics Technology (SET) Panel that belongs to the Research & Technology Organization (RTO), NATO from 1999.
jerzypie@wel.wat.waw.pl
Faculty of Electronics, Institute of Radar Technology
Military University of Technology
Gen. S. Kaliski st 2
00-908 Warsaw, Poland

Paper

Geometrical representation of a monochromatic electromagnetic wave using the tangential vector approach

Laura Carrea and Gerd Wanielik

Abstract — The aim of this work is to develop a coherent polarimetric model and to find a geometrical description of a monochromatic wave. The spinor form of the electrical field, its links to the coherency matrix and the Poincare' sphere are introduced with the aim to obtain a geometrical representation of the spinor. It consists, from the "polarization point of view", on the polarization vector and a tangential plane to the Poincare' sphere where it is possible to visualize the zero phase.

Keywords — polarimetric, coherent model, Poincare' sphere.

1. Introduction

Pulse radar has a very narrow band, so, to describe the state of the signal, it is possible to consider one single pulse like a monochromatic electromagnetic wave, which is completely polarized [1, 2]. A very useful representation of the electrical field is its spinor form which contains the complete information even the zero phase[1]. The aim of this work is to develop a coherent polarimetric description which has a geometrical representation.

2. Spinors and quadrivectors – the coherency matrix

The two-component complex field of the Jones representation may be treated as a spinor η^A:

$$\begin{pmatrix}\eta^1\\ \eta^2\end{pmatrix}=\begin{pmatrix}E_x\\ E_y\end{pmatrix}=\begin{pmatrix}a_x e^{i\delta_x}\\ a_y e^{i\delta_y}\end{pmatrix}, \tag{1}$$

where a_x, a_y are the amplitudes and δ_x, δ_y are the phases of the phasor representation of a RF signal.
A quadrivector $x^\mu=(x^0,x^1,x^2,x^3)$ may be regarded as a Hermitian second-rank spinor. The spin matrix X [3]:

$$X=x^0+(\vec{x}\cdot\vec{\sigma})=\left\|\begin{matrix}x^0+x^4 & x^1-ix^2\\ x^1+ix^2 & x^0-x^4\end{matrix}\right\|=\left\|\begin{matrix}X^{1\dot{1}} & X^{1\dot{2}}\\ X^{2\dot{1}} & X^{2\dot{2}}\end{matrix}\right\| \tag{2}$$

is transformed like a second rank spinor namely the coefficients in the law for the transformation of the components of the spin matrix $X^{A\dot{V}}$ are identical with the coefficient in the law for the transformation of the second rank spinor $\chi^A\xi^{\dot{V}}$ (the dots are used for the conjugate complex, not transpose). In more compact form:

$$X^{A\dot{V}}=\left[x^0+(\vec{x}\cdot\vec{\sigma})\right]^{A\dot{V}}=x^\mu\sigma_\mu^{A\dot{V}}\quad(\mu=0,\,1,\,2,\,3), \tag{3}$$

where σ_0 is the unit matrix and σ_1, σ_2, σ_3 are the Pauli matrices:

$$\sigma_1\sigma_2=-\sigma_2\sigma_1=i\sigma_3 \tag{4}$$

and cyclic permutations. In this way a geometric representation of the spinor η^A which the spinor form of the Jones vector, is possible. Then, if $X^{A\dot{V}}$ is calculated as

$$X^{A\dot{V}}=\eta^A\left(\overline{\eta}\right)^{\dot{V}} \tag{5}$$

it results: $X^{1\dot{1}}=E_xE_x^*$, $X^{1\dot{2}}=E_xE_y^*$, $X^{2\dot{1}}=E_yE_x^*$, $X^{2\dot{2}}=E_yE_y^*$, which are the components of the coherency matrix J [4] (where E_i^* is the conjugate complex of the complex number E_i).
The correspondent 4-vector x^μ is obtained from the Eq. (3) and from Eq. (5):

$$\left\|\begin{matrix}x^0+x^1 & x^2-ix^3\\ x^2+ix^3 & x^0-x^1\end{matrix}\right\|=\left\|\begin{matrix}\eta^1\overline{\eta}^{\dot{1}} & \eta^1\overline{\eta}^{\dot{2}}\\ \eta^2\overline{\eta}^{\dot{1}} & \eta^2\overline{\eta}^{\dot{2}}\end{matrix}\right\|, \tag{6}$$

where the cyclic permutation: $\sigma_1\to\sigma_2$, $\sigma_2\to\sigma_3$, $\sigma_3\to\sigma_1$ is considered. Substituting the components of the Jones vector, the components of the Stokes vector are found:

$$x^0=\frac{1}{2}g^0,\quad x^1=\frac{1}{2}g^1,\quad x^2=\frac{1}{2}g^2,\quad x^3=\frac{1}{2}g^3. \tag{7}$$

For a monochromatic wave, (g^0,g^1,g^2,g^3) is a real null 4-vector

$$(g^0)^2-(g^1)^2-(g^2)^2-(g^3)^2=0\Rightarrow(x^0)^2-(x^1)^2+-(x^2)^2-(x^3)^2=0. \tag{8}$$

All the directions of the 4-vectors x^μ in the Minkowski space-time for which the components satisfy (8) are null directions and they build the null cone [5]. The space of the null directions can be represented in the Euclidean space by the intersections of the null cone with the hyper planes $x^0=const$ and so $g^0=const$ (with the same intensity of the electrical field, because $g^0=I$). If the $const=\pm1$, the intersection is a sphere which can be regarded as a Riemann sphere of an Argand plane, which is the Poincare'

[1] D. H. O. Bebbington, "Analytical foundations of polarimetry: I" – to be published.

sphere. But in general for any value of the constant, unless $g^0 = 0$, we get from the relation (8):

$$\left(\frac{g^1}{g^0}\right)^2 + \left(\frac{g^2}{g^0}\right)^2 + \left(\frac{g^3}{g^0}\right)^2 = 1 \tag{9}$$

and we can define

$$p^1 = \frac{g^1}{g^0}, \quad p^2 = \frac{g^2}{g^0}, \quad p^3 = \frac{g^3}{g^0} \tag{10}$$

which are the components of the polarization vector. The equation of the Poincare' sphere is in general:

$$(p^1)^2 + (p^2)^2 + (p^3)^2 = 1\,. \tag{11}$$

The exterior of the sphere represents space-like directions namely unpolarized or partially polarized light.
Multiplying the spinor η^A by a complex number $p = \lambda e^{i\theta}$ (λ and θ real) the 4-vector x^μ is stretched of λ^2 but is unchanged in direction (cfr. (5)), namely it is independent from the choice of the angle θ. The 4-vector is uniquely defined by the spinor but to a 4-vector correspond a lot of spinors, which differ by the multiplicative factor $e^{i\theta}$.
On the other side we want find a coherent description of a monochromatic wave, which contains the so-called "zero phase" $\alpha = \delta_x$ $(0 < \alpha < 2\pi)$. In order to do this, we look at the spinor in its polarization vector form [6]:

$$\begin{pmatrix}\eta^1\\ \eta^2\end{pmatrix} = \sqrt{\frac{I}{2}}\, e^{i\alpha} \begin{pmatrix} (1+p^1)^{1/2} \\ (1+p^1)^{-1/2}(p^2+ip^3)\end{pmatrix}. \tag{12}$$

This form of the spinor contains explicitly the zero phase and, as we have stated below, the corresponding 4-vector (g^0, g^1, g^2, g^3), is unaffected by the choice of the angle α.

3. The tangential plane and the angle α

Let us consider the spinor mate [3] ξ^B of η^A:

$$\begin{pmatrix}\xi^1\\ \xi^2\end{pmatrix} = \sqrt{\frac{I}{2}}\, e^{-i\alpha} \begin{pmatrix} -(1+p^1)^{-1/2}(p^2-ip^3) \\ (1+p^1)^{1/2}\end{pmatrix}. \tag{13}$$

The spinor and the spinor mate so defined satisfy the condition:

$$\eta_A \xi^A = I\,. \tag{14}$$

They build a basis normalized to I and if we consider $I = 1$ the two spinor build a basis normalized to 1. The spinor and the spinor mate are linked by the equations:

$$\eta^A \xi^B - \xi^A \eta^B = \varepsilon^{AB} \quad (A, B = 1, 2)\,, \tag{15}$$

where ε^{AB} is an antisymmetric symbol such that: $\varepsilon^{12} = = \varepsilon_{12} = 1$, $\varepsilon^{AB} = -\varepsilon^{BA}$. The spinor and the spinor mate constitute a spinor basis.

As we have stated below that $X^{A\dot{V}}$ is transformed like a second rank spinor $\chi^A \overline{\xi}^{\dot{V}}$, we can calculate the component of $Q^{A\dot{V}}$ using the spinor mate:

$$Q^{A\dot{V}} = \eta^A \left(\overline{\xi}\right)^{\dot{V}}. \tag{16}$$

Now multiplying the spinor η^A by a complex number $\rho = \lambda e^{i\theta}$, the vector is stretched but also it depends on the choice of the angle θ and in particular it depends on 2θ. The calculation of $Q^{A\dot{V}}$ gives:

$$\begin{aligned} Q^{1\dot{1}} &= -\tfrac{I}{2} e^{2i\alpha}(p^2 + ip^3), & Q^{1\dot{2}} &= \tfrac{I}{2} e^{2i\alpha}(1+p^1), \\ Q^{2\dot{1}} &= -\tfrac{I}{2} e^{2i\alpha}(1+p^1)^{-1}(p^2+ip^3)^2, & Q^{2\dot{2}} &= \tfrac{I}{2} e^{2i\alpha}(p^2+ip^3) \end{aligned} \tag{17}$$

which corresponds to a complex point. Infact, by the Eq. (3) the components of the corresponding 4-vector q^μ are:

$$\begin{aligned} q^0 &= 0, \\ q^1 &= -\frac{I}{2} e^{2i\alpha}(p^2 + ip^3), \\ q^2 &= \frac{I}{4} e^{2i\alpha}\, \frac{(1+p^1)^2 - (p^2+ip^3)^2}{1+p^1}, \\ q^3 &= -\frac{I}{4i}\, \frac{(p^2+ip^3) - (1+p^1)^2}{1+p^1}. \end{aligned} \tag{18}$$

If the real and imaginary parts are separated, the two real 4-vectors have components $q^\mu_R = (0, \vec{q}_R)$ and $q^\mu_I = (0, \vec{q}_I)$ which are:

$$\begin{aligned} q^0_R &= 0, \\ q^1_R &= I(-p^2\cos 2\alpha + p^3 \sin 2\alpha), \\ q^2_R &= I\left(\frac{p^1(1+p^1) + (p^3)^2}{1+p^1}\cos 2\alpha + \frac{p^2 p^3}{1+p^1}\sin 2\alpha\right), \\ q^3_R &= I\left(-\frac{p^2 p^3}{1+p^1}\cos 2\alpha - \frac{p^1(1+p^1)+(p^2)^2}{1+p^1}\sin 2\alpha\right). \end{aligned} \tag{19}$$

$$\begin{aligned} q^0_I &= 0, \\ q^1_I &= I(-p^2\sin 2\alpha - p^3 \cos 2\alpha), \\ q^2_I &= I\left(\frac{p^1(1+p^1) + (p^3)^2}{1+p^1}\sin 2\alpha - \frac{p^2 p^3}{1+p^1}\cos 2\alpha\right), \\ q^3_I &= I\left(-\frac{p^2 p^3}{1+p^1}\sin 2\alpha + \frac{p^1(1+p^1)+(p^2)^2}{1+p^1}\cos 2\alpha\right). \end{aligned} \tag{20}$$

The 4-vector q^μ is space-like and in particular of magnitude equal to I. The 4-vector $p^\mu(1, p^1, p^2, p^3)$, $q^\mu_R(0, \vec{q}_R)$, $q^\mu_1(0, \vec{q}_I)$ are orthogonal in the sense:

$$p^\mu (q_R)_\mu = 0, \quad p^\mu (q_I)_\mu = 0, \quad (q_I)^\mu (q_R)_\mu = 0\,. \tag{21}$$

And it is easy to see that even $\vec{g} = (g^1, g^2, g^3)$, $\vec{q}_R = (q_R^1, q_R^2, q_R^3)$ and $\vec{q}_I = (q_I^1, q_I^2, q_I^3)$ are orthogonal and of modul equal to I in the Euclidean space. So the vectors $\vec{q}_R$ and $\vec{q}_I$ provide basis vectors ($I = 1$) in the two-dimensional space which is the tangential plane at the point $\vec{p}$ on the Poincare' sphere. When the angle α varies, the vectors $\vec{q}_R$ and $\vec{q}_I$ rotate in the tangential plane.

The aim is now to visualize the angle α and to find a reference for $\alpha = 0$. For the horizontal polarization $\vec{p}_H = (1, 0, 0)$ and for $\alpha = 0$, $\vec{q}_R$ is the tangential vector to the equatorial great circle. If α increases, $\vec{q}_R$ rotates in the tangential plane clockwise through an angle of 2α. Keeping $\alpha = 0$, the fact that the point $\vec{p}_H$ moves into the point $\vec{p}$ corresponds to a rotation applied to the spinor η^A. This means a change of the basis, which means different $\vec{q}_{R(\alpha=0)}$ and $\vec{q}_{I(\alpha=0)}$. The rotation matrix, which preserves the angle α and which moves the point $\vec{p}_H$ to the point $\vec{p}$ is:

$$R = \left(\frac{1}{1+|\rho|^2}\right)^{-1/2} \begin{pmatrix} 1 & -|\rho|e^{-i\delta} \\ |\rho|e^{i\delta} & 1 \end{pmatrix}, \qquad (22)$$

where $\rho = \frac{E_y}{E_x} = |\rho|e^{i\delta}$ ($\delta = \delta_y - \delta_x$, cfr. (1)) is the polarization ratio. This is a rotation around the axis $\vec{n}(0, -\sin\delta, \cos\delta)$ through an angle such that $\cos\theta = \frac{1-|\rho|^2}{1+|\rho|^2} = p^1$. The rotation (22) preserves the angle between the directions but not the direction, so the vector $\vec{q}_{R(\alpha=0)}$ changes its direction. The direction r (cfr. Fig. 1), obtained by the intersection of the great circle through $\vec{p}_H$ and $\vec{p}$, forms with the vector $\vec{q}_{R(\alpha=0)}$ an angle δ and with the vector $\vec{q}_R$ the angle $2\alpha + \delta$. It is very important to find a reference for $\alpha = 0$ because $\vec{q}_R$ forms an angle δ with the direction r but δ is different for every point on the sphere. To solve this problem, let us consider $\vec{p}$ and $\vec{q}_R$ and $\vec{q}_I$ for any α, consider the correspondent spinor, apply the rotation which preserves the angle α and move the vector $\vec{p}$ in the point $\vec{p}_H$ to obtain the vector $\vec{q}_{RH}$ and the angle 2α is the angle between $\vec{q}_{RH}$ and $\vec{q}_{RH(\alpha=0)}$.

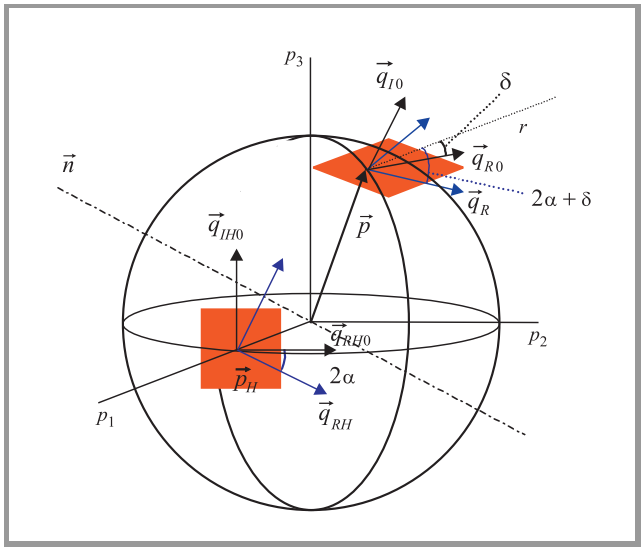

Fig. 1. The Poincare' sphere and the tangential planes in the point $\vec{p}_H$ and in the point $\vec{p}$.

The spinor and the spinor mate constitute a spinor basis. It is easy to see that the correspondent 4-vectors (cfr. Eq. (6)) fix on the Poincare' sphere two antipodal points ((p^1, P^2, p^3) and $(-p^1, -p^2, -p^3)$) which are the basis states of polarization [7]. If the corresponding $\vec{q}_R$ and $\vec{q}_I$ vectors are calculated, the result is:

$$\vec{p} \to \vec{q}_R, \vec{q}_I \qquad -\vec{p} \to -\vec{q}_R, \vec{q}_I\,. \qquad (23)$$

With the help of the spinor, the change of basis is easy because it corresponds to a unitary transformation of the spinor which corresponds to a rotation in the three dimensional space. Infact the group of two-dimensional special unitary transformations (with unit determinants), which preserve the invariants, are homomorphic to the three-dimensional rotation group [5]. The general form of the spin rotation matrix is:

$$R = \cos\frac{\theta}{2} - i\sin\frac{\theta}{2}(\sigma_1 n_1 + \sigma_2 n_2 + \sigma_3 n_3)\,, \qquad (24)$$

where θ is the angle of rotation, (n_1, n_2, n_3) are the components of the axis $\vec{n}$ of rotation in the Euclidean space and σ_i are the Pauli matrices. The transformation law of a spinor is:

$$\eta \to \eta' = R\eta\,. \qquad (25)$$

It is possible to show that the rotation spin matrix is a unitary matrix and its determinant is necessarily unity.

Acknowledgment

Laura Carrea is supported by the TMR Network for Radar Polarimetry, Theory and Applications (Network Contract number: ERB-FMRX-CT98-0211).

References

[1] W. M. Boerner, Wie-Ling Yan, An-Quing Xi, and Yoshio Yamaguchi, "Basic concepts of radar polarimetry", in *Proc. NATO Adv. Res. Worksh. Dir. Inv. Meth. Radar Polar.*, Bad Windsheim, Franconia, Germany, Sept. 1988.

[2] Z. H. Czyż, "Comparison of fundamental approaches to radar polarimetry", in *Proc. NATO Adv. Res. Worksh. Dir. Inv. Meth. Radar Polar.*, Bad Windsheim, Franconia, Germany, Sept. 1988.

[3] C. Misner, K. Thorne, and J. Wheeler, *Gravitation*. W. H. Freeman and Company, 1973.

[4] M. Born and E. Wolf, *Principles of Optics*. Cambridge University Press, 1980.

[5] R. Penrose and W. Rindler, *Spinor and Space-Time*. Cambridge University Press, 1884.

[6] G. Wanielik, "Signaturuntersuchungen an einem polarimetrischen Pulseradar". Dissertation. VDI Verlag, 1988.

[7] R. Azzam and N. Bashara, *Ellipsometry and Polarized Light*. North Holland Publishing Company, 1977.

Laura Carrea received the "Laurea" degree in physics from the University of Turin, Turin, Italy in 1997. She is currently pursuing the Ph.D. degree at the Faculty of Electrical Engineering and Information Technology at the Chemnitz University of Technology, Chemnitz, Germany. She is supported by the European Research Network Training and Mobility of Researcher (T.M.R.) "Radar polarimetry – Theory and Applications". Her main interests center on radar polarimetry with special emphasis on polarimetric SAR image processing.
e-mail: carrea@infotech.tu-chemnitz.de
Faculty of Electrical Engineering
and Information Technology
University of Technology
Reichenhainer st 70
09126 Chemnitz, Germany

Gerd Wanielik received his diploma in 1979 from the Technical University of Darmstadt (Germany) and his Ph.D. in 1988 from the Technical University of Karlsruhe (Germany), all in electrical engineering. From 1979 he has worked as a scientist at the AEG-Telefunken Research Institute and later at the Daimler Chrysler Research Center. Since 1999 he is Professor of Communication Engineering at the Chemnitz University of Technology (Germany). His research interests include multisensor processing and systems, polarimetry, communication and navigation systems. He is a senior member of the IEEE, member of the ITG and DGON. He received the ITG Award in 1991 and the Daimler Chrysler Research Award in 1997.
e-mail: wanielik@infotech.tu-chemnitz.de
Faculty of Electrical Engineering
and Information Technology
University of Technology
Reichenhainer st 70
09126 Chemnitz, Germany

Paper

New type of microstrip antenna with ferroelectric layer

Józef Modelski and Yevhen Yashchyshyn

Abstract — A new type of microstrip antenna is proposed using a voltage-controlled ferroelectric thin tape in the multilayered structure. This paper presents the ferroelectric thin tape, its theoretical analysis and design. The results indicate that this concept has many advantages, is very practical and promising. It gives possibilities of several applications, e.g. in smart antennas.

Keywords — microstrip antenna, multilayered structure, ferroelectric thin tape, smart antennas.

1. Introduction

Microstrip antennas have over thirty years history [1], but during the last decade, microstrip antenna technology has been the most rapidly developing research topic in the antenna field [2], because of the huge demand in markets of personal and satellite communications, wireless local networks and intelligent vehicle systems. Microstrip antennas are well known for their highly desirable physical characteristics such as low profile, light weigh, low cost, ruggedness and they are well suited to integration with MICs. In comparison to traditional antenna elements, however, the electrical performance of the basic microstrip antenna suffers from a number of serious drawbacks, e.g. narrow bandwidth, high feed network losses, poor cross polarization, and low power handling capacity. In many applications, the electrically shaping of the radiation pattern has received a great deal of attention. New possibilities are emerged by using new materials and structures. Below, a new type of multilayered microstrip antenna has been proposed, which seems to be very promising for applications in smart antennas and phase-arrays.

2. Antenna configuration

Figure 1 shows a basic configuration of the discussed microstrip antenna. The main feature of the ferroelectric antennas is the change of ferroelectric material permittivity with an applied dc (direct current) control voltage. The multilayer substrate consists of thin ferroelectric tape sandwiched between dielectric slabs (also for the heat transferring). Substrates are located on the conducting plate. Ferroelectric tape has thickness h_3 and is made up of ferroelectric material which permittivity (ε_3) can be changed by applying and varying the dc electric field. DC voltage source V is used as shown in Fig. 1. Dielectric slabs have thicknesses h_2 and h_4 and permittivities ε_2 and ε_4, respectively, and conducting plate is described by thickness h_1 and conductivity σ. Microstrip line with current J_x^e is a source which excites the multilayer structure. Characteristics of this microstrip antenna depends on parameters of dielectric substrate (i.e. thicknesses and permittivities). Radiating elements employing ferroelectric materials may give much better performance with compared to ferrite ones, because of their high power handling capability, low drive power, full military temperature range of operation and low cost [3].

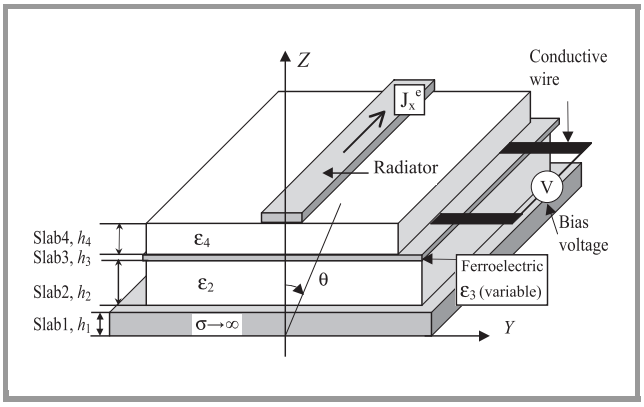

Fig. 1. Basic configuration of the ferroelectric microstrip antenna.

Ferroelectric materials of series (Ba-Sr)TiO_3 (BSTO), (Pb-Sr)TiO_3 and (Pb-Ca)TiO_3 and similar titanates (for which the Curie temperature is in the vicinity of room temperature) are well suited for microstrip applications. Ferroelectric materials for high performance microwave applications should exhibit: a large variation of the dielectric constant with applied dc biasing fields, low loss tangent over the range of operating dc bias voltages, insensitivity of dielectric properties to changes in environmental condition (e.g. ambient temperature variation), and maximum reproducibility of the dielectric properties with respect to the applied dc voltage. Materials such as (Ba-Sr)TiO_3 series exhibit a significant variation of the dielectric constant with applied dc biasing fields at microwave frequencies (e.g. from 1000 to 6000) because the Curie temperature is close to the room temperature. Also, the loss tangent value of barium-strontium titanate materials can be reduced to 0.005 by adding a small percentage (1 to 4 percent) of iron, nickel or magnesium to the material mixture. The dielectric constant variation with dc biasing field is larger if the Curie temperature for a BSTO composition is closer to the ambient temperature (25°C) [4, 5].

3. Antenna analysis

The full-wave method has been applied for theoretical analysis. Analysis of the multilayered substrate is based on the calculations of electromagnetic field excited by the source inside multilayered space (with different variable parameters as permittivity, permeability and conductivity).

Assume, that dependence on the time is $e^{-i\omega t}$ and distribution of the current density is $\vec{j}(M)$ in space V. The associated electric and magnetic fields due to this current are given by:

$$\vec{H} = rot\vec{A};\quad \vec{E} = i\omega\left\{-\vec{A} + grad\left[\frac{\mu}{k^2} div\frac{\vec{A}}{\mu}\right]\right\}, \qquad (1)$$

where

$$\vec{A}(M) = \frac{1}{4\pi}\iiint_V \widehat{G}(M, M_0)\,\vec{j}(M_0)\,dv_{M_0} \qquad (2)$$

is the vector potential integral and $\widehat{G}(M, M_0)$ is tensor function given by

$$\widehat{G}(M, M_0) = \begin{Bmatrix} G_0(M,M_0) & 0 & 0 \\ 0 & G_0(M,M_0) & 0 \\ \mu(z)\frac{\partial g(M,M_0)}{\partial x} & \mu(z)\frac{\partial g(M,M_0)}{\partial y} & \frac{\mu(z)}{\widetilde{\varepsilon}(z_0)}G_1(M,M_0) \end{Bmatrix}, \qquad (3)$$

where: $k = \omega\sqrt{\widetilde{\varepsilon}\mu}$ – wave number; μ – permeability; $\widetilde{\varepsilon} = \varepsilon + i\frac{\sigma}{\omega}$ – complex permittivity.

Functions G_0, g, G_1 are solutions of the boundary problem. They depend only on coordinates z, z_0 and $\rho = \sqrt{(x-x_0)^2 + (y-y_0)^2}$ and can be written as:

$$G_0 = \int_0^\infty J_0(\chi\rho)\Phi_0(\chi, z, z_0)\chi d\chi;\quad g = \int_0^\infty J_0(\chi\rho)\varphi(\chi, z, z_0)\chi d\chi;$$

$$G_1 = \int_0^\infty J_0(\chi\rho)\Phi_1(\chi, z, z_0)\chi d\chi. \qquad (4)$$

If we will introduce the fundamental function $U_a^\alpha(\chi, z, z_0)$, then dependence (4) can be given as

$$\Phi_0 = U_\mu^0;\quad \varphi = \frac{1}{\chi^2}\left\{U_{\widetilde{\varepsilon}}^1 - \frac{1}{\mu}\cdot\frac{dU_\mu^0}{dz}\right\};\quad \Phi_1 = U_{\widetilde{\varepsilon}}^0. \qquad (5)$$

The fundamental function for the field in half-space above radiator ($z \geq z_0$) can be accomplished in the form:

$$U_a^\alpha(z) = 2\frac{(1-\alpha)Z_1(z_o)Z_2(z_0) - \alpha Z_2(z_0)}{Z_2(z_o) - Z_1(z_0)}e^{-\zeta_0(z-z_0)}. \qquad (6)$$

Because we examine antenna with nonmagnetic substrate, the functions $Z_{1/2}$ are given by:

$$Z_2(z_0) = -\frac{\mu_0}{\zeta_0};\qquad Z_1(z_0) = Z_1^l;$$

$$Z_1^l = \frac{\mu_0}{\zeta_4}\cdot\frac{A_4 - B_4e^{-2\zeta_4 h_4}}{A_4 + B_4e^{-2\zeta_4 h_4}};\quad A_4 = \mu_0 + \zeta_4 Z_1^4;\quad B_4 = \mu_0 - \zeta_4 Z_1^4$$

$$Z_1^4 = \frac{\mu_0}{\zeta_3}\cdot\frac{A_3 - B_3e^{-2\zeta_3 h_3}}{A_3 + B_3e^{-2\zeta_3 h_3}};\quad A_3 = \mu_0 + \zeta_3 Z_1^3;\quad B_3 = \mu_0 - \zeta_3 Z_1^3$$

$$Z_1^3 = \frac{\mu_0}{\zeta_2}\cdot\frac{A_2 - B_2e^{-2\zeta_2 h_2}}{A_2 + B_2e^{-2\zeta_2 h_2}};\quad A_2 = \mu_0 + \zeta_2 Z_1^2;\quad B_2 = \mu_0 - \zeta_2 Z_1^2$$

$$Z_1^2 = \frac{\mu_0}{\zeta_1}\cdot\frac{1 - e^{-2\zeta_1 h_1}}{1 + e^{-2\zeta_1 h_1}}, \qquad (7)$$

where: $k_1 = \sqrt{\frac{\omega\mu_0\sigma}{2}}(1-i)$; $\zeta_m = \sqrt{\chi^2 - k_m^2}$; $k_m = \omega\sqrt{\widetilde{\varepsilon}_m\mu_0}$ (m = 0, 2, 3, 4) – wave number of the mth layer.

The structure has been restricted to the 2D geometry (is not depended on coordinate "x"). In this case the electromagnetic field can be presented as:

$$E_x = i\omega\frac{J_x^e}{4\pi^2}\int_{-\infty}^{\infty}\frac{Z_1(z_0)}{Z_2(z_0) - Z_1(z_0)}e^{-i\chi(y-y_0) - i\zeta_0(z-z_0)}d\chi. \qquad (8)$$

This equation is simply a Fourier transform. It permits to utilize the fast Fourier transform (FFT) for numerical calculation. The far field has been obtained on the base of stationary phases method. Then pattern of the ferroelectric microstrip antenna can be written as:

$$F(\theta) = -j\frac{Z_1(\theta)\beta_0}{Z_2(\theta) - Z_1(\theta)}, \qquad (9)$$

where:

$$Z_2(\theta) = -\frac{\mu_0}{\beta_0};$$

$$Z_1(\theta) = \frac{\mu_0}{\beta_0}\cdot\frac{\mu_0(1-\vartheta_4) + \beta_0 Z_1^4(1+\vartheta_4)}{\mu_0(1+\vartheta_4) + \beta_0 Z_1^4(1-\vartheta_4)};$$

$$Z_1^4(\theta) = \frac{\mu_0}{\beta_3}\cdot\frac{\mu_0(1-\vartheta_3) + \beta_3 Z_1^3(1+\vartheta_3)}{\mu_0(1+\vartheta_3) + \beta_3 Z_1^3(1-\vartheta_3)};$$

$$Z_1^3(\theta) = \frac{\mu_0}{\beta_2}\cdot\frac{\mu_0(1-\vartheta_2) + \beta_2 Z_1^2(1+\vartheta_2)}{\mu_0(1+\vartheta_2) + \beta_2 Z_1^2(1-\vartheta_2)};$$

$$Z_1^2(\theta) = \frac{\mu_0}{\beta_1}\cdot\frac{(1-\vartheta_1) + (1+\vartheta_1)\beta_1/\beta_0}{(1+\vartheta_1) + (1-\vartheta_1)\beta_1/\beta_0},$$

where:

$\vartheta_m = e^{-2H_m B_m}$; $\beta_m = j\sqrt{k_m^2 - k_0^2\sin^2\theta}$, $m = 0, 1, 2, 3, 4$; $k_m = \omega\sqrt{\mu_0\varepsilon_m}$, $m = 0, 2, 3, 4$.

4. Results

The characteristics of the ferroelectric microstrip antenna have been investigated. Figure 2 shows H-plane radiation pattern of this antenna for different permittivity values. As shown in the Fig. 2, the permittivity change (by varying the dc bias) gives possibility to create different radiation patterns. The following cases have been calculated: slab1 – $h_1 = 0.02\lambda$ and $\sigma \to \infty$; slab2 – $h_2 = 0.004\lambda$ and $\varepsilon_2 = 9 \cdot \varepsilon_0$; slab3 (ferroelectric) – $h_3 = 0.00002\lambda$ and ε_3 can be changed (e.g. from 900 to 9000); slab4 – $h_4 = 0.007\lambda$ and $\varepsilon_4 = 2 \cdot \varepsilon_0$, where λ – length wave. Beamwidth pattern for case 2 ($\varepsilon_3 = 3600 \cdot \varepsilon_0$) is about 33° with two zeros. For case 3 beamwidth pattern is about 52° ($\varepsilon_3 = 9000 \cdot \varepsilon_0$) without zeros (see Fig. 2, curve 2 and 3, respectively). The pattern of radiating element changes its shape and zeros localization of the beam by varying permittivity of ferroelectric tape. Figure 3 shows dependence of the zeros localization in the radiating element pattern, by varying the dc electric field of ferroelectric material (parameters of the structure have been shown above). This permits to use such radiating element into several applications, e.g. for smart antenna arrays [6]. A linear N-isotropic elements array has $N-1$ degrees of the freedom. Therefore, it is possible to own $N-1$ independent control zeros pattern. If the pattern of the radiating nonisotropic element has own two zeros, then the linear N-nonisotropic elements array has own $N+1$ control zeros (e.g., two more degrees of freedom). This permits to shape assignment pattern for smart antenna.

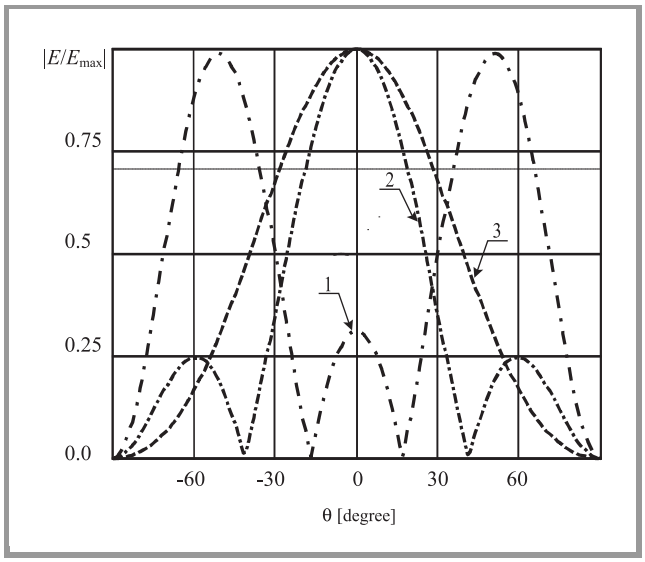

Fig. 2. H-plane radiation pattern of the ferroelectric microstrip antenna for different permittivity. Explanations: *1* – $\varepsilon_3 = 1800\varepsilon_0$; *2* – $\varepsilon_3 = 3600\varepsilon_0$; *3* – $\varepsilon_3 = 9000\varepsilon_0$.

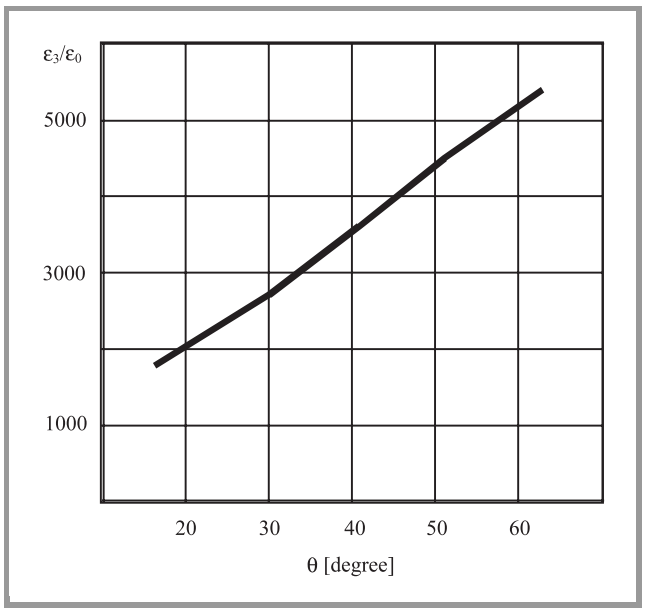

Fig. 3. Dependence of the zero localization from change permittivity of ferroelectric.

5. Conclusion

In this paper, a new type of microstrip antenna with ferroelectric layer has been presented. This novel antenna consists of multilayered structure with thin ferroelectric tape (voltage-controlled) sandwiched between two dielectric slabs, located on the conductive plate. The results of investigations indicate that proposed microstrip antenna type is perspective.

References

[1] I. J. Bahl and P. Bhartia, *Microstrip Antennas*. Norwood (MA): Artech House, 1980.

[2] D. Pozar and D. Schaubert, *Microstrip Antennas*. New York: IEEE Press, 1995.

[3] V. K. Varadan, D. K. Ghodgaonkar, V. V. Varadan, J. F. Kelly, and P. Glikerdas, "Ceramic phase shifters for electronically steerable antenna systems", *Microw. J.*, vol. 35, no. 1, pp. 116–127, 1992.

[4] J. B. L. Rao, D. P. Patel, and V. Krichevsky, "Voltage-controlled ferroelectric lens phased arras", *IEEE Trans. Anten. Propagat.*, vol. 47, no. 3, pp. 458–468, 1999.

[5] T. N. Verbickaya, "Ferroelectrics". Guide of the Electrical Materials. *Energoatom*, vol. 3, pp. 550–579, 1988 (in Russian).

[6] D. Robbins and M. G. Amin, "Testing of smart antenna systems", *Microw. J.*, vol. 42, no. 1, pp. 112–118, 1999.

Józef Modelski received the M.Sc., Ph.D. and D.Sc. (habilitation) degrees in electronics from Warsaw University of Technology in 1973, 1978, and 1987, respectively. In 1994 he obtained the State title of Professor. Since 1973 he has been with the Institute of Radioelectronics, Warsaw University of Technology (WUT) holding in sequence all academic positions from teaching/research assistant to tenured

professor (1991). In 1976/77 he spent 13 months in U.S. as a Fulbright grantee working with the microwave laboratories: at the Texas University at Austin, Cornell University, and Communication Satellite Corporation COMSAT. In 1986 he joined for two years the Braunschweig Technical University (Germany) as a senior scientist. His research interests are in the areas of microwave phase modulators and shifters with semiconductor and ferrite elements, dielectric resonators and their applications, integrating waveguide technology for mass-production components, and design of communications antennas. He has published over 120 technical papers and 4 books, obtained 8 patents and many awards. Since 1996 J. Modelski has been Director of the Institute of Radioelectronics, WUT. He is chairing scientific boards in two research centers and International Microwave Conference MIKON, is a member of the TPCs of MTTS International Microwave Symposium, European Microwave Conference and many local conferences. He is IEEE Fellow Member.

e-mail: j.modelski@ire.pw.edu.pl
Institute of Radioelectronics
Warsaw University of Technology
Nowowiejska st 15/19
00-655 Warsaw, Poland

Yevhen Yashchyshyn was born in Lvov, Ukraine, in 1957. He received the M.Sc. degree in radioelectronics engineering from the Lvov University of Technology in 1979 and Ph.D. degree in microwave devices and antennas from the Moscow Institute of the Electronic Machine Building in 1986. In 1991 he obtained the Senior Scientist title. From 1979 to 1993 he was with the Radio Engineering Faculty, Lvov University of Technology (LUT) holding in sequence all academic positions from teaching/research assistant to head of VHF laboratory. From 1993 to 1999 he was Associate Professor of Telecommunication Department Lvov Polytechnic National University. Since 1999 he has been with the Institute of Radioelectronics, Warsaw University of Technology (WUT), Poland, as an Associate Professor. His research interests are in the areas of antenna theory and technique, smart beamforming and design of communications antennas. He has published over 50 technical papers and obtained 4 patents. Since 1996 he has been a member of the IEEE.

e-mail: e.jaszczyszyn@ire.pw.edu.pl
Institute of Radioelectronics
Warsaw University of Technology
Nowowiejska st 15/19
00-655 Warsaw, Poland

Paper

A broadband uniplanar quasi-Yagi antenna – parameter study in application to a spatial power combiner

Marek E. Białkowski, Hyok J. Song, and Paweł Kabacik

Abstract — A parameter study is performed of a broadband uniplanar quasi-Yagi antenna with regard to its design and use in a spatial power combiner. A 3D full-wave electromagnetic field analysis is applied to identify parameters, which mostly affect the design frequency and operational bandwidth of this antenna. Optimal design conditions are determined. Using these design criteria a passive spatial power combiner employing trays of back-to-back connected quasi-Yagi antennas is developed. This combiner is investigated in terms of insertion losses and field uniformity, which are key factors in obtaining high power combining efficiency.

Keywords — broadband quasi-Yagi antenna, passive spatial power combiner.

1. Introduction

In recent years a lot of interest has been shown in spatial power combining methods to overcome difficulties in generating high power levels from solid-state devices at millimeter-wave frequencies [1]. Although oscillators and amplifiers can be spatially combined, most of the recent research activities have been devoted to amplifiers due to their more predictable performance and a larger operational bandwidth. In order to obtain low manufacturing costs, **tile** and **brick** configurations of planar antenna arrays have attracted a lot of attention [2] as suitable power combining structures. In these arrays antenna elements are connected to the input and output ports of the individual amplifiers. The input antenna element receives the signal and passes it to the amplifier. The amplifier passes the amplified signal to the output antenna where it is radiated. Power from the array is intercepted in free space by a receiving/collecting antenna such as a horn antenna. Due to the fact that the tile configuration usually employs resonant type antenna elements, such as microstrip patch antennas, this type of power combiner is narrow-band in operation. The resulting operational bandwidth is usually smaller than that of the individual amplifiers when they are assessed without radiating elements [3, 4]. The motivation of the work presented in this paper is to explore new antenna elements arranged in the brick configuration to fully utilize the surplus bandwidth of transistor amplifiers.

One possible choice, which has already been explored in [5], is a planar-type linear tapered slot antenna (LTSA). This antenna element, when properly designed, features large (multi-octave) operational bandwidth and because of an end-fire radiation characteristic it is suitable for inclusion as an element of a brick or tray array. One flaw of this solution is that the LTSA features a relatively large size with length L being in the order of $2\lambda_0 \leq L \leq 12\lambda_0$ and the termination width of $W \geq \lambda_0/2$ [6]. In [7] Qian *et al.* proposed an uniplanar quasi-Yagi antenna whose size is significantly smaller than that of the LTSA. A large operational bandwidth in the order of 48% for VSWR < 2 was demonstrated in X-band [8]. Although this antenna element is compact and provides a suitable bandwidth to match individual transistor amplifiers its design strategy has not been well documented.

This paper investigates the effects of five main design parameters of the uniplanar quasi-Yagi antenna on its operational frequency and impedance bandwidth. The study identifies parameters most affecting the performance of this antenna. The presented findings should be of interest to the designers of the quasi-Yagi antenna for applications such as a spatial power combining and other wireless communications applications.

2. Configuration

Figure 1 shows the configuration of the uniplanar quasi-Yagi antenna, which consists of a director and a driver fed by a broadband microstrip to coplanar strip transition [7]. A delay of half wavelength introduced in one of the two microstrip arms is required to obtain the odd mode coupling. The truncated ground plane on the backside of the substrate is used as a reflector. The operation of this antenna has been described in [7, 8] and hence it is not repeated here. Instead, the effects of different parameters of this antenna on its performance are studied here.

3. Parameter study

Due to the complex structure of the quasi-Yagi antenna, a 3D full-wave electromagnetic simulation package is necessary to efficiently carry out the parameter study. A commercially available 3D full-wave EM package, IE3D of Zeland Software, based on the method of moment (MoM) is used here to analyze the antenna performance in terms of its return loss.

Five design parameters considered in the present study include: parameter *l* – length of the director, parame-

ter *2* – distance between the director and the driver, parameter *3* – distance between the coupled microstrip lines, parameter *4* – length of the driver, parameter *5* – distance from the driver to the reflector. All these parameters are respectively shown in Fig. 1.

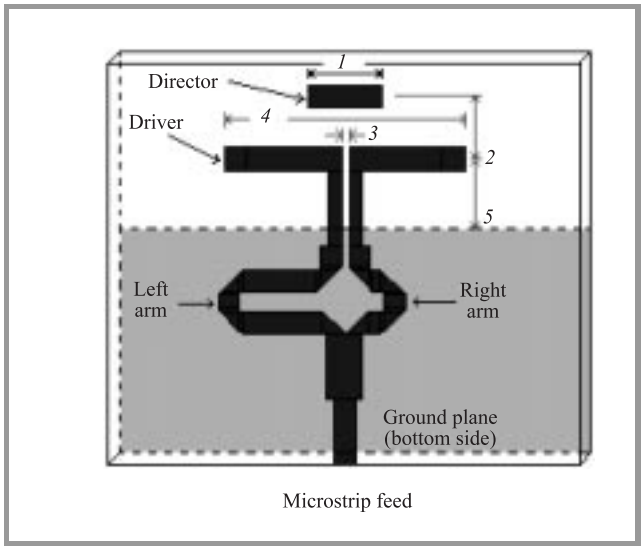

Fig. 1. Configuration of uniplanar quasi-Yagi antenna.

In order to gain the confidence in the accuracy of the EM software used in this study, a prototype quasi-Yagi antenna was designed, developed and tested and the measured results were compared against the theoretical ones. The design frequency was selected as 12.5 GHz and the initial antenna dimensions were chosen by referring to the design of a normal Yagi-Uda antenna. A substrate with a relative dielectric constant of 2.45 and thickness of 0.48 mm was assumed. The design was performed using IE3D. A manual iteration procedure was applied to achieve impedance bandwidth comparable to that demonstrated in [8]. The final antenna dimensions included: length of director (parameter *1*) = 4.8 mm, distance between the director and the driver (parameter *2*) = 4.0 mm, distance between the coupled microstrip lines (parameter *3*) = 0.5 mm, length of the driver (parameter *4*) = 15.5 mm, and distance from the driver to the reflector (parameter *5*) = 4.13 mm. Figure 2 shows both simulated and measured return loss of the final design. It can be seen that the simulation result closely follows the measured one. The frequency shift can be due to an insufficiently fine grid of the structure used in simulations. Nevertheless, a relatively good agreement confirms the validity of the chosen software to be used in the parameter study.

The results of simulations for the return loss with respect to parameters *1* to *5* are presented in Fig. 3(a–e). Figure 3a shows the results when parameter *1* is varied by 1 mm from 3.8 mm to 5.8 mm. The results show that the return loss is not sensitive to the changes of parameter *1*. Figure 3b shows the results when parameter *2* is varied

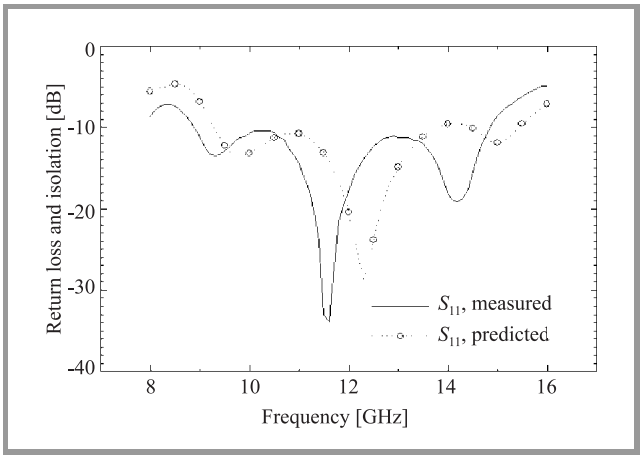

Fig. 2. Measured return loss of the optimized Ku-band quasi-Yagi antenna.

by 1 mm from 3 mm to 5 mm. The results show that parameter *2* only slightly affects the return loss. Figure 3c shows the results for the return loss when the gap between the coupled microstrip lines (parameter *3*) is varied in steps of 0.2 mm from 0.5 mm to 0.7 mm. The results reveal that the return loss degrades when the gap between the two microstrip lines is reduced. Figure 3d shows the results when the length of the driver (parameter *4*) is varied by increments of 2 mm from 13.5 mm to 17.5 mm. As observed in Fig. 3d the return loss is very sensitive to the changes of this parameter. This parameter affects both the impedance bandwidth and the center frequency. Finally Fig. 3e shows the results when parameter *5*, which is the distance from the driver to the reflector, is varied by increments of 1 mm from 3.13 mm to 5.13 mm. As seen in Fig. 3e the return loss is sensitive to this parameter. It affects the impedance bandwidth as well as the design frequency. The results presented in Fig. 3(a–e) reveal that the length of the driver (parameter *4*) is optimum when it is about a guide wavelength and the distance between the driver and the reflector (parameter *5*) is about a quarter guide wavelength.

4. Design of a power combiner

Having successfully designed a single quasi-Yagi antenna, the next step is to show that this antenna can properly operate when used as an element of a spatial power combiner. Here only a passive power combining structure is investigated. The investigations are restricted to practical experiments because the highly complicated 3D structure of the combiner is difficult to study theoretically.

Figure 4a shows the construction of a power combiner that includes two horn antennas for power launching and receiving purposes and several trays each consisting of two Yagi antennas positioned back-to-back, as shown in Fig. 4b.

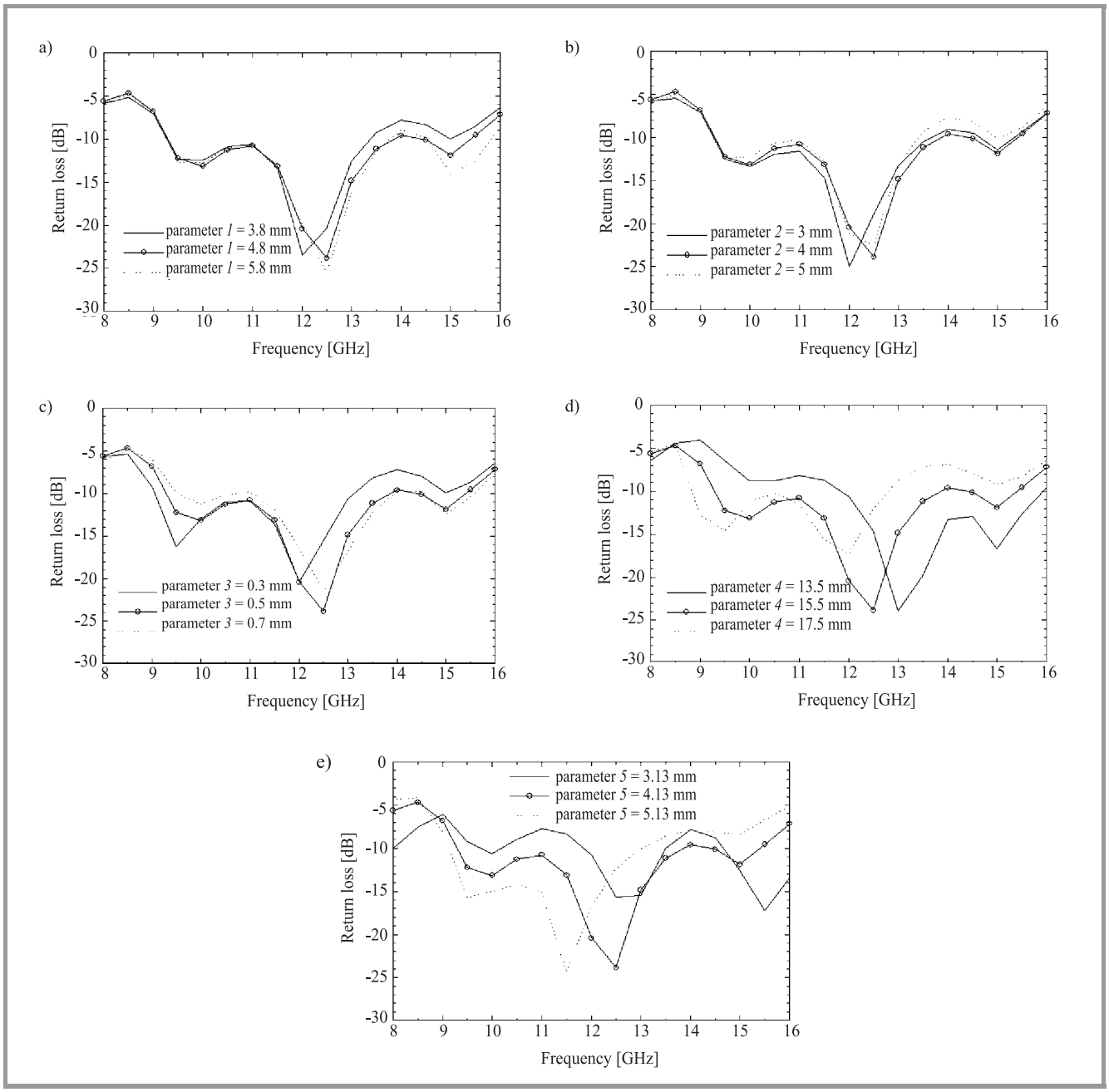

Fig. 3. Simulations results for the return loss of an uniplanar quasi-Yagi antenna when: (a) parameter *1* – length of the director; (b) parameter *2* – distance between the director and the driver; (c) parameter *3* – distance between the coupled microstrip lines; (d) parameter *4* – length of the driver, and (e) parameter *5* – distance from the driver to the reflector are varied.

As seen in Fig. 4a the trays are positioned parallel to the E-plane of the horns and hence they are stacked along the H-plane. The space between the input ports of the antennas in the tray in Fig. 4b is left to test the tray for isolation between the two ports. High isolation is required when an amplifier is included so that possible oscillations due to the feedback between amplifier's input and output ports are not present. Blocks of 6.4 mm Rohacell foam featuring the relative constant of 1.07 located on the sides of the trays are used to support the trays. The replacement of these foam spacers by spacers made in copper did not show any significant difference in all the measured results. The overall setup dimensions are as follows. The two horns feature aperture dimensions of 34 mm × 48 mm respectively in the direction of E- and H-field. The single tray features physical dimensions of 60 mm × 60 mm with its aperture width of about 16 mm that corresponds to the length of the driven element of the Yagi antenna.

Figure 5 shows the measured isolation for the tray configuration of Fig. 4. Note that in the experiment, the input ports to the two antennas were separated by 8 mm to enable their input ports to be connected to the vector network

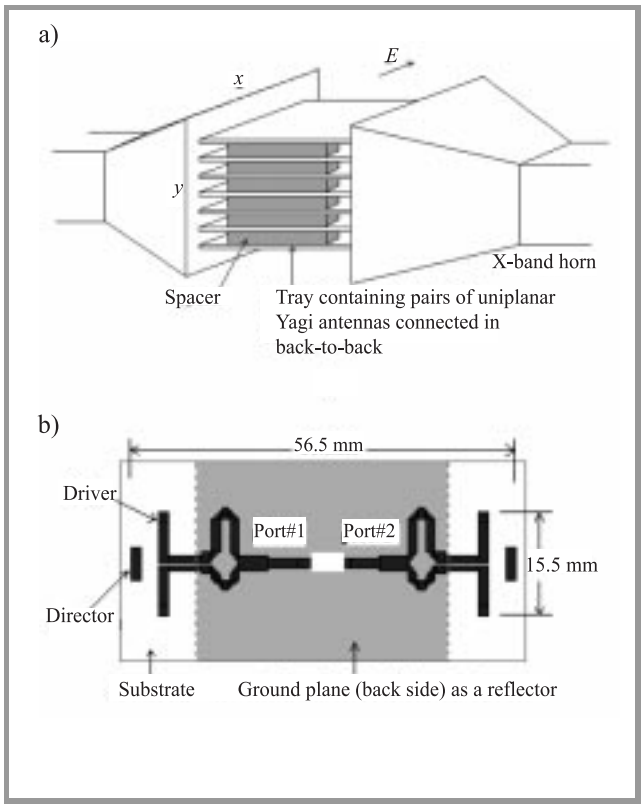

Fig. 4. (a) A perspective view of the power combiner consisting of 7 passive trays with horn antennas as distributing/combining devices, and (b) a layout of a passive tray containing two uniplanar quasi-Yagi antennas connected back-to-back.

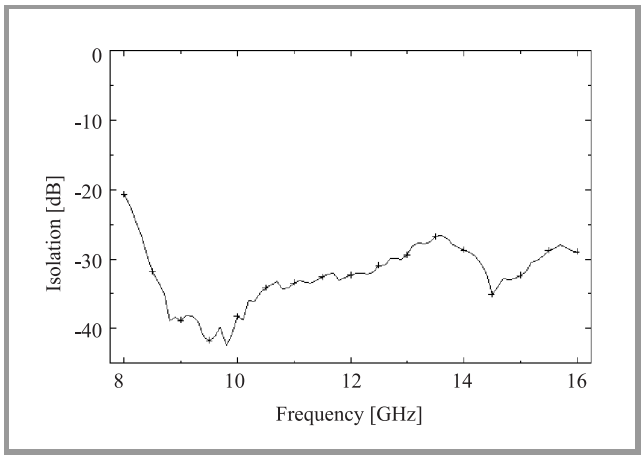

Fig. 5. Measured isolation (S_{12}) between input ports of the passive tray formed by two back-to-back connected quasi-Yagi antennas.

analyzer. High value of isolation, being greater than 25 dB over the frequency band from 8.5 GHz to 16 GHz is observed. This result indicates that the developed passive tray is ready to accommodate a broadband amplifier designed for the 50-ohm input/output operation whose gain does not exceed 25 dB across the frequency band from about 9 GHz to 15 GHz.

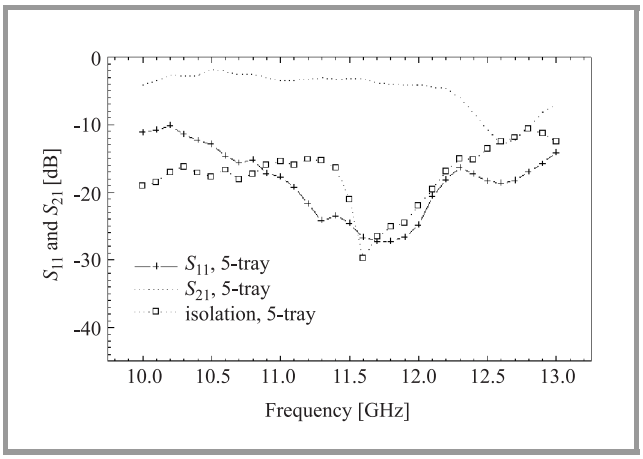

Fig. 6. Return loss (S_{11}) and insertion loss (S_{21}) as measured with respect to the horn ports for the 5-tray combiner. Also shown is isolation for this combiner when driven elements of Yagi antennas are short-circuited.

Figure 6 shows the measured results for return loss and insertion loss as observed from the coaxial ports of the transmitting and receiving horns of the 5-tray combiner.

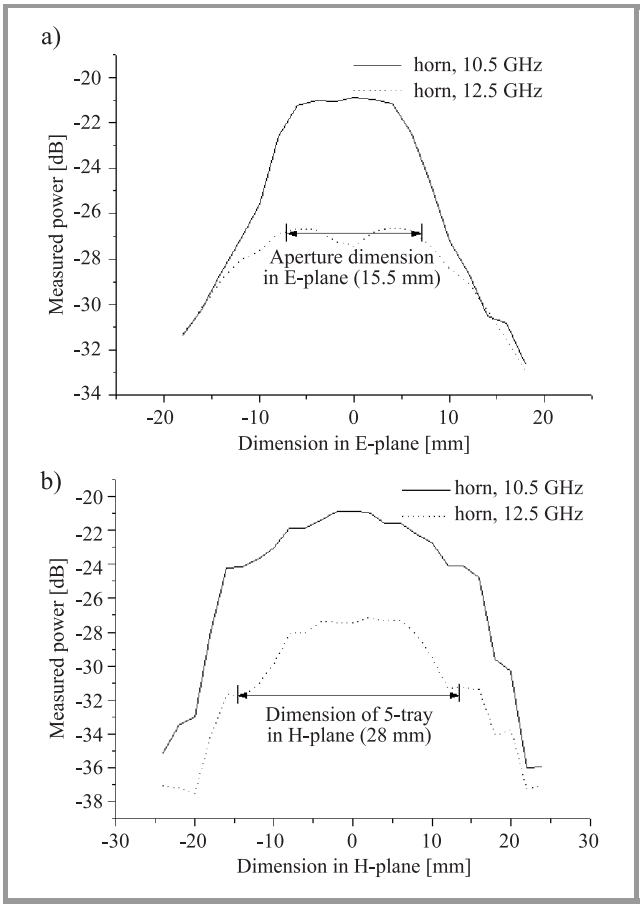

Fig. 7. Measured power distribution across two principal planes at the aperture of the X-band pyramidal horn, having dimensions 34 mm × 48 mm respectively in the E- and H-planes, at 10.5 GHz and 12.5 GHz: (a) E-plane cut, (b) H-plane cut.

Also shown in Fig. 6 is the isolation when the quasi-Yagi antennas of the 5-tray combiner become short-circuited. The lowest insertion loss of 1.8 dB occurs at 10.5 GHz with 3 dB bandwidth covering from 10 to 12.2 GHz. It is also observed that the insertion loss curve rolls off as frequency increases toward 12.5 GHz. It was found that the rise of insertion loss was mainly due to the near-field interaction between the tray and the horns. When the separation between the tray and the horns was slightly increased, the roll-off at 12.5 GHz in the insertion loss plot disappeared. The isolation between the receiving and transmitting horn ports when the Yagi antennas are short-circuited in the 5-tray structure takes a minimum value of 16 dB. This result shows that the back-to-back connected Yagi antennas are indeed responsible for power transmission between the two horns.

The next step to assess the performance of the combiner is to measure field uniformity across the stack. Obtaining a highly uniform field across the stack (which is in the H-plane of the quasi-Yagi antenna) is important from the point of view of achieving high power combining efficiency. If excitations of individual trays in the stack are uniform (constant in magnitude and phase), each amplifier contributes equally to the output power. Also when large power levels are established all the amplifiers reach their saturation simultaneously.

The measured amplitude of the field distribution across the launching horn aperture at 10.5 GHz and 12.5 GHz using a near-field measurement facility is shown in Fig. 7. An open-ended circular waveguide probe was used to scan the near field. As observed in Fig. 7, the 5-tray combiner fits well the region of uniform amplitude distribution at the horn aperture at 10.5 GHz compared with that at 12.5 GHz.

The measured amplitude of the field distribution across the output aperture of the 5-tray structure when excited by the horn at 10.5 GHz and 12.5 GHz is shown in Fig. 8.

As can be seen in Fig. 8, the outer trays are not excited as strong as the central trays. The measured phase variation across the stack (not shown here) was only within $\pm 15^\circ$. The uniformity of the field amplitude can be improved by using a hard horn as the launching/receiving horns [9].

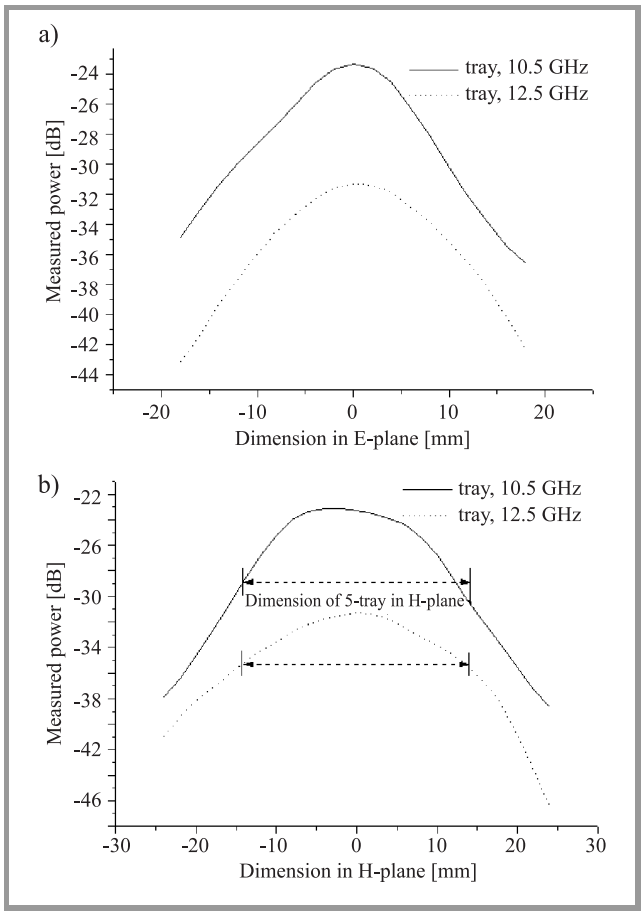

Fig. 8. Measured power distribution across two principal planes at the output of the 5-tray structure at 10.5 GHz and 12.5 GHz: (a) E-plane cut, (b) H-plane cut.

5. Conclusions

A parameter study has been performed of a broadband uniplanar quasi-Yagi antenna with regard to its design and use in a spatial power combiner. It has been found that the design frequency and the operational bandwidth are insensitive to the changes in the length of director (parameter *1*) and the distance between the director and the driver (parameter *2*). The length of gap between the coupled microstrip lines (parameter *3*) affects the bandwidth moderately. The most sensitive parameters of the quasi-Yagi antenna have been found the length of the driver (parameter *4*) and the distance from the driver to the reflector (parameter *5*). These two parameters affect both the antenna's design frequency and its operational bandwidth.

Following this theoretical study, a single tray consisting of two back-to-back connected quasi-Yagi antennas and a 5-tray combiner for operation in X/Ku-band have been developed and tested. Two ordinary pyramidal horn antennas have been used to distribute and receive microwave power. Investigated parameters have included return loss, insertion loss and field uniformity across the trays to achieve optimal combining conditions. The overall results for the single tray of two elements and the 5-tray configuration have shown that the quasi-Yagi antenna is a suitable element to develop a broadband spatial power combiner.

References

[1] J. A. Navarro and K. Chang, Eds., *Integrated Active Antennas and Spatial Power Combining*. New York: Wiley, 1996.

[2] R. A. York and Z. B. Popovic, Eds., *Active and Quasi-Optical Arrays for Solid-State Power Combining*. New York: Wiley, 1997, ch. 2.

[3] M. E. Białkowski and H. J. Song, "Investigations into power combining efficiency of microstrip patch transmit-arrays," *Microw. Opt. Technol. Lett.*, vol. 22, no. 4, pp. 284–287, 1999.

[4] H. J. Song and M. E. Białkowski, "A fully planar power combiner using microstrip patch arrays", in *IEEE AP-S Int. Symp. Dig.*, Orlando, Florida, USA, July 1999, vol. 4, pp. 2398–2401.

[5] R. N. Simons and R. Q. Lee, "Spatial frequency multiplier with active linearly tapered slot antenna array", in *Dig. Int. IEEE MTT-S Symp.*, San Diego, CA, 1994, vol. 3, pp. 1557–1560.

[6] K. F. Lee and W. Chen, Eds., *Advances in Microstrip and Printed Antennas*. New York: Wiley, 1997, ch. 9.

[7] Y. Qian, W. R. Deal, N. Kaneda, and T. Itoh, "Microstrip-fed quasi-Yagi antenna with broadband characteristics", *Electron. Lett.*, vol. 34, no. 23, pp. 2194–2196, 1998.

[8] Y. Qian, W. R. Deal, N. Kaneda, and T. Itoh, "A uniplanar quasi-Yagi antenna with wide bandwidth and low mutual coupling characteristics", in *1999 IEEE AP-S Int. Symp.*, July 1999, vol. 2, pp. 924–927.

[9] T. Ivanov and A. Mortazawi, "A two-stage spatial amplifier with hard horn feeds", *IEEE Microw. Guid. Wave Lett.*, vol. 6, no. 2, pp. 88–90, 1996.

Marek E. Białkowski (SM IEEE 1988) received the M.Eng.Sc. degree (1974) in applied mathematics and the Ph.D. degree (1979) in electrical engineering both from the Warsaw University of Technology and the D.Eng. degree (2000) in computer science and electrical engineering from the University of Queensland. In 1977 he joined the Institute of Radioelectronics, Warsaw University of Technology, and in 1979 became an Assistant Professor there. In 1981, he was awarded a Postdoctoral Research Fellowship by the Irish Department of Education and spent one year at the University College Dublin carrying out research in the area of microwave circuits. In 1982, he won a Postdoctoral Research Fellowship from the University of Queensland, Brisbane, Australia, where he worked on electromagnetic models for waveguide diode mounts. In 1984, he joined the Department of Electrical and Electronic Engineering, James Cook University, Townsville, Austrialia, as a Lecturer and then Senior Lecturer in the field of communications. In 1988, he was a Visiting Lecturer in the Department of Electronics and Computer Science, University of Southampton, U.K. In 1989, he joined the Department of Computer Science and Electrical Engineering at the University of Queensland, Brisbane, Austrialia where he is the Head of the Communications Systems Division. In 1994, he held an appointment as a Visiting Professor in the University of Victoria, Canada. In 1998–99, he held an appointment as a Visiting Professor at Nanyang Technological University, Singapore. In 2001, he was a Visiting Professor at City University of Hong Kong. Dr Białkowski's research interests include phased array antennas for cellular and satellite communications, technologies and signal processing techniques for smart antennas, low profile antennas for reception of satellite broadcast TV programs, near-field/far-field antenna measurements, electromagnetic modelling of waveguide feeds and transitions, conventional and spatial power combining techniques, six-port vector network analysers and industrial applications of microwaves. He has published about 270 technical papers and one book. Also he holds one patent. His name appears in a number of international biographical references including *Marquis Who's Who in the World* (USA), *International Biographical Dictionary* (UK) and *Polonia 2000* (France).

e-mail: meb@csee.uq.edu.au Bialkowski@ieee.org
Computer Science and Electrical Engineering Department
The University of Queensland
Brisbane, Qld 4072, Australia

Hyok J. Song was born in South Korea, on July 15, 1970. He received the B.E. (Honors) and M.Eng.Sc. degrees both in electrical engineering from the University of Queensland, Australia, in 1995 and 1998, respectively. Between 1998 and 2000 he was a Ph.D. student and a Research Assistant in the School of Computer Science and Electrical Engineering at the same university. He was a recipient of the UQGSA (University of Queensland Graduate School Award) scholarship. In February 2001, he joined HRL Laboratories LLC in Malibu, California. His research interests include passive and active microstrip patch array antennas and rf/microwave circuits for wireless communications applications. His other research interests include quasi-optical and spatial power combining techniques.

e-mail: song@ieee.org
Computer Science and Electrical Engineering Department
The University of Queensland
Brisbane, Qld 4072, Australia

Paweł Kabacik was born in Wroclaw, Poland, on January 1, 1963. He received the M.Sc. (telecommunications) and Ph.D. (electrical engineering) degrees, both from the Wroclaw University of Technology, Poland, in 1986 and 1996, respectively. From 1986 to 1988, he studied computer science at the Wroclaw University of Technology. In January 1987, he joined the Institute of Telecommunications and Acoustics, Wroclaw University of Technology, and in 1996, he became an Assistant Professor. In 1994, he completed a one-year management course that was organized by the Central Connecticut University,

New Britain, and the Wroclaw University of Technology. He was a Visiting Scholar at the Electromagnetics Institute, Technical University of Denmark, Lyngby, Denmark, from 1991 to 1992 and at the University of Queensland, Brisbane, Australia in 1997. He has published about 50 technical papers and participated in many scientific events in Europe, the United States, and Far-East Asia. His research interests include antenna arrays, phased arrays, near-field antenna measurements, digital beam-forming techniques, and smart antennas for mobile and wireless communications systems. Dr. Kabacik was a member of the EU COST 245 Project. Currently, he is a member of the EU COST 260 Project and supervises a research team working on conformal arrays within this project. In 1993, he received the Award for Young Scientists at the VIIth National URSI Symposium, Poland. His name is listed in *Marquis Who's Who in Science and Engineering* and in *Marquis Who's Who in the World*.

e-mail: pawel@zr.ita.pwr.wroc.pl
Institute of Telecommunications and Acoustics
Wroclaw University of Technology
50-370 Wroclaw, Poland

Paper

Photonic band gaps in complex layered arrays

Sergey L. Prosvirnin, Sergey A. Tretyakov, Tetyana D. Vasilyeva, Arlette Fourrier-Lamer, and Said Zouhdi

Abstract — Reflective and transmitting properties of several layers of double-periodic arrays are studied. In the arrays, elements are conducting inclusions of various shapes. It is shown that in these structures all the phenomena recently found in dense wire grids with periodical defects (so-called photonic band gap structures) can be observed and explained in simple terms of inter-layer and inclusion resonances. Frequency-selective (with two and more stop bands) and polarization transformation properties of these arrays are demonstrated.

Keywords — photonic band gap structures, double-periodic arrays, reflective and transmitting properties.

1. Introduction

In recent years, much attention has been given to so-called photonic band gap (PBG) materials. Full band gaps for electromagnetic waves of arbitrary polarization and propagation direction have been found in many 3D periodic structures. These results stimulated renewed interest to 2D and even 1D periodic structures in the microwave regime. Some new applications have been recently proposed [1 – 3]. A very interesting behavior has been observed in a system which is intermediate between bulk 3D periodic media and 2D regular arrays, see [4]. A relatively thin layer of conducting wire mesh has been investigated. Experimental results of [4] lead to the following observations: 1) in a regular periodic structures, the layer is highly reflective at low frequencies and rather transparent at high frequencies; 2) there is a sharp cut-off boundary between the two regimes; 3) if the wires are cut periodically (mesh with defects), transmission peaks appear in the low-frequency band of high reflectivity.

These phenomena were explained in [4] in terms of an effective dielectric constant. The cut-off frequency is identified as that similar to the plasma frequency for electrons flowing in the mesh. Regular 3D wire meshes with cubic cells were considered in papers [5, 6]. Here, the phenomena in regular structures have been explained in terms of the effective mass of electrons moving in conducting wires. However, these simple models fail if the system is studied in a wide frequency range. When the characteristic sizes become comparable to the wavelength (which is the most interesting case where photonic band gaps exist), the system is spatially dispersive. More complicated constitutive relations are needed to model spatial dispersion [7, 8]. We show that similar phenomena can be found in much simpler systems formed of a few parallel planar layers of conducting resonant inclusions, and explained in a very simple and physically clear way.

Let us start from an observation (made already in [4]) that in the low frequency regime the cell structure is not important. And indeed, phenomena 1 and 2 have been also observed in [5, 6] in 3D arrays of parallel conducting wires. Phenomenon 1 can be explained very simply just noticing that at low frequencies when the period of the grid is much smaller than the wavelength, the wire grid behaves as a conductor. On the other hand, when the frequency is high and the period is large compared to the wavelength, the grid is quite transparent for electromagnetic waves. These properties can be modeled for wire grids in terms of the averaged induced current [9]. Sharp cut-off between the two regimes is there because of the finite thickness of the structure and periodicity in the normal direction. Finally, if the wires in each layer are periodically cut (introducing defects), new resonances of high transmission appear. The resonance frequencies correspond to the condition that the length of conducting sections equals one or several half-wavelengths. If the section length is large enough (sparse defects), these resonances appear in the low frequency stopband.

We explore properties of periodical structures of several layers of metal elements of various forms in detail and show that indeed all the properties observed in [4] can be found in these arrays. These structures can find practical applications in polarization-selective filters (very sharp resonances due to screening the internal layers of the structure, polarization sensitivity or polarization transformation due to the inclusion shape).

2. Operator of electromagnetic wave scattering by double-periodic arrays

Let us consider the incidence of a plane electromagnetic wave $\mathbf{E}^i = \mathbf{P}\exp(i\mathbf{k}^i \cdot \mathbf{r})$ on an infinite double-periodic array in the plane $z = 0$. Incident and scattered electromagnetic fields can be conveniently represented using transverse to Oz axis components of TE- and TM-wave sets. Consider in the beginning the incidence of a wave having transverse component of the electric field in the form

$$\mathbf{E}_t^i(\mathbf{r}) = \boldsymbol{\psi}_{m'n'}^{(p)}(\boldsymbol{\rho})\exp(-i\Gamma_{m'n'}z), \qquad (1)$$

where index t denotes transverse to Oz axis components of the electric field, $p = 1$ corresponds to TE-waves, and $p = 2$ corresponds to TM-waves,

$$\boldsymbol{\psi}_{mn}^{(1)}(\boldsymbol{\rho}) = \frac{1}{\sqrt{Q}} \frac{\boldsymbol{\chi}_{mn} \times \mathbf{e}_z}{\chi_{mn}} e^{i\boldsymbol{\chi}\cdot\boldsymbol{\rho}}, \quad \boldsymbol{\psi}_{mn}^{(2)}(\boldsymbol{\rho}) = \frac{1}{\sqrt{Q}} \frac{\boldsymbol{\chi}_{mn}}{\chi_{mn}} e^{i\boldsymbol{\chi}\cdot\boldsymbol{\rho}} \tag{2}$$

are vector harmonics; $\boldsymbol{\chi}_{mn} = \mathbf{e}_x(k_x^i - 2\pi m/d_x) + \mathbf{e}_y(k_y^i + -2\pi n/d_y)$, $\Gamma_{mn} = \sqrt{k^2 - \chi_{mn}^2}$, $\boldsymbol{\rho} = \mathbf{e}_x x + \mathbf{e}_y y$, $Q = d_x d_y$, d_x and d_y are the array periods along Ox and Oy axes, respectively. The corresponding reflected field we write as

$$\mathbf{E}_t^r(\mathbf{r}) = \sum_{q=1}^{2} \sum_{m=-\infty}^{\infty} \sum_{n=-\infty}^{\infty} a_{mn}^{(pq)}(\boldsymbol{\chi}_{m'n'}) \boldsymbol{\psi}_{mn}^{(q)}(\boldsymbol{\rho}) \exp(i\Gamma_{mn} z). \tag{3}$$

If the set of partial waves

$$\mathbf{E}_t^i(\mathbf{r}) = \sum_{p=1}^{2} \sum_{m'=-\infty}^{\infty} \sum_{n'=-\infty}^{\infty} q_{m'n'}^{(p)} \boldsymbol{\psi}_{m'n'}^{(p)}(\boldsymbol{\rho}) \exp(-i\Gamma_{m'n'} z) \tag{4}$$

is incident upon an array, the reflected field may be represented in the form

$$\mathbf{E}_t^r(\mathbf{r}) = \sum_{q=1}^{2} \sum_{m=-\infty}^{\infty} \sum_{n=-\infty}^{\infty} b_{mn}^{(q)} \boldsymbol{\psi}_{mn}^{(q)}(\boldsymbol{\rho}) \exp(i\Gamma_{mn} z). \tag{5}$$

Let us define an operator of scattering by a double-periodic grating as an operator which connects coefficients $b_{mn}^{(q)}$ of the reflected field and the coefficients $q_{m'n'}^{(p)}$ of the incident field:

$$b_{mn}^{(q)} = \sum_{p=1}^{2} \sum_{m'=-\infty}^{\infty} \sum_{n'=-\infty}^{\infty} a_{mn}^{(pq)}(\boldsymbol{\chi}_{m'n'}) q_{m'n'}^{(p)} \tag{6}$$

or, in short operator notation, $b = rq$, where r is the operator of reflection. Coefficients $a_{mn}^{(pq)}(\boldsymbol{\chi}_{m'n'})$ may be found by using any known method of the analysis of electromagnetic wave scattering by single double-periodic arrays. Method of moments may be used particularly in the cases of wave scattering by arrays of thin strips [10 – 12].

Let us consider the incidence of a plane electromagnetic wave with the frequency that is below the lowest of the so-called sliding frequencies, i.e. the frequency values which divide frequency regions corresponding to propagating or evanescent spatial partial waves. Further, only the amplitudes of propagating waves will be important, i.e., we will consider characteristics of the reflected fields at positions spaced from the array plane so that the influence of non-propagating partial waves can be neglected. Operator of reflection in this case may be defined approximately by expression $b^{(q)} = \sum_{p=1}^{2} a^{(pq)} q^{(p)}$, where the lower indices are omitted for shortness, they are all equal to zero. All the statements formulated above regarding operator of reflection are correct also for operator of transmission t.

3. Operators of reflection and transmission for a system of a finite number of arrays

The structure is assumed to be equidistant and to consist of identical arrays. The field in each gap between planar arrays may be represented in the form of a set of partial TE- and TM-waves. The amplitudes of the transverse components of the partial waves are denoted as following: q for the incident field, $r^{(n)}q$ for the reflected field, $t^{(n)}q$ for the transmitted field, and $A^{(n-1)}$, $B^{(n-1)}$ for the fields in the gap between the next to the last array and the last array of the structure, see Fig. 1.

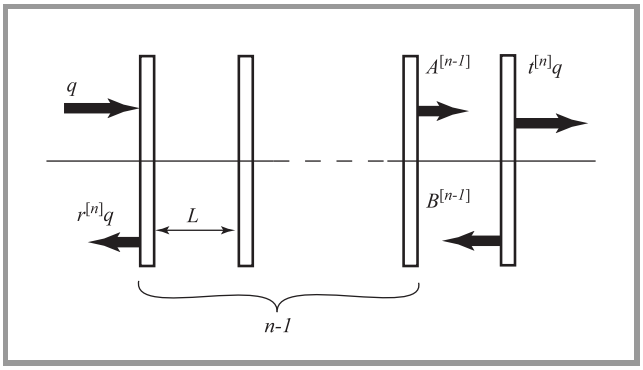

Fig. 1. Layered array: amplitudes of the reflected, transmitted, and partial waves.

Let us assume operators r, t for a single array to be known, as well as $r^{(n-1)}$, $t^{(n-1)}$ for the system of $(n-1)$ arrays, and show that the operators for the whole system can then be found recursively. The amplitudes of the partial waves satisfy equations

$$A^{(n-1)} = t^{(n-1)}q + r^{(n-1)}eB^{(n-1)},$$

$$B^{(n-1)} = reA^{(n-1)},$$

$$r^{(n)}q = r^{(n-1)}q + t^{(n-1)}eB^{(n-1)},$$

$$t^{(n)}q = teA^{(n-1)}, \tag{7}$$

where e is the plane-wave propagator operator from the plane of one array to the next array plane. After elimination of vectors $A^{(n-1)}$ and $B^{(n-1)}$ one obtains recurrent expressions which allow to find operators $r^{(n)}$ and $t^{(n)}$ in the form

$$r^{(n)} = r^{(n-1)} + t^{(n-1)}ere(I - r^{(n-1)}ere)^{-1}t^{(n-1)}, \tag{8}$$

$$t^{(n)} = te(I - r^{(n-1)}ere)^{-1}t^{(n-1)}. \tag{9}$$

4. Numerical results and discussion

For shortness, we will call straight strips I-shaped inclusions, the shape of open loops we associate with the shape of letter C, and an Ω-shaped conductive inclusion we call the omega particle. The frequency dependence of the transmission and reflection coefficients of an array of I-shaped elements has a resonant behavior. The resonance appears when the length of an element approximately equals to one half of the incident wavelength. Naturally, an increase of the element length leads to a decrease of the resonant frequency. Frequency dependence of the reflection coefficient of an array of infinitely long strips (an array without defects as periodic cutting of strips) has no resonances.

Further reduction of the resonance frequency is possible by changing the element shape so that it is more compact but has a longer stretched length. In the frequency dependencies for an array of C-shaped elements there are two resonances. The second resonance appears when the length of an element is close to one and one half of the wavelength. Knowing the resonant behavior of layered structures as dependent on the shape, length of strips, periods of arrays, elements and distance between the layers we can create systems of layers with interesting and useful properties. A 4-layer structure of I-shaped strips exhibits the same behavior as the 3D wire mesh with defects described in [4].

A system with two zones of full reflection can be made using a 4-layer structure ($L = 5/6d_x$) with C-shaped elements ($a = 5/12d_x$, $\phi_1 = \pi/18$, $2w = 1/30d_x$, $d_x = d_y$). Its frequency characteristics are shown in Fig. 2. The first reflection zone is in the low frequency area. It is the first resonance (polarization along axis *Oy*) depending on the element length ($S = 2.47d_x$, $d_x = d_y$) with the resonance between the first and the fourth layers ($d_x/\lambda \approx 0.2$). The second zone is the second length resonance with resonances between layers: layer 1 and layer 2 ($L_{12} \approx \lambda/2$), layer 1 and layer 3 ($L_{13} \approx \lambda$), layer 1 and layer 4 ($L_{14} \approx 3\lambda/2$), when $d_x/\lambda \approx 0.6$.

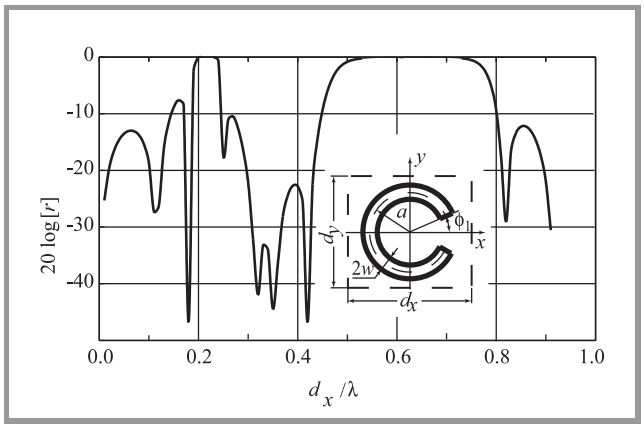

Fig. 2. Reflection coefficient from a four-layer array of C-shaped inclusions.

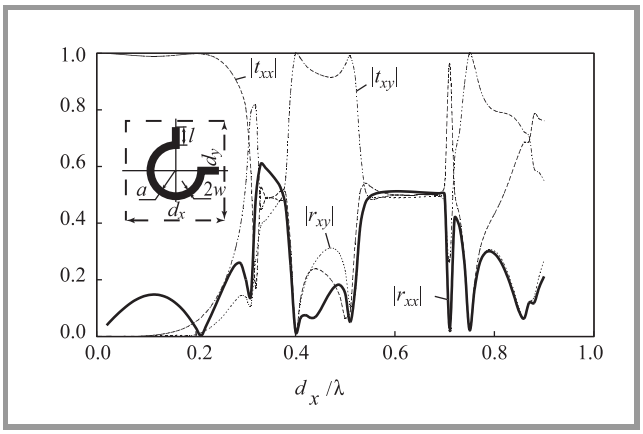

Fig. 3. Reflection and transmission coefficients from a four-layer array of Ω-shaped inclusions.

Similar behavior of the frequency dependence of the reflection coefficient we can see in Fig. 3 in the case of a 4-layer structure ($L = 0.5d_x$) with Ω-shaped elements ($a = 0.25d_x$, $l = 0.35d_x$, $2w = 0.019d_x$, $d_x = d_y$). Because we have chosen in this case symmetrical displacements of elements with respect to the diagonal of the array cells, cross-polarized field components exist in the transmitted and reflected field. There are no frequencies of full reflection in this case because of the polarization transformation. Different responses of the array on different polarizations allow to use such structures not only as frequency selective filters but also as polarization-sensitive filters.

5. Conclusion

There are three reasons for resonant behavior of the frequency dependencies of the reflection coefficient for such structures. The first reason is interference phenomena between layers. The second reason is introduced by defects (cut strips, in our case) that leads to finite length of array elements and, as a consequence, to additional resonances. The third reason is interference between layers on frequencies near to the resonant frequencies of elements in a single array. In the last case new resonances can appear because of strong dispersion of the phase of the transmission coefficient for a single array.

Regular structures of conducting elements without defects are strongly reflecting in the low frequency region. Layered structures of arrays of finite-length elements are transparent in the low frequency region and have properties of PBG structures in the frequency region where the main sizes of the elements and the whole array thickness are approximately equal to the wavelength.

Acknowledgement

This work has been supported in part by the NATO Science Programme, linkage grant HTECH.LG 974668.

References

[1] E. R. Braun, C. D. Parker, and E. Yablonovich, "Radiation properties of a planar antenna on a photonic-crystal substrate", *J. Opt. Soc. Am. B,* vol. 10, no. 2, pp. 404–407, 1993.

[2] H. Y. D. Yang, N. G. Alexopoulos, and E. Yablonovitch, "Photonic bandgap materials for high-gain printed circuit antennas", *IEEE Trans. Anten. Propag.,* vol. 45, no. 1, pp. 185–187, 1997.

[3] F.-R. Yang, K.-P. Ma, Y. Qian, and T. Itoh, "A uniplanar compact photonic-bandgap (UC-PBG) structure and its applications for microwave circuits", *IEEE Trans. Microw. Theory Techn.,* vol. 47, no. 8, pp. 1509–1514, 1999.

[4] D. F. Sievenpiper, M. E. Sickmiller, and E. Yablonovitch, "3D wire mesh photonic crystals", *Phys. Rev. Lett.,* vol. 76, no. 14, pp. 2480–2483, 1996.

[5] J. B. Pendry, A. J. Holden, W. J. Stewart, and I. Yongs, "Extremely low frequency plasmons in metallic mesostructures", *Phys. Rev. Lett.,* vol. 76, no. 25, pp. 4773–4776, 1996 (comment by S. A. Mikhailov and author's reply: vol. 78, no. 21, pp. 4135–4136, 1997).

[6] J. B. Pendry, A. J. Holden, D. J. Robbins, and W. J. Stewart, "Low frequency plasmons in thin-wire structures", *J. Phys.: Condens. Matter,* vol. 10, pp. 4785–4809, 1998.

[7] H. F. Contopanagos, C. A. Kyriazidou, W. M. Merrill, and N. G. Alexopoulos, "Effective response functions for photonic bandgap materials", *J. Opt. Soc. Am. A,* vol. 16, no. 7, pp. 1682–1699, 1999.

[8] S. I. Maslovski, S. A. Tretyakov, and C. R. Simovski, "Electromagnetic modelling of composite media with second-order spatial dispersion", in *XXVIth URSI General Assembly,* University of Toronto, Canada, 1999, p. 91.

[9] M. I. Kontorovich, M. I. Astrakhan, V. P. Akimov, and G. A. Fersman, *Electrodynamics of Grid Structures*. Moscow: Radio i Sviaz, 1987 (in Russian).

[10] S. L. Prosvirnin, "Analysis of electromagnetic wave scattering by plane periodical array of chiral strip elements", in *Proc. 7th Int. Conf. Complex Media Bianisotropics'98*, Technische Universität Braunschweig, Germany, 3–6 June 1998, pp. 185–188.

[11] T. D. Vasilyeva and S. L. Prosvirnin, "Electromagnetic wave diffraction by the plane array of chiral strip elements of complex shape", *Phys. Wave Proc. Radio Syst.*, vol. 1, no. 4, pp. 5–9, 1998 (in Russian).

[12] S. Zouhdi, G. E. Couenon, and A. Fourrier-Lamer, "Scattering from a periodic array of thin planar chiral structures – calculations and measurements", *IEEE Trans. Anten. Propag.*, vol. 47, no. 6, pp. 1061–1065, 1999.

Sergey L. Prosvirnin graduated from Kharkov Institute of Radio Electronics in 1971, and obtained the degrees of Ph.D. and D.Sc. in radio physics, and Professor Rank from Kharkov State University, Ukraine in 1974, 1986, and 1992, respectively. From 1974 to 1985, he was with the Institute of Radio Physics and Electronics. Since 1985, he has been with the Institute of Radio Astronomy (IRA), Academy of Sciences of Ukraine. He has been Head of Department of Computational Mathematics, IRA since 1989, Professor of Kharkov National University since 1987, Professor of Kharkov Institute of Air Forces of Ukraine since 1997. His main scientific interests are analytical-numerical methods in the theory of scattering and radiation of electromagnetic waves, complex media electromagnetics, and microwave engineering. He is a Senior Member of the IEEE.
e-mail: prosvirn@rian.ira.kharkov.ua
Institute of Radio Astronomy
Chervonopraporna st 4
61002 Kharkov, Ukraine

Sergey A. Tretyakov received the Dipl. Engineer-Physicist, the Ph.D., and the Doctor of Sciences degrees (all in radiophysics) from the St. Petersburg State Technical University (Russia), in 1980, 1987, and 1995, respectively. From 1980 to 2000 he was with the Radiophysics Department of the St. Petersburg State Technical University. Presently, he is Professor of radio engineering in the Radio Laboratory, Helsinki University of Technology. His main scientific interests are electromagnetic field theory, complex media electromagnetics and microwave engineering. Prof. Tretyakov served as Chairman of the St. Petersburg IEEE ED/MTT/AP Chapter from 1995 to 1998.
e-mail: sergei.tretyakov@hut.fi
Radio Laboratory
Helsinki University of Technology
P.O. Box 3000, FIN-02015 HUT, Finland

Tetyana D. Vasilyeva received the Dipl. in electronics engineering from Kharkov University of Radio Electronics, Ukraine, the Ph.D. in radiophysics from Kharkov State University, Ukraine in 1981, and 1992 respectively. She was with the Institute of Radio Physics & Electronics from 1981 to 1985, and with the Institute of Radio Astronomy (IRA), Academy of Sciences of Ukraine from 1985 to 2000. Presently, she is application analyst in HiTech Network Inc., Toronto, ON, Canada. Her main scientific interests are numerical modeling and analysis in the electromagnetic theory of complex media, and in microwave techniques.
e-mail: tetyana.vasilyeva@sympatico.ca
2500 Keele st, #602
Toronto ON, M6L 2N5, Canada

Arlette Fourrier-Lamer
afl@ccr.jussieu.fr
Laboratoire de Genie Electrique de Paris LGEP
Supelec, France

Said Zouhdi
sz@ccr.jussieu.fr
Laboratoire de Genie Electrique de Paris LGEP
Supelec, France

Paper

Antennas of vehicles landing on a planet surface

Kira K. Belostotskaya

Abstract — The antenna systems designed under the international projects "Mars-96" and "Phobos" are described. The antenna system of Small station landing on Mars, in flight is packed under protective petals of the station and is opened on a surface with the help of flexible legs. The original scheme of excitation in the form of compact strip-geometry is described. The antenna system of the mobile vehicle landing on Phobos, provides the omnidirectional pattern on the basis of the combination of antenna methods with methods of processing of the received signal. The high efficiency of the antenna results from its construction in the form of an active antenna.

Keywords — antenna system, omnidirectional pattern, active antenna.

The small vehicles which are landed on a surface of planets, must have, as a rule, very limited sizes and weight. At a phase of overfly in a transport position the antenna devices should be packed inside the vehicle and in working position it is appropriate to use the elements of the vehicle in a design as components of the antenna. The radio system of Small automatic station landed on a surface of Mars (international project "Mars-96"), was equipped with receiving system. The system received a command from the orbital spacecraft to switch on the equipment for the scientific information transmission.

The communication was realized by transmiting-receiving antenna. The antenna provided a reception on a frequency of 437.1 MHz and transmission on a frequency of 401.5272 MHz. The requirements to the pattern were determined by communication angles with the orbital spacecraft. The antenna should have a radiation characteristic in the upper half-space (on azimuth – omnidirectional, on an elevation – $\pm 70^\circ$ from a direction in zenith). The field of radiation – circular right hand with elliptic coefficient not worse then 4 dB in a zone of working angles.

The external outlines of the upper hemisphere of the station and system of legs in the form of flexible contoured metal ribbons for the lift of the antenna and installation it into working position were determined during the designing of the antenna. Besides, the scientific devices were placed above the antenna and on the elements of legs.

The antenna system represents a dipole antenna of turnstile type (Figs. 1 and 2). Four arms of dipole assume the position at which the pattern on two frequencies is satisfactorily formed. The metallized top of a station surface served as the reflector for the antenna, forming its radiation in the upper hemisphere.

The height of dipole above a station surface, and also their inclination to a vertical axis of station was selected from conditions of synthesis of maximum gain within working angles on two operational frequencies. The increase of the antenna bandwidth was reached by selection of strip width

Fig. 1. Mars Small station.

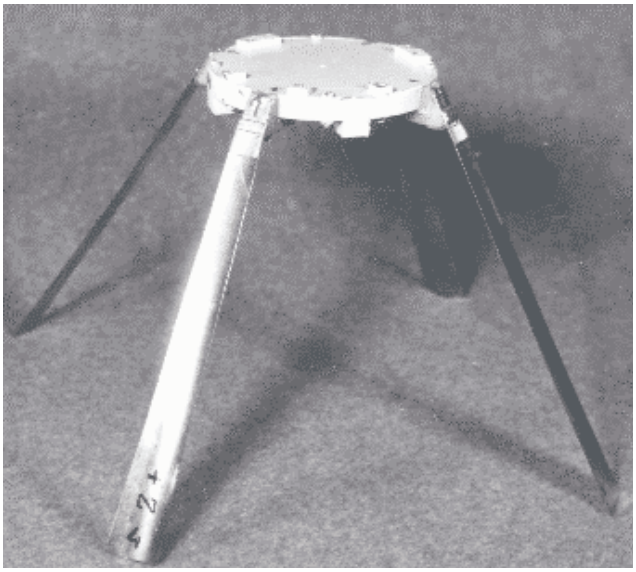

Fig. 2. Antenna system of Mars Small station.

of dipole. As dipoles are for long in a folded bent condition in notches of protective dielectric coating of station, the plates have a special configuration and special limiter. The material of a plate – bronze with special thermal treatment. Four dipole were excited with shift of 90°, providing the

circular polarization field which is omnidirectional in an azimuth plane.

The essential problem has arisen at working out of the device of excitation, phasing and matching. The necessity of the installation of scientific devices practically in "body" of the antenna was the reason of this problem. As a result the dipole lost its ordinary point of a feed, because the arms of dipole have been strongly removed one from the other. From the diplexer of transponder to the antenna could be made only one flexible cable along the one of four legs and whole beam-forming network (BFN) should be placed in a small volume under the scientific device occupying the center of a symmetry of the station. The height of this volume was limited also. As a result the beam forming network and design of a feeding unit became complicated and required fine turning. The scientific devices and flexible legs change the input impedance. The input impedance has a sharp frequency response because the arms have nonresonance sizes on working frequencies. As a result, matching could be fulfilled on two separate working frequencies only (Fig. 3). The scheme of excitation and matching of turnstile antenna are made as a three

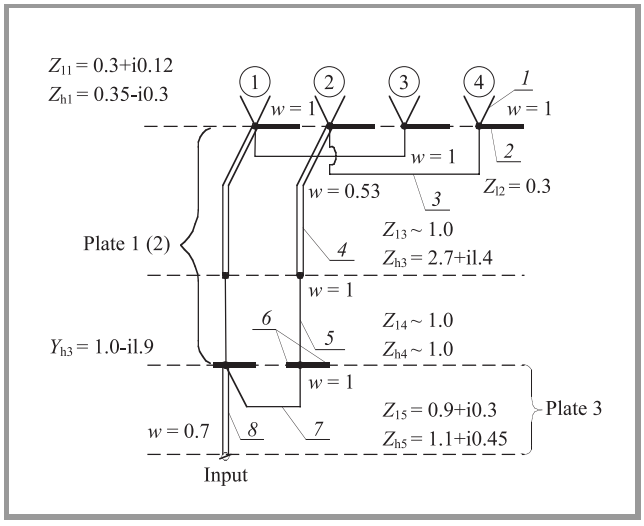

Fig. 3. Excitation and matching scheme of turnstile antenna. Explanations: *1* – dipole; *2* – symmetrizing section $1/4(\lambda_1+\lambda_h)$; *3* – matching stub for f_1; *4* – $\lambda_1/4$ transformer; *5* – shift transformer for f_h; *6* – resonant stub $\lambda_1/2$; *7* – $\lambda/4$ phasing section $1/8(\lambda_1+\lambda_h)$; *8* – matching transformer $1/2(f_h+f_1)$.

plate set of symmetrical microstrips of a complex configuration on disks with a diameter of 78 mm. There is a 180°-phase shifter on the first plate for first pair of opposite arms (Fig. 4). There is a 180°-phase shifter on the second plate for identical matching of the second pair of arms. At first the antenna matching is made on low frequency with the help of a transformer and a stub. Then after transformation on the low frequency the stub which provided the matching on the upper frequency is connected. The phasing on 90° and final matching is executed on the third plate. The scheme is terminated by the connector such as SMA, to which was connected cable mounted on a leg. The antenna system must operate with high reliability in conditions of low temperatures (−100°C ... 140°C). For this reason conductors connecting the dipoles with BFN as well as the connectors between plates must had redundant length. The feed points of dipole are protected by a polyurethane compound. The full losses in the antenna system are evaluated in 1.7 dB.

The antenna system gain with polarization losses in 95% in the zone of working angles had values: −4.2 dB on $f = 401.5272$ MHz and −3.9 dB on $f = 437.1$ MHz. Weight of the antenna system with a cable 1060 mm long was 240 g. The tests in conditions of statistical, dynamic and impact accelerations, and also at reduced temperature were conducted on the antenna system which was a component of a technological experimental model of Small station. After these tests the parameters of the antenna were kept.

Other example of unique development is the antenna system of the vehicle landing on the surface Phobos. The multipurpose international space project "Phobos" provided the activity of mobile vehicle on a surface during a long period (Fig. 5).

The vehicle was equipped with radio telemetry system for transmission of the data of ground research to the spacecraft and also command radio link for periodic turn on of transmitting system of vehicle. The orientation of the mobile vehicle on a surface could be any. The task of formation of the omnidirectional characteristics of radiation requires a combination of antenna means with certain circuit designs. Here double-frequency transmission and two-channel signal reception was used. By this principle two independent patterns were added so that the zones of a low gain of one pattern were filled by radiation with a high gain from the another. The number of antennas in a system is selected from a condition $n \geq 1.5 \ldots 1.8$ ka, where ka-electrical radius of the vehicle. Depending on processing methods the synthesized pattern is equal either sum, or envelope of large values of the pattern of separate channels. On the vehicle two antennas on sphere surface separated on 90°. The small frequency separation of antennas (about 7%) has allowed to use the antenna devices of the identical sizes in channels $f_1 = 280$ MHz; $f_2 = 300$ MHz. It is necessary to mark, that of the double-frequency principle provides an actual hot-standby operation of a system, the failure of one channel does not result in a full communications breakdown, and only limits a zone of working angles.

The requirement concerning absence of outstanding antenna elements over a shell of the mobile vehicle has determined the size of antenna vertical parts. The size of outstanding parts must be not greater than 0.025 wavelengths. This task was decided by designing the antenna system of an active type. The antenna was made as the Γ-shaped quarter-wave oscillator of a shunt feed directly incorporated with a transmission device (Fig. 6).

For selection of an optimum regime of an antenna matching with the transistors the power diagram of the transis-

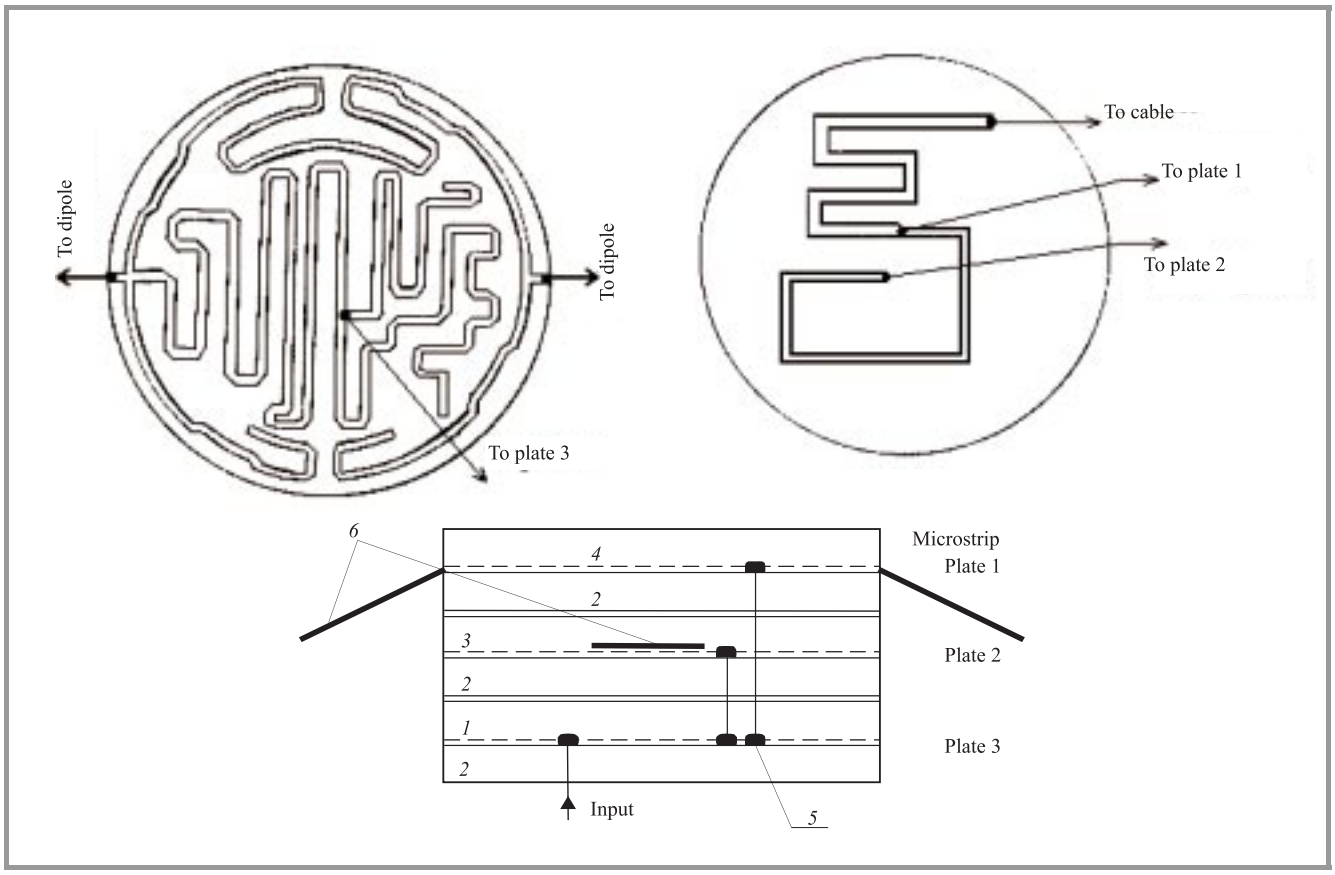

Fig. 4. Beam forming microstrip plates. Explanations: *1* – 90°-shift plate; *2* – empty layer; *3* – 180°-shift and matching plate (1 – 3); *4* – 180°-shift and matching plate (2 – 4); *5* – coaxial strip; *6* – dipole.

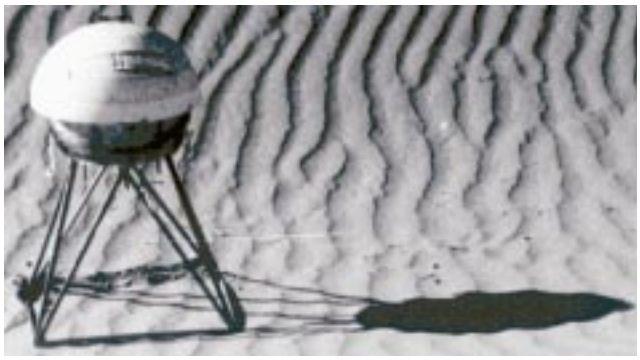

Fig. 5. Phobos mobile vehicle.

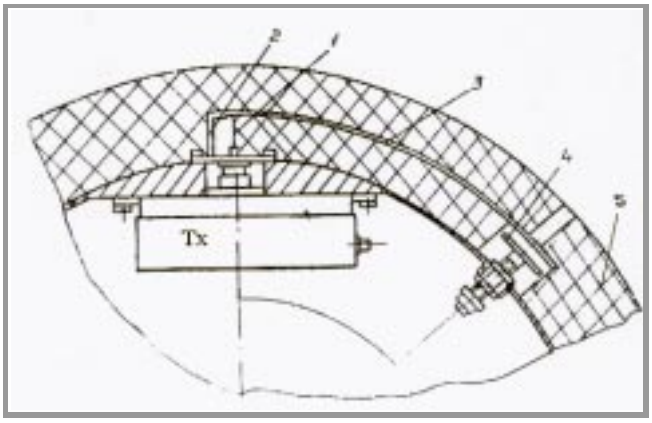

Fig. 6. Active antenna. Explanations: *1* – exciter; *2* – short-circuit vertical part; *3* – stub turner; *4* – capacity disk; *5* – dielectric shell.

tor of an output circuit was used. Active component of input impedance was determined by the position of an exciting element relative to a short-circuit vertical part of the antenna, and reactance component was provided with selection of length of a horizontal part-stub and tuning elements – capacity disk. In a whole sphere the gain of a double-frequency telemetry system was greater than 0.4. Thus efficiency of an active antenna was determined only by thermal losses in antenna elements and shell, and at the height of vertical parts equal to $1/40\lambda$ it was high enough (about 70%). At flight tests the estimation of ground influence on the characteristics of the antenna was carried out. The tests were conducted with the completely assembled mobile vehicle covered a protective dielectric shell. It has been found that the direct contact of the mobile vehicle with soil can reduce the value of a gain by 3 dB. The thermal frequency stability of tuning was evaluated using the variation of a resonance frequency in range of temperatures

from +50°C to −40°C. For the given design the variation of an input impedance practically did not change a radiation power which was given back by the transmitter to the antenna.

Kira K. Belostotskaya was born in Moscow, Russia, in December 1934. She received the Candidate of Technical Science (Ph.D.) degree in electrical engineering (antennas and microwave devices) from the Moscow Power Engineering Institute (MPEI) in 1971. In 1958–1966 a Research Scientist in the Special Research Bureau of MPEI (OKB MEI). In 1967–1980 a Leading Research Scientist in OKB MEI. Since 1981 a Chief of Laboratory (design of telemetry and telecommand radiolinks; energy budget of radiolinks; design of onboard antenna system; electromagnetic compatibility of onboard systems) in OKB MEI. Member of various projects, including: "Venus 15, 16" – Antenna system of SAR, "Phobos" – Antenna system of moving vehicle, "Mars 96" – Antenna system of Small station, IRS (India) – design of radiolinks, "Solar Sail" – VHF antenna. She is author of more then 100 publications, including Planetary and Space science, Telecommunications and Information Technology.
Kirabelst@inbox.ru
Special Research Bureau
of Moscow Power Engineering Institute (OKB MEI)
Krasnokazarmennaya st 14
Moscow 111250, Russia

Paper

Characteristics of the indoor propagation channel in 1.9 GHz band

Krzysztof Kurek, Dariusz Janusek, Tomasz Kosiło, and Józef Modelski

Abstract — This paper presents results of propagation measurements carried out in the frequency range 1.8 – 2.0 GHz inside a building, using network analyser. Wideband properties of the channel, described through mean delay and delay spread, and a narrowband local statistics of the received power have been presented. For each transmitter and receiver antennas location two propagation cases have been considered, line of sight (LOS) and obstructed line of sight (NLOS) – the direct path component was attenuated by radio absorbing mat near the receiver.

Keywords — indoor propagation channel, channel impulse response, time dispersion.

1. Introduction

In last years the number of mobile system applications is growing very fast. Such systems as cellular (GSM 900, GSM 1800) and cordless (DECT, PHS) are widely used, the next generation cellular system (UMTS 2000) is planed for the year 2002 [4]. WLAN and ISM (e.g. Bluetooth [5]) systems are also extensively developed. In many situations those systems will be used in highly urbanised areas and inside buildings. Indoor signal propagation strongly depends on building configuration and material used. The received signal is a sum of multipath components reflected, diffracted and diffused on surrounding objects (walls, obstacles, etc.). Because amplitude, phase and delay of each component changes very fast as a result of terminal movement (or movement of surrounding objects, peoples in building for example) the received signal fluctuates. For narrowband observation the main result is fading – variation of the signal strength, and for wideband observation time dispersion, causing intersymbol interferences is the main effect. The more detailed description of indoor propagation can be found in literature e.g. [1 – 3].

The knowledge of the propagation channel properties is necessary for a communications system design allowing determining maximal signal bandwidth, kind of equalisation in receiver and transmitter locations as well. The problem of effective indoor channel measuring and modelling is discussed in many papers e.g. [6 – 10]. This paper presents results of the channel measurements, in 1.9 – 2 GHz band. We were mainly interested in the influence of direct ray on channel properties. After description of measurement procedure, wideband characteristics of the channel and the narrowband statistics of the received power variations are presented. Conclusions are presented at the end.

2. Procedure of measurements

The wideband channel propagation characteristics were measured in frequency domain, by use of HP8720C vector network analyser [6]. Block diagram of the measuring system is presented in Fig. 1. An output signal from the analyser (output power −10 dBm) is connected to the transmitting antenna through 6 m coaxial cable. Signal from the receiving antenna is amplified by additional 35 dB amplifier and sent through 24 m cable to analyser input. The 2 dBi omnidirectional, vertical polarised antennas, placed at 1.3 m height over the floor were used for transmission and reception.

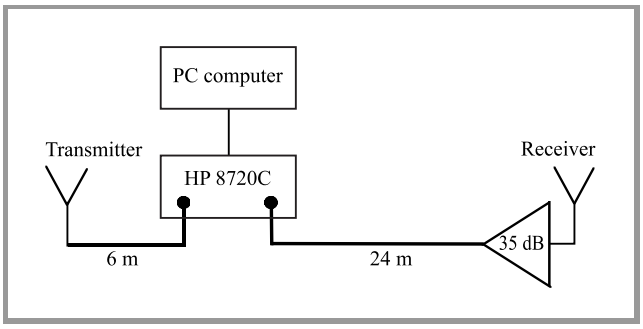

Fig. 1. Block diagram of the measuring system.

The direct measurements result was channel transfer function. The channel impulse response was calculated, using IFFT, with 5 ns time resolution. It means that all multipath components that reached the receiver antenna in 5 ns time interval are shown as one impulse whose amplitude depends on vector sum of these components. Measurements were done in the building of the Faculty of Electronics and Information Technology, Warsaw University of Technology at two locations: in a laboratory room (5.5 m wide and 6 m long) and in a corridor (2.6 m wide and 30 m long). The external walls of those places are concrete with glass windows, internal walls are of brick. For each measuring session the transmitting antenna (Tx) was fixed, and the receiving antenna (Rx) was moved along lines parallel to walls:

- in the laboratory room along two lines: towards the Tx antenna and perpendicular to them;
- in the corridor along line towards the Tx antenna only.

For each Rx antenna location two types of propagation were arranged: LOS and NLOS. The direct ray was at-

tenuated by putting radio wave absorbing plate (Laminated absorber AEL – 4.5, of Advanced ElectroMagnetic INC., dimensions 0.6×0.6 m, reflection attenuation > 20 dB, for freq. $>$ 0.6 GHz) in front of the receiving antenna.
We characterise the channel dispersive properties by typical parameters: mean delay and delay spread, calculated from the power delay profile [1]. The following assumptions have been done during measured data treatment:

a) threshold level 30 dB below maximum component of the impulse response is assumed; e.g. all the smaller values are treated as noise and are not taken into analysis;

b) the impulse response delay is defined relatively to the first component (first received path).

3. Analysis of results

Typical examples of measured propagation channel transfer functions and normalised impulse responses for LOS and NLOS situation are presented in Fig. 2. Both impulse responses are normalised to the level of non obstructed direct ray for LOS. During NLOS direct ray is attenuated because of that a relative level of multipath components in the received signal is larger and channel is more time dispersive. Additionally received power for this case is smaller. Changes of the channel properties for LOS and NLOS situations are especially large for small distances between *Tx* and *Rx* antennas, when amplitude of non attenuated direct ray is dominant in the received signal (about 20 dB above multipath components for distances $1-2$ m). Figure 3 shows average values of these dispersive parameters for the propagation in laboratory room. Attenuation of LOS component causes an increase of average mean delay from 6 ns to 10 ns and average delay spread from 8.8 ns to 10.7 ns. In the case of measurements at the corridor average values are respectively 10.8 ns and 23.4 ns, and after LOS ray obstruction average mean delay changed to 14.1 ns and average delay spread to 29.1 ns. Values of dispersive parameters also depend on distance between transmitter and receiver antennas, local average values of them are larger with increasing of distance.

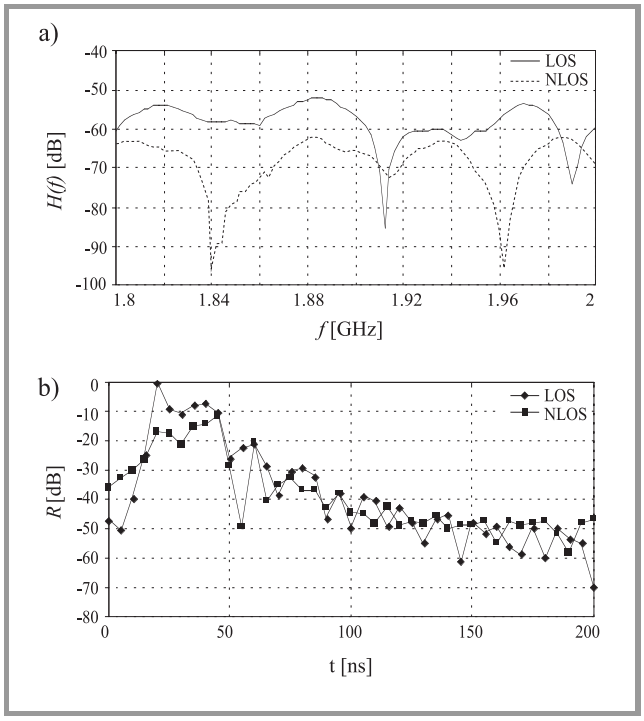

Fig. 2. Transfer functions (a) and normalised impulse responses (b) of the propagation channel for LOS and NLOS situations.

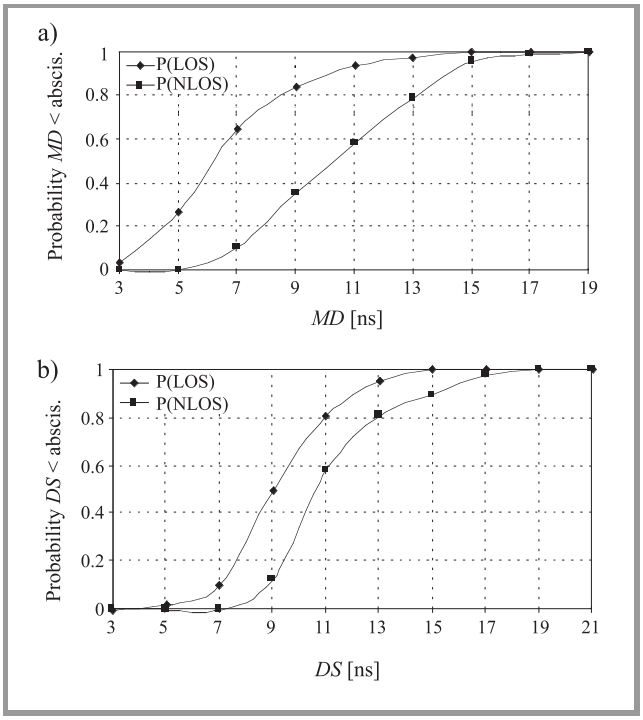

Fig. 3. Cumulative probability distributions of the mean delay (a) and delay spread (b) for measurements in laboratory room.

Figure 4 shows the average power delay profiles for two analysed places. That curves were calculated from all the measurements for the laboratory and the corridor respectively. The laboratory profile is very regular. At the corridor profiles there are two strong components: a) first (direct) component which is a sum of direct ray and rays reflected from walls and floor with delay less than the time resolution of measurements (because the corridor is long and narrow); b) large amplitude multipath component with delay 100 ns, which is caused by a ray reflected from the metal door at one end of the corridor.
In Fig. 4 the aproximation of the delay profiles by a simple exponential function is also shown. The laboratory room propagation is modeled by the function $p(t) = e^{-mt}$, where m is slope of the profile. For the LOS propagation case m is -1.2 and for NLOS situation m is -0.8. The

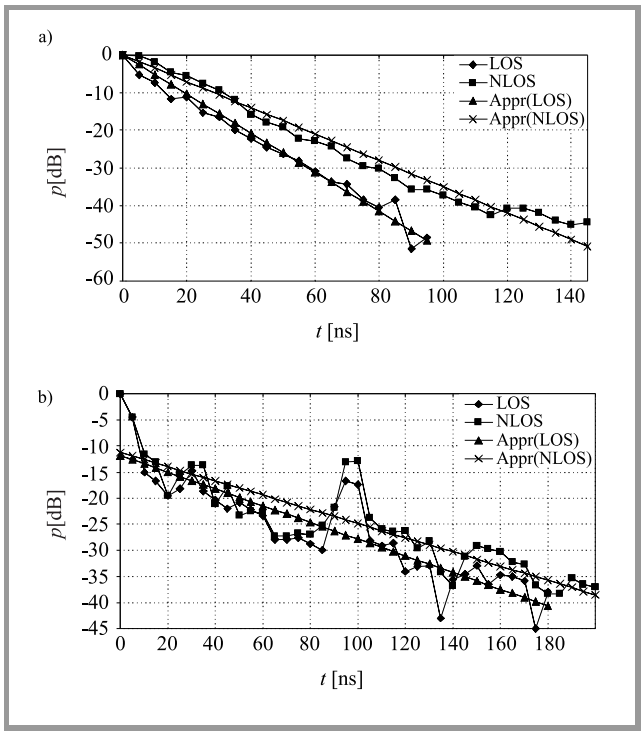

Fig. 4. Average power delay profiles of the propagation channel and their exponential approximations: (a) for laboratory room; (b) for corridor.

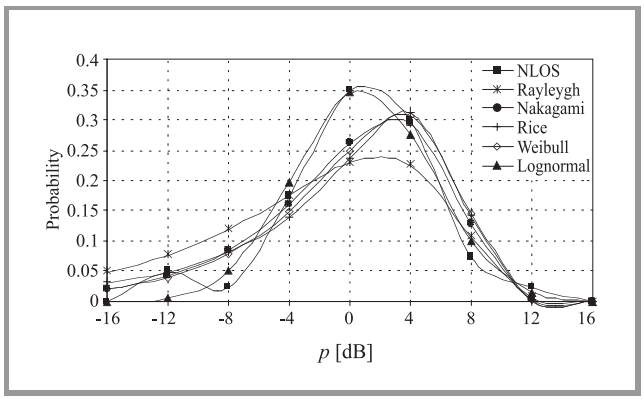

Fig. 5. Probability density function of the received power for NLOS situation and its approximations by commonly used distributions (with identical mean values and standard deviation).

corridor propagation is aproximated by a modified function $p(t) = k \cdot e^{-mt}$, where m is 0.37 and k is 0.066 for LOS, and m is 0.31 and k is 0.076 for NLOS situation.

Figure 5 presents an example of narrowband signal properties. We analysed the probability density function of received power at one frequency (1.9 GHz) from measurement taken at laboratory room. The receiving antenna was moved along a line parallel to the transmitter in 10 cm steps from wall to wall of the laboratory. The distance between the measuring line and the Tx antenna was 6 m. Then statistics of the power variation normalised to the mean values have been calculated. For both LOS and NLOS situations local mean power changes with the receiver location, and obtained statistics are similar. Example of probability density function (PDF) of the received power at the frequency 1.9 GHz for NLOS situations is presented in Fig. 5, for comparison PDF's of common used distributions [7]: Rayleigh, Rice, Nakagami, Weibull, lognormal all with identical mean values and standard deviations are also shown. From our analysis its clear that for both LOS and NLOS situations, lognormal distribution best fits to experimental data.

4. Conclusions

Results of measurements for the indoor propagation channel in 1.9 GHz band have been presented. Wideband characteristics of the channel and the received power depend strongly on existence of visibility between antennas. Obstruction of line of sight path causes decrease of received power and increase of time dispersive properties of the propagation channel, especially for small distances between antennas. From our measurements there is a clear indication that in micro-cellular systems direct ray propagation situation should be preferred. That can be rather easy realised by putting base-station high on the walls or on a ceiling.

References

[1] T. H. Rappaport, *Wireless Communications: Principles and Practices*. Piscataway: IEEE Press, 1996.

[2] G. L. Stüber, *Principles of Mobile Communication*. Boston: Kluwer, 1996.

[3] J. D. Parsons, *The Mobile Propagation Channel*. London: Pentech Press, 1992.

[4] R. Prasad, *Universal Wireless Personal Communication*. Boston/London: Artech House, 1998.

[5] Specification of the Bluetooth System, Bluetooth, July 1999. [Online]. Available WWW: www.bluetooth.com

[6] S. J. Howard and K. Pahlavan, "Measurement and analysis of the indoor radio channel in the frequency domain", *IEEE Trans. Instr. Measur.*, vol. 39, no. 5, pp. 751–755, 1990.

[7] H. Hashemi, "The indoor radio propagation channel", *Proc. IEEE*, vol. 81, no. 7, pp. 943–968, 1993.

[8] V. Erceg, S. J. Fortune, J. Ling, A. J. Rustako, and R. A. Valenzuela, "Comparisons of a computer-based propagation prediction tool with experimental data collected in urban microcellular environments", *IEEE Trans. Select. Areas Commun.*, vol. 15, no. 4, pp. 677–684, 1997.

[9] G. Wölfle, B. Gschwendtner, and F. M. Landstorfer, "Intelligent ray tracing – a new approach to the field strength prediction in microcells", in *IEEE 47th Vehic. Technol. Conf. (VTC)*, Phoenix, May 1997, pp. 790–794.

[10] A. J. Motley and J. M. Keenan, "Personal communication radio coverages in buildings at 900 and 1700 MHz", *Electron. Lett.*, vol. 24, no. 12, pp. 763–764, 1988.

Krzysztof Kurek was born in Jadow, Poland in 1970. He received the M.Sc. degree in electronics engineering from Warsaw University of Technology, Institute of Radioelec-

tronics in 1996. He is currently working towards the Ph.D. degree at Warsaw University of Technology, Institute of Radioelectronics. His research interest is in modelling of the propagation channel in mobile communications systems. He worked on several projects related to radiowave propagation: "Wideband analysis of the propagation channel in mobile broadband system" in 1997 (at Technical University of Lisbon, Portugal), "Characterisation of the indoor propagation channel in 1.9 GHz band" in 1999/2000, "Analysis of the propagation channel properties in wireless communications systems" in 2001. He is student member of IEEE.
e-mail: k.kurek@ire.pw.edu.pl
Institute of Radioelectronics
Warsaw University of Technology
Nowowiejska st 15/19
00-665 Warsaw, Poland

Dariusz Janusek was born in Wroclaw, Poland. He received the M.Sc. degree from Warsaw University of Technology, Institute of Radioelectronics, Radiocommunications Division in 1997. He was graduated with honours. Since 1997 he is a Ph.D. student at Warsaw University of Technology, Institute of Radioelectronics, Nuclear and Medical Electronics Division. Since 2000 he is a member of Technical Commission 183 "Safety of Information Technology, Telecommunications and Business Equipment", Polish Committee for Standardisation. During his Ph.D. studies he worked on several projects related to radio communication: in 1998 "Short radio for the remote power meter reading", in 1999 "Remote power control using LW radio transmitter" and in 2000 "Characteristic of the indoor propagation channel in 1.9 GHz". He has open project: "New algorithms of T-wave alternans identification in high resolution ECG", which is his Ph.D. thesis.
e-mail: janusek@ire.pw.edu.pl
Institute of Radioelectronics
Warsaw University of Technology
Nowowiejska st 15/19
00-665 Warsaw, Poland

Tomasz Kosiło was born in Lublin, Poland on November 19, 1946. He received the M.Sc. degree in radiotechnics in 1970 and Ph.D. degree in radiocommunication in 1978, both from Warsaw University of Technology. From 1971 he was employed at the Warsaw University of Technnology where he is now an Assistant Professor and head of the Radiocommunication Group. His field of interests is in advanced communication system, digital modulation and demodulation, measurements of channels and propagation media.
Institute of Radioelectronics
Warsaw University of Technology
Nowowiejska st 15/19
00-665 Warsaw, Poland

Józef Modelski – for biography, see this issue, p. 39.

Paper

Distortion and noise problems of subcarrier multiplexed optical systems

Eszter Udvary and Tamás Marozsák

Abstract — In this paper investigation of subcarrier multiplexed optical subsystems for optically supported communication systems is presented. Noise and spurious free dynamic range are the main parameters, which are determined by the applied optical transmission. The frequency dependence of these parameters and optimal frequency chosen is presented.

Keywords — wireless communications, distortion and noise problems, subcarrier multiplexed optical subsystems.

1. Introduction

In many applications of analog fiber optic links the link noise figure or output signal to noise ratio and intermodulation free dynamic range are two of the most important parameters. Great dynamic range and high linearity are necessary in the subcarrier multiplexed optical transmission system to have good system performance and avoid channel cross-talk. These parameters can be determined by the optical transmitter and depend on frequency and level of optical reflection. This dependence has not been satisfactory investigated, here some measurement results and noise calculations are presented in connection of realization of an optically supported millimeter wave (MMW) cellular radio system.

2. Optical link in radio systems

One possible radio system can be seen in Fig. 1. This proposed system is based on the simultaneous transmission of the information and the reference signal via intensity modulated optical distribution system. The reference and information signals are placed in the low microwave frequency range (about 1 GHz). In this approach instead of transmitting the millimeter-wave signal, one of its subharmonic is optically transmitted and at the reception side the millimeter-wave is generated utilizing the subharmonic signal as a reference frequency. A single mode laser is intensity modulated by the subharmonic reference signal and several subcarriers, which are used for the optical transmission of the information channels [1]. Hence, the key parameters of the optical transmission system are noise and linearity which can be dominant in the whole system.

3. Optical noise sources

A typical microwave fiber optic link consists of a laser source may be with an external modulator (Mach-Zehnder or electro-absorption modulator), the fiber optic transmission medium, optical amplifier (fiber or semiconductor) and an optical detector. These components are the noise sources of the optical link. Because these noise sources are independent, they can be simply added.

Conventional direct modulation of laser diodes has the problems with an adverse frequency spread (chirp) and with a frequency response, which is limited by the internal resonance between the electrons and photons. The amplitude, power and frequency of the laser as an oscillator have some fluctuations. The semiconductor laser source is characterized by the relative intensity noise (RIN) and the equivalent electrical noise power $(N_L(f))$ is generated in the laser:

$$RIN(f) = \frac{\langle \Delta P^2(f) \rangle}{P_L^2}, \quad N_L(f) = RIN(f) \cdot P_L \cdot B, \qquad (1)$$

where $\langle P^2(f) \rangle$ – spectral density of the square of the laser optical power fluctuation, P_L – steady-state optical power output from laser, B – bandwidth.

The frequency dependence of the *RIN* is rather high, it can change more than 10 dB in the lasers bandwidth (Fig. 2). This way in the data sheet given usual value, 140 dB/Hz cannot be always used for accurate calculations. The *RIN* also changes with biasing, to eliminate this effect as high bias current should be applied as possible. This is also good for laser stability and linearity also.

The linearity of the direct modulated laser source depends on bias current, level of optical reflection in the system, and frequency. This is shown in Fig. 3, where a conventional Fabry-Perot laser was biased over 1 mW optical power in the single mode fiber, the RF power was 0 dBm which created $m = 23\%$ modulation depth. The measurement was done by two carriers with 1 MHz spacing, and the level of the third order mixing product was measured. The $3-5$ dB proving effect of the isolator can be observed. In the $1-1.6$ GHz range the linearity changes a lot with frequency, it even overtakes the non-isolator case. This effect was reproducible, and therefore 1.6 and 1 GHz was chosen for the system as optimum frequency for the optical transmission. The laser *RIN* was also lower than in higher frequencies.

Two types of the external modulators are widely used. The first one is the electro-optic (EO) $LiNbO_3$ Mach-Zehnder modulator and the second one is the multiple-quantum-well (MQW) electro-absorption optical modulator. For an

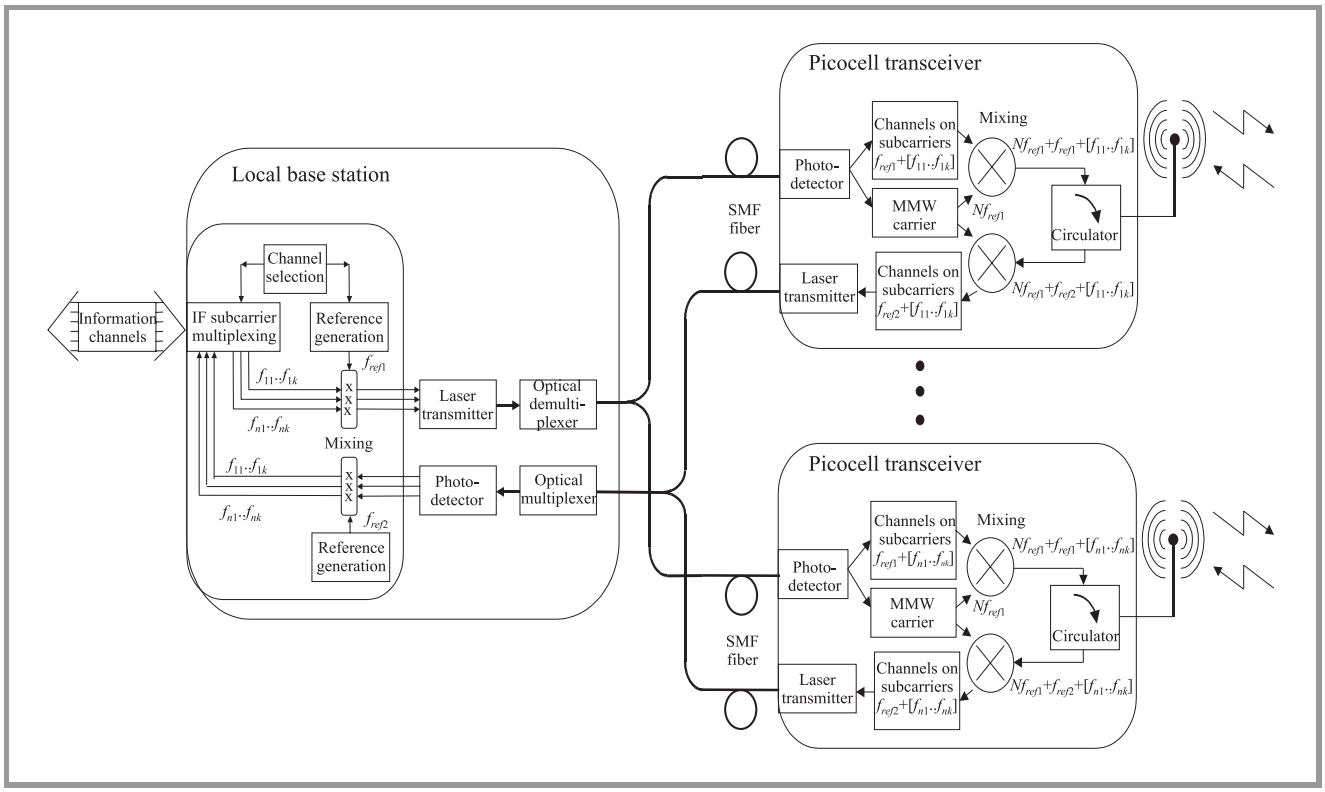

Fig. 1. Optical supported fiber radio system.

externally modulated link the noise figure decreases with increasing laser power. The shot noise of photodiode increases linearity, while the link gain increases as the square of the laser power. This is because the modulation depth depends only on the external modulator RF input power. However, for a direct modulated optical transmitter the noise figure increases, because the link gain is independent of laser power, it depends only on the RF power [2].

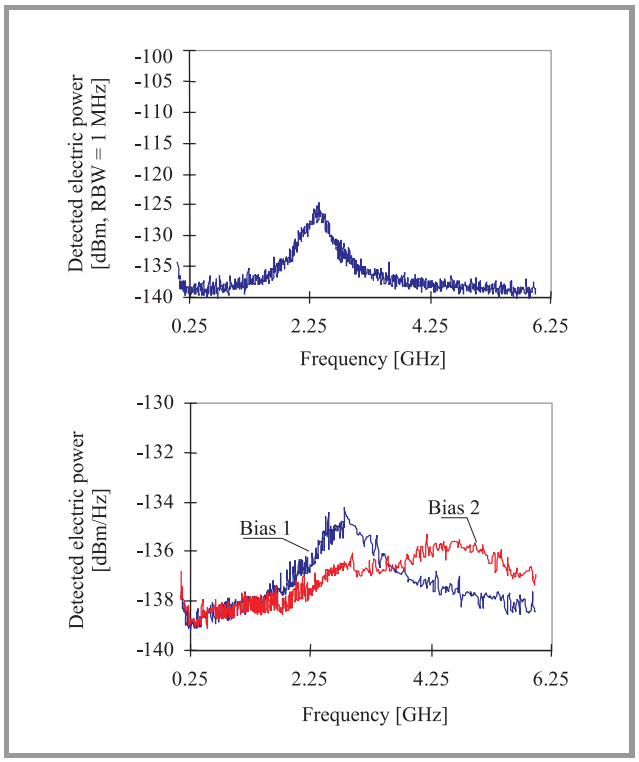

Fig. 2. The frequency and bias dependence for two different laser diodes.

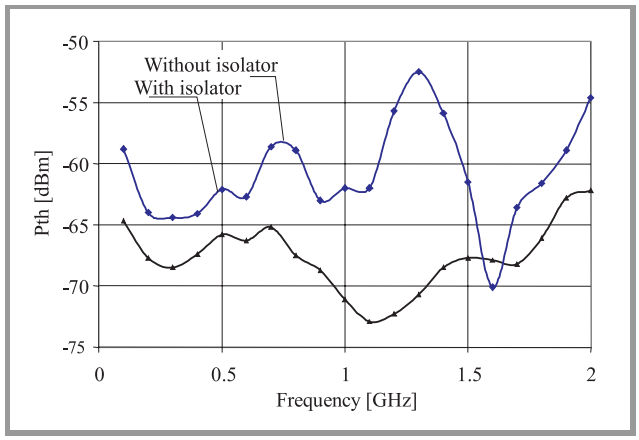

Fig. 3. Third order distortion product dependence on modulation frequency.

The drawback of a MZ modulator is, that it requires high RF power, and has low linearity. In the experiments a HP 83422A external modulator was used, which had less than 8% modulation depth with 10 dBm input power. The

linearity was measured at 8 and 25% modulation depth, and the result was 40.93 dBm and 31.07 dBm respectively for the third order mixing product (Fig. 4).

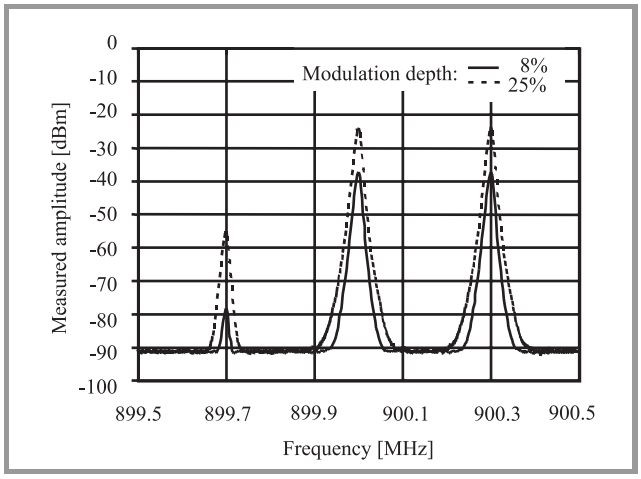

Fig. 4. Third order distortion products of MZ.

The optical loss is very high in case of long optical link or usage of several optical dividers for several cellular transceivers. Hence, some optical amplifiers may be needed to compensate this optical loss. The spontaneous emission is the source of noise in semiconductor optical amplifier and it is a random process, which is statistically stationary and will cause fluctuations in both amplitude and phase of optical signal. In addition, the spontaneous emission photons can interact directly the signal. So several type of noises (the shot noise owing to spontaneous emissions, beat noise between signal and spontaneous emissions, beat noise between spontaneous emissions components and excess noise owing to incoherence of the input signal) can be observed, when the output photons are detected by a photodetector. So the resulting noise power at the detector with load resistance R_p and bandwidth B with perfect coupling is:

$$N_A(f) = \frac{\langle \Delta N_p^2(f) \rangle}{\tau_{p2}^2} \cdot R_p \cdot B \cdot \eta_Q^2 \cdot e^2 , \tag{2}$$

where $\langle \Delta N_p^2(f) \rangle$ – second-order moments of photon number, η_Q – quantum efficiency of the photo-detector, τ_{p2} – photon lifetime.

In practical three main applications are used. In first method, SOAs operate as a post-amplifier to optical transmitter. In a non-regenerative repeater the incoming optical signals are directly amplified and so this process is compensate the fiber loss. Finaly, the SOA can be used as a pre-amplifier to the receiver, it can amplify the incoming weak signal, thereby improving the sensitivity of receiver. For these applications SOAs with a wide bandwidth and low noise figure are required.

If M pices of identical SOAs are used as in-line repeaters, each specified by an amplifier gain (G) and noise figure (F), we can derive the signal to noise ratio of the optical receiver [3]:

$$SNR_r = \frac{SNR_t}{F + \frac{F}{G} + \frac{F}{G^2} + \cdots + \frac{F}{G^{M-1}}} , \tag{3}$$

where SNR_t is the signal to noise ratio of the transmitter. It can be seen that the noise figure of the first amplifier is the most significant contribution to SNR_r. So when different SOAs can be used, the minimum noise figure amplifier should be the first in the chain [4]. The typical value of the noise figure of semiconductor optical amplifier is $6-8$ dB, but the theoretical limit is 3 dB.

Several sources of optical loss along the link are indicated:

- L_{TF}: optical transmitter to fiber coupling loss (typical value: 3 dB),
- L_F: optical fiber loss (0.3 dB/km),
- L_C: connector and splice losses $(0.1-0.4$ dB),
- L_{FR}: fiber to optical receiver coupling loss (<3 dB),
- L_{FA}: fiber to optical amplifier coupling loss (3 dB),
- L_{AF}: optical amplifier to fiber coupling loss (typical value: 3 dB).

Hence the whole optical insertion loss of the link:

$$L_{opt} = P_L / P_P , \tag{4}$$

where P_P is the optical power delivered to photodiode.

The electrical insertion loss (L) which is proportional to the square of the optical loss of the link:

$$L = \frac{P_{tr}}{P_{rec}} = \frac{I_{tr}^2 \cdot R_L}{I_P^2 \cdot R_P} = \left(\frac{L_{opt}}{\eta_L \cdot \eta_P} \right)^2 \cdot \frac{R_L}{R_P} ,$$
$$L[\text{dB}] = 2 \cdot L_{opt}[\text{dB}] . \tag{5}$$

Here P_{tr} and P_{rec} are the electrical power supplied to the laser diode and delivered by the photodiode, respectively. R_L is the laser diode incremental drive impedance about its point of bias, R_P is the photodiode load impedance, I_{tr} is the modulation current of the laser diode, I_P is the photo current of the photodetector and finally η_L and η_P are the responsibility of laser diode and photodiode, respectively.

Supposing a pin diode photo receiver the electrical noise power in the photodiode output comes from shot noise of average photocurrent (N_q), dark current (N_d), leakage current (N_l) and the Johnson noise of photodiode equivalent resistance (N_T). Although the main noise source are the thermal noise and the shot noise, which are due to the quantum statistic nature of photons and electrons. The noise sources are statistically independent, so they can be added and the resultant electrical noise power of photodetector (N_P) is:

$$N_P = N_q + N_d + N_l + N_T \cong N_q + N_T =$$
$$= 2 \cdot q \cdot I_{ph} \cdot B \cdot R_P + k \cdot T \cdot B , \tag{6}$$

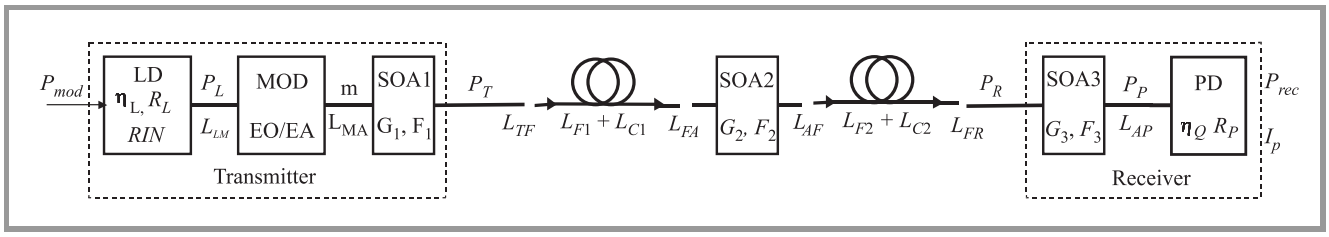

Fig. 5. Block diagram of the optical link.

where q is the electron charges, k is the Boltzmann constant, T is the absolute temperature, B is the bandwidth and I_{ph} is the average photo current.

Summarizing the noise performance and signal power of the optical link (the block can be seen in Fig. 5):

$$L_{opt} = \frac{L_{LM} \cdot L_{MA} \cdot L_{TF} \cdot L_{F1} \cdot L_{C1} \cdot L_{FA} \cdot L_{AF} \cdot L_{F2} \cdot L_{C2} \cdot L_{FR} \cdot L_{AP}}{G_1 \cdot G_2 \cdot G_3}, \tag{7}$$

where L_{LM}, L_{MA}, L_{TF}, L_{FA}, L_{AF}, L_{FR}, L_{AP} are the optical coupling loss between the different blocks and L_{F1}, L_{C1}, L_{F2}, L_{C2}, are the fiber and connectors loss in the different sections.

Examining the electrical signal power in the output of photodiode a sinusoidal modulating signal is assumed:

$$i_{rms} = \frac{1}{\sqrt{2}} \cdot I_P = \frac{1}{\sqrt{2}} \cdot \frac{q \cdot \eta_Q \cdot P_P}{h \cdot \nu}, \tag{8}$$

where h is the Planck constant and ν is the light frequency. Hence the signal to noise ratio is in the output of receiver:

$$\frac{S}{N} = \frac{\left(\frac{1}{\sqrt{2}} \cdot \frac{q \cdot \eta_Q \cdot P_L \cdot L_{opt}}{h \cdot \nu} \right)^2 \cdot R_P}{\frac{N_L}{L} + \frac{N_{\mathrm{mod}}}{\left(L_{LM}\right)^2} + \frac{N_{A1}}{\left(L_{LM} \cdot L_{MA}\right)^2} + \frac{N_{A2}}{\left(L_2\right)^2} + \frac{N_{A3}}{\left(L_{AP}\right)^2} + N_P}, \tag{9}$$

where N_L, N_M, N_A and N_L are the noises of laser diode, external modulator, optical amplifier and photodiode respectively, L is the electrical loss of the whole optical link and L_2 is the optical loss from optical amplifier to photodiode.

4. Conclusion

In the paper sources of nonlinearity and noise in subcarrier multiplexed optical transmission were investigated. The different types of optical modulation methods were experimentally compared. The external modulation is advantageous when high dynamic range is more important than linearity. The direct modulation has higher linearity and needs lower driving signal. The frequency and optical reflection dependence of linearity was presented. Calculation method of the signal to noise ratio in optical transmission including optical amplifiers was also presented.

Acknowledgment

The authors acknowledge the Hungarian Scientific Research Fund for their support to their research work (under the projects of OTKA no. F024113, T030148, T026557).

References

[1] T. Berceli, G. Járó, T. Marozsák, S. Mihály, E. Udvary, Z. Varga, and A. Zólomy, "A novel optical cellular millimeter wave radio system", in *29th Eur. Microw. Conf.*, München, Germany, Oct. 1999, vol. 1, pp. 230–233.

[2] C. H. Cox, G. E. Betts, and L. M. Johnson, "An analytic and experimental comparison of direct and external modulation in analog fiber-optic links", *IEEE Trans. Microw. Theory Techn.*, vol. 38, no. 5, pp. 501–509, 1990.

[3] H. Ghafouri-Shiraz, *Laser Diode Amplifiers*. Chichester: Wiley, 1996.

[4] H. A. Haus, "The noise figure of optical amplifiers", *IEEE Phot. Technol. Lett.*, vol. 10, no. 11, pp. 1602–1604, 1998.

Eszter Udvary received the M.Sc. degree in electrical engineering from Technical University of Budapest (TUB), Hungary in 1997. Her M.Sc. thesis was on the design and test of microwave oscillators. Now, she is a Ph.D. student at the TUB, Department of Microwave Telecommunications. Her research interests include optical and microwave communication systems, optical and microwave interactions and applications of special electro-optical devices. It principally means application semiconductor optical amplifier as a modulator, and a detector in optical networks. She is student member of the IEEE and author or co-author of more than 15 technical papers.
e-mail: udvary@mht.bme.hu
Department of Microwave Communications
Technical University of Budapest
H-1111 Budapest, Goldmann György-tér 3, Hungary

Tamás Marozsák received the M.Sc. degree in electrical engineering from Technical University of Budapest, Hungary in 1995. From 1995 he is a Ph.D. student there. He was involved in several research projects in the field of optical

communications. He designed hybrid integrated microwave circuits and high speed electro-optical converters. He investigated dispersion effects in millimeter-wave optical transmission systems and the optical transmitters in subcarrier multiplexed systems. His special interest is modeling semiconductor laser diodes. He took part in the design of variety microwave and optical devices for telecommunication and military applications. His recent research area is modeling VCSELs.

Department of Microwave Communications
Technical University of Budapest
H-1111 Budapest, Goldmann György-tér 3, Hungary

INFORMATION FOR AUTHORS

The *Journal of Telecommunications and Information Technology* is published quarterly. It comprises original contributions, both regular papers and letters, dealing with a broad range of topics related to telecommunications and information technology. Items included in the journal report primary and/or experimental research results, which advance the base of scientific and technological knowledge about telecommunications and information technology.

The *Journal* is dedicated to publishing research results which advance the level of current research or add to the understanding of problems related to modulation and signal design, wireless communications, optical communications and photonic systems, speech devices, image and signal processing, transmission systems, network architecture, coding and communication theory, as well as information technology. Suitable research-related manuscripts should hold the potential to advance the technological base of telecommunications and information technology. Tutorial and review papers are published by invitation only.

Papers published by invitation and regular papers should contain up to 15 and 8 printed pages respectively (one printed page corresponds approximately to 3 double-space pages of manuscript, where one page contains approximately 2000 characters).

Manuscript: An original and two copies of the manuscript must be submitted, each completed with all illustrations and tables attached at the end of the papers. Tables and figures have to be numbered consecutively with Arabic numerals. The manuscript must include an abstract limited to approximately 100 words. The abstract should contain four points: statement of the problem, assumptions and methodology, results and conclusion, or discussion, of the importance of the results. The manuscript should be double-spaced on only one side of each A4 sheet (210 × 297 mm). Computer notation such as Fortran, Matlab, Mathematica etc., for formulae, indices, etc., is not acceptable and will result in automatic rejection of the manuscript. The style of references, abbreviations, etc., should follow the standard IEEE format.

References should be marked in the text by Arabic numerals in square brackets and listed at the end of the paper in order of their appearance in the text, including exclusively publications cited inside. The **reference entry** (correctly punctuated according to the following rules and examples) **has to contain**.

From journals and other serial publications: initial(s) and second name(s) of the author(s), full title of publication (transliterated into Latin characters in case it is in Russian, possibly preceded by the title in Russian characters), appropriately abbreviated title of periodical, volume number, first and last page number, year. E.g.:

[1] Y. Namihira, „Relationship between nonlinear effective area and modefield diameter for dispersion shifted fibres", *Electron. Lett.*, vol. 30, no. 3, pp. 262–264, 1994.

From non-periodical, collective publications: as above, but after title – the name(s) of editor(s), title of volume and/or edition number, publisher(s) name(s) and place of edition, inclusive pages of article, year. E.g.:

[2] S. Demri, E. Orłowska, „Informational representability: Abstract models versus concrete models" in *Fuzzy Sets, Logics and Reasoning about Knowledge*, D. Dubois and H. Prade, Eds. Dordrecht: Kluwer, 1999, pp. 301–314.

From books: initial(s) and name(s) of the author(s), place of edition, title, publisher(s), year. E.g.:

[3] C. Kittel, *Introduction to Solid State Physics*, New York: Wiley, 1986.

Figure captions should be started on separate sheet of papers and must be double-spaced.

Illustration: Original illustrations should be submitted. All line drawings should be prepared on white drawing paper in black India ink. Drawings in Corel Draw and Postscript formats are preferred. Colour illustrations are accepted only in exceptional circumstances. Lettering should be large enough to be readily legible when drawing is reduced to two- or one-column width – as much as 4:1 reduction from the original. Photographs should be used sparingly. All photographs must be gloss prints. All materials, including drawings and photographs, should be no larger than 175 × 260 mm.

Page number: Number all pages, including tables and illustrations (which should be grouped at the end), in a single series, with no omitted numbers.

Electronic form: A floppy disk together with the hard copy of the manuscript should be submitted. It is important to ensure that the diskette version and the printed version are identical. The diskette should be labelled with the following information: a) the operating system and word-processing software used, b) in case of UNIX media, the method of extraction (i.e. tar) applied, c) file name(s) related to manuscript. The diskette should be properly packed in order to avoid possible damage during transit.

Among various acceptable word processor formats, TEX and LATEX are preferable. The *Journal's* style file is available to authors.

Galley proofs: Proofs should be returned by authors as soon as possible. In other cases, the article will be proofread against manuscript by the editor and printed without the author's corrections. Remarks to the errata should be provided within two weeks after receiving the offprints.

The copy of the „Journal" shall be provided to each author of papers.

Copyright: Manuscript submitted to this journal may not have been published and will not be simultaneously submitted or published elsewhere. Submitting a manuscript, the authors agree to automatically transfer the copyright for their article to the publisher if and when the article is accepted for publication. The copyright comprises the exclusive rights to reproduce and distribute the article, including reprints and also all translation rights. No part of the present journal may be reproduced in any form nor transmitted or translated into a machine language without permission in written form from the publisher.

Biographies and photographs of authors are printed with each paper. Send a brief professional biography not exceeding 100 words and a gloss photo of each author with the manuscript.

National Institute
of Telecommunications
Szachowa st 1
04-894 Warsaw, Poland

Editorial Office
tel. +48(22) 872 43 88
tel./fax: +48(22) 512 84 00
e-mail: redakcja@itl.waw.pl
http://www.itl.waw.pl/jtit